Monthly Notices of the ROYAL ASTRONOMICAL SOCIETY

MNRAS **00,** 1 (2021) https://doi.org/10.1093/mnras/stab1620

The GALAH survey and symbiotic stars – I. Discovery and follow-up of 33 candidate accreting-only systems

U. Munari [1]★ G. Traven,[2] N. Masetti,[3,4] P. Valisa,[5] G.-L. Righetti,[5] F.-J. Hambsch,[5] A. Frigo,[5] K. Čotar [6] G. M. De Silva,[7,8] K. C. Freeman,[9] G. F. Lewis [10] S. L. Martell [11,12] S. Sharma [10,12] J. D. Simpson [11,12] Y.-S. Ting,[13] R. A. Wittenmyer[14] and D. B. Zucker[8,12,15]

[1]*INAF – Astronomical Observatory of Padova, I-36012 Asiago (VI), Italy*
[2]*Lund Observatory, Department of Astronomy and Theoretical Physics, Box 43, SE-221 00 Lund, Sweden*
[3]*INAF – Osservatorio di Astrofisica e Scienza dello Spazio, via Gobetti 93/3, I-40129 Bologna, Italy*
[4]*Departamento de Ciencias Físicas, Universidad Andrés Bello, Fernández Concha 700, Las Condes, Santiago, Chile*
[5]*ANS Collaboration, c/o Astronomical Observatory, I-36012 Asiago (VI), Italy*
[6]*Faculty of Mathematics and Physics, University of Ljubljana, Jadranska 19, 1000 Ljubljana, Slovenia*
[7]*Australian Astronomical Optics, Macquarie University, 105 Delhi Rd, North Ryde, NSW 2113, Australia*
[8]*Macquarie University Research Centre for Astronomy, Astrophysics and Astrophotonics, Sydney, NSW 2109, Australia*
[9]*Research School of Astronomy and Astrophysics, Australian National University, ACT 2611, Australia*
[10]*Sydney Institute for Astronomy, School of Physics (A28), The University of Sydney, NSW 2006, Australia*
[11]*School of Physics, UNSW, Sydney, NSW 2052, Australia*
[12]*Centre of Excellence for Astrophysics in Three Dimensions (ASTRO-3D), Australia*
[13]*Department of Astrophysical Sciences, Princeton University, Princeton, NJ 08544, USA*
[14]*Centre for Astrophysics, University of Southern Queensland, USQ, Toowoomba, QLD 4350, Australia*
[15]*Department of Physics and Astronomy, Macquarie University, Sydney, NSW 2109, Australia*

Accepted 2021 June 3. Received 2021 June 3; in original form 2020 December 13

ABSTRACT

We have identified a first group of 33 new candidates for symbiotic stars (SySt) of the accreting-only variety among the 600 255 stars so far observed by the GAlactic Archaeology with HERMES (GALAH) high-resolution spectroscopic survey of the Southern hemisphere, more than doubling the number of those previously known. GALAH aims to high latitudes and this offers the possibility to sound the Galaxy for new SySt away from the usual plane and bulge hunting regions. In this paper, we focus on SySt of the M spectral type, showing an Hα emission with a peak in excess of 0.5 above the adjacent continuum level, and not affected by coherent radial pulsations. These constraints will be relaxed in future studies. The 33 new candidate SySt were subjected to an array of follow-up confirmatory observations [X-ray/ultraviolet (UV) observations with the *Swift* satellite, search for optical flickering, presence of a near-UV upturn in ground-based photometric and spectroscopic data, radial velocity changes suggestive of orbital motion, and variability of the emission-line profiles]. According to *Gaia* Early Data Release 3 (EDR3) parallaxes, the candidate new SySt are located at the tip of the giant branch, sharing the same distribution in $M(K_s)$ of the well-established SySt. The accretion luminosities of the candidate new SySt are in the range 1–10 $L_\odot$, corresponding to mass accretion rates of 0.1–1 $\times$ 10^{-9} $M_\odot$ yr^{-1} for white dwarfs of 1 $M_\odot$. The M giant of one of them presents a large lithium overabundance.

Key words: methods: data analysis – binaries: symbiotic – Galaxy: stellar content.

1 INTRODUCTION

Symbiotic stars (SySt) are interacting binaries where a red giant (RG) fuels a white dwarf (WD) or a neutron star (NS) companion via accretion (either through Roche lobe overflow or wind intercept). Systems harbouring NSs are a recent addition to this class of celestial objects (Masetti et al. 2006, 2007a,b, 2011; Bozzo et al. 2018; Yungelson, Kuranov & Postnov 2019) and constitute a few per cent of the known total (Merc, Gális & Wolf 2019a), the vast majority containing WDs (Mukai et al. 2016; Sokoloski et al. 2017; Akras et al. 2019). For some time, a main-sequence star accreting from the RG at very high rates (10^{-6} to 10^{-4} $M_\odot$ yr^{-1}) was considered a viable scenario for SySt in general (Kenyon & Webbink 1984), but this has been progressively abandoned in the light of expanding observational data, especially in the far-ultraviolet (UV) and X-rays (Skopal et al. 2006; Sokoloski et al. 2006; Mohamed & Podsiadlowski 2012; Luna et al. 2013; Skopal & Cariková 2015; Lutovinov et al. 2020).

The RG+WD SySt are broadly divided into two major groups (see the recent review by Munari et al. 2019 for details): those *accreting-only* (*acc*-SySt) whose optical spectra are dominated by the RG with no or weak emission lines, and the *burning-type* (*burn-*

★ E-mail: ulisse.munari@oapd.inaf.it

SySt) displaying a strong nebular continuum and a rich emission line spectrum: they originate from the wind of the RG, which is largely ionized by the very hot and luminous WD undergoing surface nuclear burning of accreted material.

SySt are believed to spend most of their time in the accreting-only phase, quietly accumulating material on the surface of the WD. When enough has been piled up, nuclear burning ignites. If the accreted matter is electron degenerate, the burning proceeds explosively. It quickly reaches the Fermi temperature (a matter of minutes; Starrfield, Iliadis & Hix 2008) and ejects most of the accreted envelope at high velocity (thousands of km s^{-1}). Radio interferometry has nicely resolved the expansion of ejecta following, for example, the 2006 outburst of RS Oph (O'Brien et al. 2006) and that of 2010 for V407 Cyg (Giroletti et al. 2020), the latter being also the first nova event ever detected in GeV γ-rays by the *Fermi* satellite (Cheung et al. 2010). The resulting nova outburst can repeat on time-scales as short as years/decades if the WD mass is close to the Chandrasekhar limit, like in the case for T CrB, RS Oph, V407 Cyg, or V3890 Sgr. If the matter accreted on the WD is instead not electron degenerate, the nuclear burning proceeds in thermal equilibrium, and no mass is ejected. The event takes a few years to reach peak brightness (Fujimoto 1982), and requires many decades to a few centuries to burn the accreted envelope and let the system return to low luminosity. Some of the best examples of this type are AG Peg, HM Sge, V1016 Cyg, and V4368 Sgr.

There is a clear disproportion among catalogued SySt in favour of the *burn*-SySt type, and the known examples of the *acc*-SySt variety are believed to be just the tip of the iceberg (Mukai et al. 2016, hereafter Mk16). Between 15 and 20 are currently known of the *acc*-SySt type. SySt were originally proposed by Munari & Renzini (1992) as possible progenitors of Type Ia supernovae, and the viability of this single-degenerate channel obviously relies on the total number of SySt spread throughout the Galaxy, which in turn heavily depends on the number of *acc*-SySt. The latter have been usually discovered as counterparts of satellite UV/X-ray sources, while the *burn*-SySt can be easily spotted at optical wavelengths through the whole Galaxy and the Local Group thanks to their outstanding emission-line spectrum (with ionization up to [Fe X] and beyond).

The subtle way the optically quiet *acc*-SySt have been usually discovered is well epitomized by SU Lyncis (SU Lyn), a $V \sim 8$ mag, M6III giant at 650 $\pm$ 35 pc distance (Gaia Collaboration et al. 2018). For decades it was a completely unnoticed field star, with just an old report about semiregular photometric variability that granted it a variable star name (Kippenhahn 1955). While looking for optical counterparts of hard X-ray sources newly discovered by the *Swift* satellite, it was noted that SU Lyn lay within the error box of one of them: 4PBC J0642.9+5528. Follow-up observations were organized with *Swift* (to refine the position and the properties of the X-ray source) and with Asiago telescopes to investigate if the optical spectra of SU Lyn could betray peculiarities supporting a physical association with the *Swift* hard X–ray source. The association was proved by a large flux excess observed at bluest optical wavelengths ($\lambda \leq 4000$ Å) and by the presence on high-resolution spectra of weak and variable emission in Hα and [Ne III] lines (cf. Mk16).

The limited sensitivity of current X-ray satellites (soon to change thanks to *eROSITA* sky survey; Merloni et al. 2012) restricts the serendipitous discovery of *acc*-SySt to those that lie within $\sim$1 kpc from the Sun, implying that many of their red giants rank among naked-eye objects (like 4 Dra, HR 1105, or *o* Cet). To sample a much larger fraction of the RG in our Galaxy, we have devised a reverse strategy, and first exploratory results are presented in this paper: digging through large spectroscopic surveys in search for the signatures of accretion on to a companion to the RG, primarily the presence of Balmer emission lines having a flux and a profile compatible with an origin in an accretion disc around a degenerate companion. The candidate *acc*-SySt identified this way can then be subjected to follow-up confirmatory observations, including pointing with X-ray/UV satellites. The GAlactic Archaeology with HERMES (GALAH) survey of the Southern hemisphere (De Silva et al. 2015) offers an ideal hunting opportunity: a large number (aiming at >1 million) of randomly selected southern stars in the $12 \leq V_{JK} \leq 14$ mag range are observed at high signal-to-noise ratio (S/N) and high spectral resolution with the Anglo-Australian Telescope (AAT) 3.9-m telescope+fibre-fed spectrograph HERMES, over four distinct wavelength ranges that include Hα and Hβ lines.

In this first paper, we outline the methodologies guiding our search among GALAH spectra for candidate *acc*-SySt, report on the discovery of a first batch of 33 new candidates (about doubling the total known so far), and describe the results of a wide range of follow-up observations aiming to confirm their *acc*-SySt nature. We encourage further observations by the community in order to validate their classification.

2 THE GALAH SURVEY

2.1 Motivation

The GAlactic Archaeology with HERMES (GALAH; De Silva et al. 2015) is an ongoing spectroscopic survey whose ambitious goal is to unveil the formation and history of the Milky Way. This is the focus of the field of Galactic archaeology, which tries to determine how the fossil remnants of star-forming regions and effects of ancient mergers paint the picture of our Galaxy that we observe and measure today. This complex endeavour can be accomplished by studying the detailed chemical composition and other properties of stars in distinct regions of the Milky Way.

The Galactic archaeology community argues that the complete Galaxy formed gradually over time. This formation history can be traced back by investigating remnants of initial building blocks or subsequent additions through mergers, which have been disrupted in the course of evolution and are now dispersed around the Galaxy. The theoretical concept of chemical tagging (Freeman & Bland-Hawthorn 2002) demonstrates that individual galactic components should have preserved their original chemical signature over time. It is therefore essential to disentangle their formation site from migration history in order to explain the current mixture of stellar populations.

GALAH aims to achieve this by measuring the abundance of up to 31 chemical elements coming from seven independent major groups with different nucleosynthetic origin: light proton-capture elements: Li, C, O; α-elements: Mg, Si, Ca, Ti; odd-Z elements: Na, Al, K; iron-peak elements: Sc, V, Cr, Mn, Fe, Co, Ni, Cu, Zn; light and heavy slow neutron capture elements: Rb, Sr, Y, Zr, Ba, La; and rapid neutron capture elements: Ru, Ce, Nd, Eu (De Silva et al. 2015).

2.2 Instrument

The goals of the GALAH survey were the main driver for the construction of the High Efficiency and Resolution Multi-Element Spectrograph (HERMES; Barden et al. 2010; Sheinis et al. 2015), a multifibre spectrograph working in tandem with the 3.9-m AAT

Table 1. Short and long wavelength limits (Å) of the four spectral intervals recorded by the GALAH survey.

Interval	Start	End
Blue	4718	4903
Green	5649	5873
Red	6481	6739
Far red	7590	7890

situated at the Siding Spring Observatory, Australia. The spectrograph has a resolving power of $R \sim 28\,000$ (or $R \sim 45\,000$ when slit mask is used) and records spectra in four separate wavelength ranges given in Table 1. The total spectral coverage is therefore approximately 1000 Å, including the important diagnostic lines Hα and Hβ, together with lines of numerous chemical elements that are necessary to fulfil the ambitions of the GALAH survey.

The AAT uses the Two-degree Field (2dF) robotic positioning system with two identical plates that are used to precisely position fibres at designated locations. This configuration allows HERMES to simultaneously record spectra from up to 392 fibres distributed over a 2° diameter field of the night sky, with an additional eight fibres used for the telescope guiding. During the exposure with the first plate, the robotic positioner places fibres on the second plate, where each complete process of fibre allocation takes about half an hour per plate. HERMES can typically achieve an S/N of ∼100 per resolution element at magnitude $V = 14$ in the red arm during a 1-h long exposure. To achieve as high S/N as possible, minimize atmospheric diffraction, and in order not to lose light due to the fibres' field of view of only 2 arcsec, all observations are ideally carried out close to the meridian.

2.3 Selection function

The main selection function of the GALAH survey is relatively simple: it avoids the crowded regions of the Galactic plane ($|b| > 10°$), accounts for the nominal telescope operations ($-80° \leq \delta \leq +10°$) and restricts observations by apparent magnitude ($12 < V_{JK} < 14$), while being colour independent. There is an additional requirement for field selection: the density of stars has to be at least 400 per π deg^2 to match the number of fibres and field of view of the fibre positioner. The input catalogue for observations is based on the Two Micron All-Sky Survey (2MASS; Skrutskie et al. 2006), with V_{JK} approximating standard V magnitude and being computed as (for more details see Martell et al. 2017)

$$V_{JK} = K + 2(J - K + 0.14) + 0.382\,\mathrm{e}^{(J-K-0.2)/0.5}. \quad (1)$$

The majority of observations are performed with the above described selection function. Additionally, GALAH employs a bright mode ($9 < V_{JK} < 12$) during twilight or poor observing conditions, and a faint mode ($12 < V_{JK} < 14.5$) when fields with normal or bright configuration are not available to be observed.

The spectroscopic data used in this work are further complemented by observations of the *K2*-HERMES survey (Wittenmyer et al. 2018) and the *Transiting Exoplanet Survey Satellite* (*TESS*)-HERMES survey (Sharma et al. 2018), which are carried out with the same observational and data reduction set-up as the GALAH survey, albeit with their peculiar selection functions focusing on K2 (Howell et al. 2014) and TESS (Ricker et al. 2015) targets, respectively.

Together, the above described observations yield a data set of 625 757 successfully reduced stellar spectra, of which a small fraction belongs to repeated observations of 600 255 unique stars observed by GALAH at the time of writing of this paper. They represent dwarf and giant stars, the former consisting of mostly nearby stars (closer than 2 kpc), while the latter probing distances as far as the Galactic Centre.

2.4 Data reduction and analysis

Every stellar spectrum recorded by the HERMES spectrograph and used in this work is homogeneously reduced by an automatic reduction pipeline, thoroughly described by Kos et al. (2017). We hereby provide only a brief explanation of this reduction procedure.

The path from a 2D image recorded in each of the HERMES arms to a one-dimensional, continuum-normalized, and zero-RV-shifted spectrum starts with the following steps: raw image cosmetic corrections, spectral tracing, optical aberrations correction, scattered light and apertures cross-talk removal, wavelength calibration, sky subtraction, and telluric absorption removal. Afterwards, spectra are continuum normalized and shifted into their rest frame by cross-correlating them with a set of 15 AMBRE model spectra (de Laverny et al. 2012). This procedure also yields initial radial velocities, while initial stellar parameters ($T_{\rm eff}$, $\log g$, [Fe/H]) are determined by a (larger) grid of 16 783 AMBRE spectra. These, internally also called GUESS parameters, were reported in the first GALAH data release (Martell et al. 2017). The spectra are then directed to the analysis pipeline with the aim of delivering precise and accurate stellar atmospheric parameters and individual elemental abundances, which constitute the core of results reported in subsequent GALAH data releases.

2.5 The new SySt probed by GALAH

Most of the known SySt have been discovered during photographic objective-prism surveys of the Galactic plane and bulge (e.g. Merrill & Burwell 1950; Sanduleak & Stephenson 1973; Henize 1976), many of which were initially classified and studied as planetary nebulae. Their true nature was generally unveiled by infrared observations catching the presence of a cool giant in the system (Allen 1982, 1984; Sabbadin, Falomo & Ortolani 1987). The same objective-prism technique was applied also to the Magellanic Clouds and several SySt were discovered there too (Walker 1983; Morgan 1992). Searches for SySt in external galaxies have steadily progressed over the years (Gonçalves et al. 2008, 2012, 2015; Kniazev et al. 2009; Angeloni et al. 2014; Mikołajewska, Caldwell & Shara 2014; Mikołajewska et al. 2017; Roth et al. 2018; Drozd et al. 2019), and the current total of known extragalactic SySt amounts to ∼70 systems (Akras et al. 2019; Chen, Liu & Shan 2019; Merc, Gális & Wolf 2019b). New surveys aiming to SySt within the Local Group (Angeloni et al. 2019) promise to increase such numbers, especially for the *burn*-SySt type.

Systematic searches for new SySt have also been performed in recent years through our Galaxy. The INT Photometric H-Alpha Survey (IPHAS; Drew et al. 2005) targeted the plane of the Milky Way for emission-line objects, among which many new candidate SySt were identified by Corradi et al. (2008, 2010, 2011) and Rodríguez-Flores et al. (2014). SySt were also hunted toward the bulge by Miszalski, Mikołajewska & Udalski (2013) and Miszalski & Mikołajewska (2014). The current total of confirmed Galactic SySt is about 250 (Akras et al. 2019; Merc et al. 2019b).

No recent survey has extensively probed the Galaxy for SySt toward directions other than low on the plane or toward the bulge. This is a gap we intend to fill with the help of the GALAH survey, that is exploring the Galaxy primarily at high latitudes. In this way a more complete census of SySt will be possible toward all stellar populations, allowing a more informed comparison with the

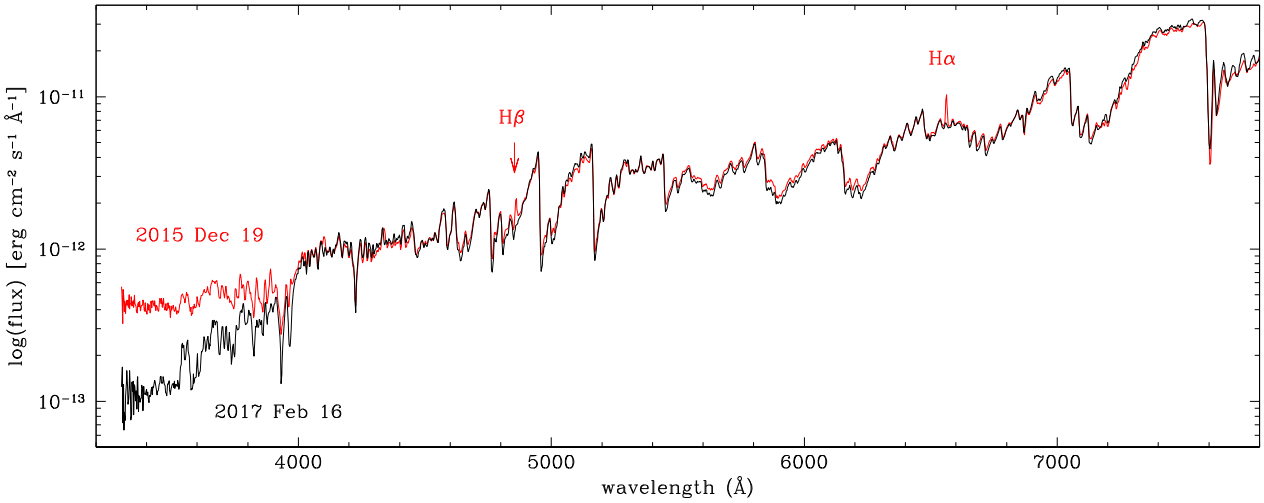

Figure 1. Two spectra of SU Lyn, a prototype of the accreting-only SySt, to illustrate the differences between low (black) and high (red) accretion rates (Asiago 1.22-m telescope). A higher rate causes a brightening of the accretion disc around the white dwarf, which manifests as an excess near-UV brightness ($\lambda \leq$ 4000 Å) and detectable emission lines (primarily hydrogen Balmer lines).

predictions about the total number of SySt spread throughout the Galaxy. Such estimates vary over a wide range: from 1200–15 000 of Lü, Yungelson & Han (2006), or 3000–30 000 of Yungelson et al. (1995) and Zhu et al. (2010), to 3000 of Allen (1984), 30 000 of Kenyon et al. (1993), and 300 000 of Munari & Renzini (1992). The large spread is in part accounted for by differences in the adopted binary evolution codes and stellar population synthesis, or by the type of SySt considered (burning or accreting only), and also by the ratio between SySt currently in an active state (and therefore detectable to observations) and those dormant (and indistinguishable from single, field cool giants). The populations of SySt containing a NS is generally estimated at 100–1000 (e.g. Lü et al. 2012), or about 1 per cent of those harbouring a WD.

3 SU LYNCIS, A PATHFINDER

As remarked earlier, several *acc*-SySt have been known for quite a while. A few of them present emission lines bright enough to be recognizable even on objective prism plates or low-resolution optical spectra. They are well epitomized by EG And, an M2III giant orbited every 481 d by a WD, whose accretion luminosity is a few 10^2 $L_\odot$ (Nuñez et al. 2016).

The discovery of SU Lyn by Mk16 revealed a '*hidden and potentially large population*' of *acc*-SySt accreting at much lower rates, with accretion luminosities a couple of orders of magnitude lower than in EG And, and therefore not detectable by conventional observations at optical wavelengths. This paper aims to specifically discover more of these SySt characterized by low accretion luminosities ($L_{acc} \sim$ 1–10 $L_\odot$). As the properties of SU Lyn will guide us as a pathfinder throughout this paper, and since no paper has so far reviewed this object at optical wavelengths, we will start with a quick overview of spectroscopic and photometric properties of SU Lyn. These are based on the very intensive monitoring we are keeping of the object since the preparatory phase leading to the Mk16 discovery paper, and whose results will be presented and discussed in detail elsewhere. The properties of SU Lyn that will be reviewed here are those that we will look for in the data set of GALAH stars with the aim to discover the new SySt.

The two most obvious distinctive characteristics of optical spectra of SU Lyn (and *acc*-SySt of that type) are shown in Fig. 1: (a) a near-UV ultraviolet excess ($\lambda \leq$ 4000 Å), and (b) weak emission lines, primarily from the hydrogen Balmer series. They both originate in the accretion disc forming around the degenerate companion, fed by the material accreted from the mass-losing RG companion.

Both can vary greatly in time, as the two epochs compared in Fig. 1 illustrate well: in just over 1 yr SU Lyn passed from an *active* state (2015 December 19), when its SySt nature was quite obvious, to a *quiet* phase (2017 Febuary 16) during which an optical spectrum would not have betrayed its binary nature. This needs to be kept in mind when comparing GALAH spectra with ancillary data taken at very different epochs.

The most important role of SU Lyn in guiding our search among GALAH stars is however the observed profile for emission lines, Hα in particular. Fig. 2 presents a temporal sequence from Asiago 1.82-m and Varese 0.84-m telescopes+echelle spectrographs illustrating the great variety of profiles observed for Hα in this star from 2015 to 2020 (for a more traditional presentation of some of these same profiles for key epochs see fig. 3 of Munari 2019). The orbital plane of SU Lyn is probably close to face-on conditions and this accounts for the negligible changes in radial velocity observed for the M6III absorption lines ($\leq$2 km s^{-1}). The observed spectroscopic and photometric changes are therefore not related to changes in the aspect angle of the binary.

The epoch marked *b* in Fig. 2 corresponds to the lowest accretion rate and it is noteworthy for the absence of emission in Hα and a null near-UV excess: at optical wavelengths SU Lyn appears like a normal and single M6III, not as an interacting binary. Only the reduced equivalent width of the Hα absorption (only about half the photospheric value of typical M6III giants) and its narrow full width at half-maximum (FWHM; again half the value for normal M6III giants) could cause doubt. The white vertical line in Fig. 2 represents the photospheric velocity of the cool giant: on epoch *b*, the velocity of the Hα absorption almost equals that of the M6III giant. This is not the case for most of the time, however, as clearly shown by Fig. 2, the Hα absorption is normally blueshifted compared to photospheric absorptions as if originating in a gentle wind blowing off the inner regions of the accretion disc (and thus appearing superimposed on to its emission), or forming in the expanding wind of the RG that engulfs the whole binary system.

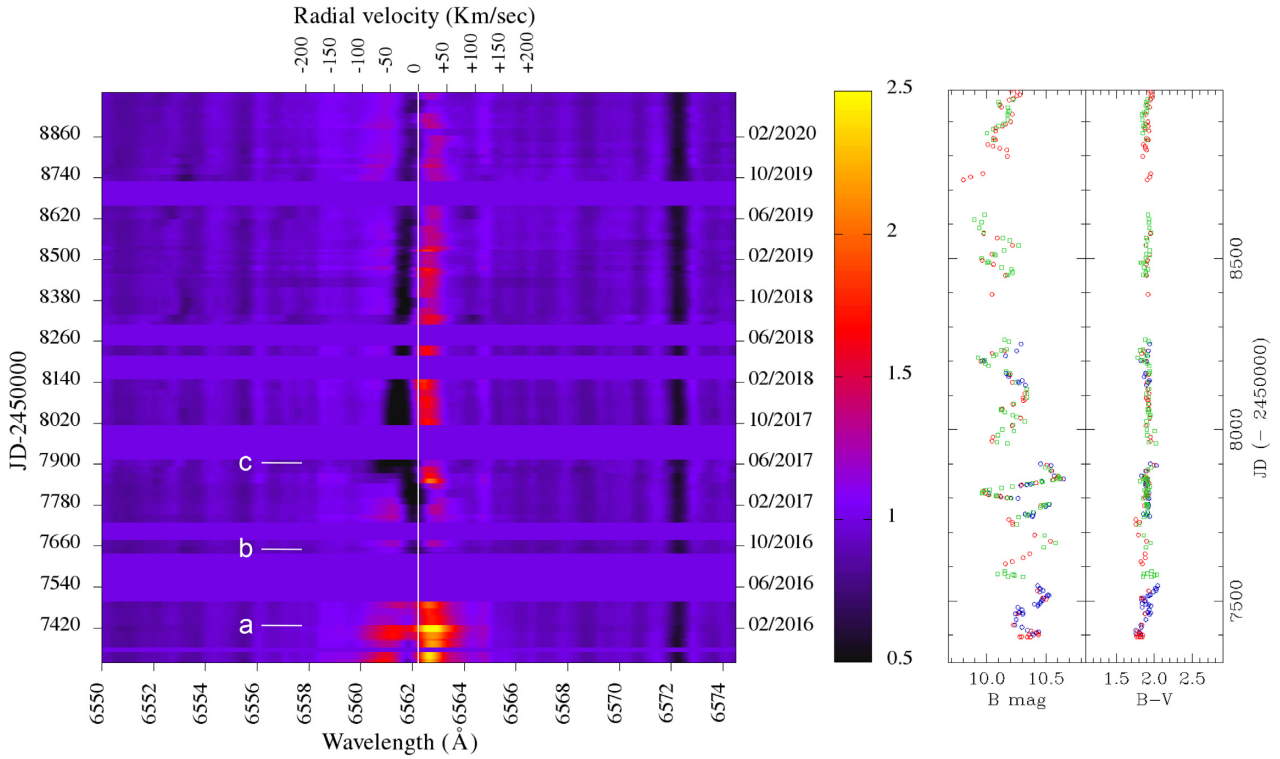

Figure 2. Temporal sequence from Asiago 1.82-m and Varese 0.84-m echelle spectra (aligned in heliocentric wavelength) illustrating the great changes observed in the Hα profile of prototype SU Lyn since its recognition in late 2015 as an accreting-only SySt. The vertical line marks the Hα rest wavelength at the stellar systemic velocity (-24 km s^{-1}). The epochs *a*, *b*, and *c* are discussed in the text (Section 3). On the right the corresponding *B*, *V* light curve of SU Lyn as built from ANS Collaboration observations.

Epoch *c* in Fig. 2 marks the sudden appearance of a second, distinct and faster moving absorption component that gradually reduced its velocity during the following months and finally merged with the slower, pre-existing absorption component. At the time of maximum equivalent width of this second absorption component, the emission in Hα briefly vanished.

Finally, epoch *a* represents the condition of highest accretion rate, with a strong near-UV excess and a prominent and structured emission in Hα, with still superimposed the blueshifted absorption component mentioned above. It is a lucky circumstance that when we first observed SU Lyn in preparation of Mk16 paper, the star was exhibiting a clear emission in Hα and the strongest near-UV upturn: if at the time, it had appeared as in epoch *b* of Fig. 2, we could not have recognized it for what it really was.

Another important point illustrated by Fig. 2 concerns the photometric activity of SU Lyn. The star is too bright to be recorded unsaturated by surveys that monitor the heaven on a nightly basis in search for transients [e.g. All-Sky Automated Survey for Supernovae (ASAS-SN), Mobile Astronomical System of TElescope Robots (MASTER), Zwicky Transient Facility (ZTF), etc.], therefore we monitored it ourselves with small instruments, and fully transformed the observations to the Landolt (1992) standard *UBVRI* system. As illustrated by the *B*, *V* light curve on the right-hand panel of Fig. 2 (synchronized to the same temporal ordinates as the spectra to the left), SU Lyn varies by up to 0.7 mag amplitude in a random fashion, with no persistent periodicity. There is no associated change in colour and no correspondence with the behaviour of the accretion disc as traced by Hα intensity and profile. Thus, the variability is not caused by brightening and fading of the accretion disc (hotter than the M6III), but must originate with the cool giant. All cool giants exhibit variability to some extent (Hoffmeister, Richter & Wenzel 1985; Sterken & Jaschek 2005), given the unstable nature of their convective outer layers (Pugh, Gray & Griffin 2015), and their tenuous atmosphere that extends across the temperatures for molecule formation and through those for dust condensation. The absence of radial velocity variability on the left-hand panel of Fig. 2 precludes an origin of the variability seen in SU Lyn with the coherent, large scale, persistent radial pulsations of the type observed in Mira long-period variables. The latter show a sinusoid-like radial velocity curve of $\sim$10–15 km s^{-1} in amplitude, in phase with the equally sinusoid-like light curve that can span up to 10 mag in amplitude, and characterized by bluer colour at maximum and redder at minimum (see fig. 27 in Hoffmeister et al. 1985).

The distinction with radially pulsating giants is important: their outer layers experience large-scale motions that lead to shocks, which in turn power emission lines. In our search for *acc*-SySt we aim to avoid the contamination from radially pulsating giants and their deceiving emission lines. The selection criteria for removing false positives from the final candidate *acc*-SySt sample are outlined in the rest of the paper.

4 SELECTION STEPS

Our search for *acc*-SySt among GALAH targets started with isolating the cool giants from the rest. In this paper, we focus on giants of the M spectral types, those most abundant ($\sim$70 per cent) among the known SySt (see the catalogues by Allen 1984; Belczyński et al. 2000; Akras et al. 2019; Merc et al. 2019b). SySt containing other types of cool giants will be explored in follow-up papers.

Table 2. Parallax for dwarf and giant M stars (under negligible reddening) at the bright ($V = 12$) and faint ($V = 14$) end of the GALAH magnitude range.

	M_V	Parallax (mas)	
		$V = 12$	$V = 14$
M0V	8.90	24	10
M5V	12.30	115	46
M0III	− 0.10	0.38	0.15
M5III	− 0.90	0.26	0.10

4.1 Colour

The intrinsic colour of M0 giants in the solar neighbourhood is $(J - K)_o = 0.97$ (Lee 1970; Koornneef 2009), so we first apply a colour selection of $(J - K_s) \geq 0.90$ to GALAH targets to both account for the natural spread with the breadth of the M0 spectral type and the slight difference in wavelength baseline between the Johnson's $(J - K)$ and 2MASS $(J - K_s)$ indices.

4.2 Parallax

On the Hertzsprung–Russell (HR) diagram, stars with an M spectral type are either very low mass main-sequence objects (down to the limit for stable H-burning in the core), or giants resulting from the evolution of more massive progenitors. The stars in our Milky Way have not lived long enough to significantly populate the range in between. M-dwarfs are intrinsically very faint and over the $12 < V_{JK} < 14$ mag range covered by GALAH targets, they represent the stars closest to the Sun, while the opposite is certainly true for the giants. In Table 2, we compare (under negligible reddening) the expected parallax of dwarfs and giants with an M spectral type at both ends of the GALAH magnitude range. No giant has a parallax larger than 0.4 mas, or a dwarf smaller than 10 mas. Therefore a second criterion was set imposing a *Gaia* Data Release 2 (DR2; Gaia Collaboration et al. 2018) parallax $\pi \leq 3$ mas. This selection criterion is fully confirmed by the improved *Gaia* Early Data Release 3 (EDR3) parallaxes (Gaia Collaboration 2020), which became available only after this paper was originally submitted.

4.3 TiO absorption bands

The above colour and parallax criteria combined together returned an initial sample of 29 514 GALAH stars. This sample could contain hotter giants of G and K spectral types affected by a large reddening or cool giants of a spectral type other than M (like the carbon giants). To prune them out and retain only those with an M-type spectrum, we looked for signatures of their distinctive TiO absorption bands in the GALAH spectra. This may have picked-up also some S-type giants whose spectra, in addition to TiO bands, show also molecules involving s-type elements (ZrO in particular; Turnshek et al. 1985). Some percentage of known SySt do indeed possess S-type giants (Jorissen 2003).

Fig. 3 presents a progression of M giant spectra with overplotted in green the wavelength range of the blue, green, and red GALAH channels. Within their span lie strong TiO bands, and the later the spectral type, the deeper such bands become. To confirm the presence of the TiO bands and objectively derive their depth, we defined eight narrow TiO wavelength bins (marked in red in Fig. 3) and an equal number of control wavelength bins (marked in yellow in Fig. 3). The control bins are all placed to the blue of their respective TiO bins given the fact that absorption bands of the TiO molecule all degrade to the red and present a steep band-head to the blue (Pearse & Gaydon 1976). We then defined eight *ratios* (b1, b2, and b3 in the blue channel, g1 and g2 in the green, and r1, r2, and r3 in the red) by integrating the flux within the control bin and dividing by it the TiO bin as

$$\text{ratio} = \frac{\int_{\lambda_A}^{\lambda_B} f(\lambda)\,d\lambda}{\int_{\lambda_C}^{\lambda_D} f(\lambda)\,d\lambda}, \qquad (2)$$

where the respective wavelength intervals A−B and C−D are listed in Table 3. These ratios were computed on spectra before continuum normalization but shifted to rest frame by the radial velocity listed in

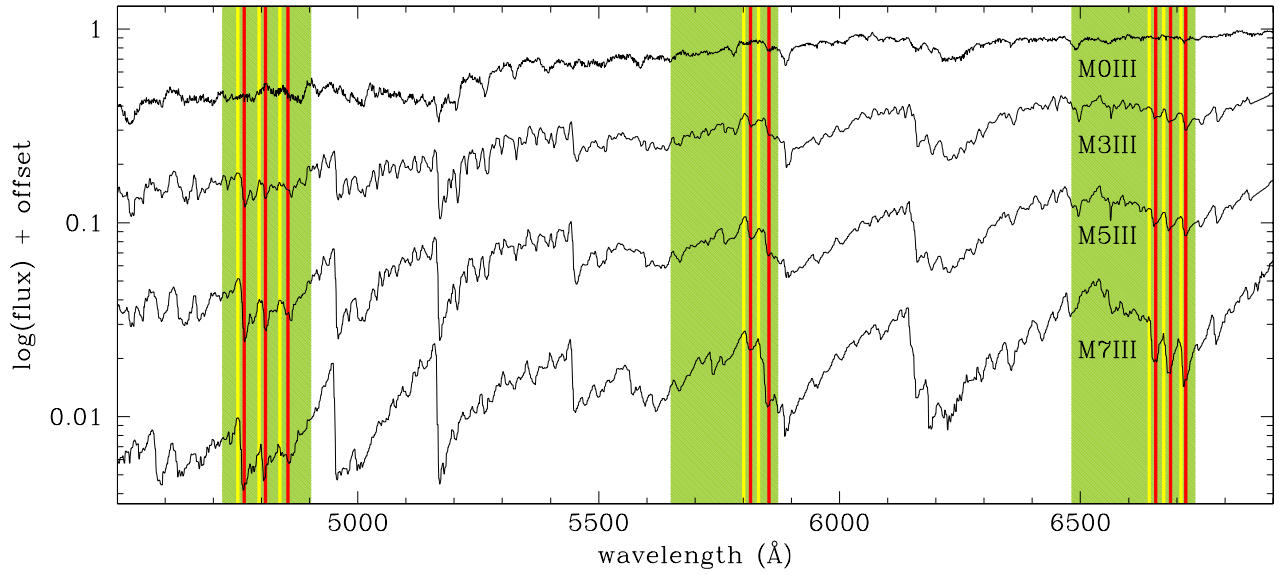

Figure 3. Definition of TiO classification indexes. The shadowed regions show the wavelength ranges covered by the GALAH blue, green, and red channels. The yellow and red bands mark the A–B and C–D wavelength intervals, respectively, used to compute the *b*, *g*, and *r* ratios according to equation (2) and Table 3. In background some Asiago 1.22-m spectra illustrating the progress in strength of TiO bands moving along the sequence of M giants (pay attention to the log-scale of the ordinates).

Table 3. Short and long wavelength limits (Å) of the intervals used to compute the ratios in equation (2) and illustrated in Fig. 3.

Ratio	λ_A	λ_B	λ_C	λ_D
b1	4751	4756	4765	4770
b2	4798	4803	4807	4812
b3	4835	4840	4850	4855
g1	5801	5806	5812	5817
g2	5829	5834	5850	5855
r1	6641	6646	6653	6658
r2	6670	6675	6684	6689
r3	6706	6711	6716	6721

GALAH DR3 as rv_guess (Buder et al. 2021). Absence of absorption by TiO returns a value around 1.0 for any of the ratios, and a progressively larger value with increasing M spectral subtype (M0 → M10). Finally, we have combined the eight ratios into a single one computed as

$$f = \frac{[0.3(\langle b\rangle - 1) + 1] + \langle g\rangle + \langle r\rangle}{3}, \quad (3)$$

where $\langle b\rangle$ stands for the arithmetic average of b1, b2, and b3, and similarly for the rest. The $\langle b\rangle$ average ratio stretches over 3.3× the range of the other two, so we have consequently reduced its impact to make it equal to the others. This is justified by the lower S/N of the spectra recorded in the blue channel compared to green and red ones.

The depth of the TiO bands has been already used in the past to classify the M giants of SySt, e.g. by Kenyon & Fernandez-Castro (1987), that used to this aim the bands at 6180 and 7100 Å (both outside the GALAH wavelength range). In these studies, equivalent widths of TiO bands were measured over their entire wavelength span (hundreds of Å), too wide compared to the breadth of GALAH channels, and therefore inapplicable in this paper (and for that matter also to more conventional, high-resolution echelle spectra covering too small a wavelength interval over a single order).

The way our ratios are defined, makes them insensitive to spectral fluxing, continuum normalization, or reddening. The relation between *f*-ratio and reddening-corrected $(J - K_s)_o$ index for the initial sample of 29 514 GALAH stars is illustrated in Fig. 4. The latter shows a number of highly reddened stars contaminating the sample. To filter them out we took all stars laying above the knee at $f > 1.02$, and considered the remaining 15 824 objects (the 15k-sample for short) as representing the true M-giants present among the 600 255 stars observed by GALAH at the time of writing of this paper. The $(J - K_s)_o$ colour index has been calculated from 2MASS photometry and the full extinction as given by Schlafly & Finkbeiner (2011). The choice of taking the full value of the tabulated extinction is justified by considering the great distance to our targets (typically several kpc, beyond which *Gaia* DR2 or EDR3 parallaxes become inaccurate) and their large galactic latitude, which makes their sightlines exit the Galactic dust slab well before reaching them.

4.4 Hα in emission

The next step has been searching the 15k-sample of true M giants for those showing Hα (and Hβ) in emission. All the SySt considered in this paper show Hα emission directly on the recorded spectrum, well before any reference spectrum is subtracted (cf. Fig. 5). To properly reconstruct the profile of the emission line, it is however necessary to subtract the underlying spectrum of the M giant. To define the latter, we grouped the M giants by similar strength of TiO bands, and computed the median of the continuum normalized spectra within each bin. The spectral progression of the templates around Hα and Hβ is compared in Fig. A1 of Appendix A.

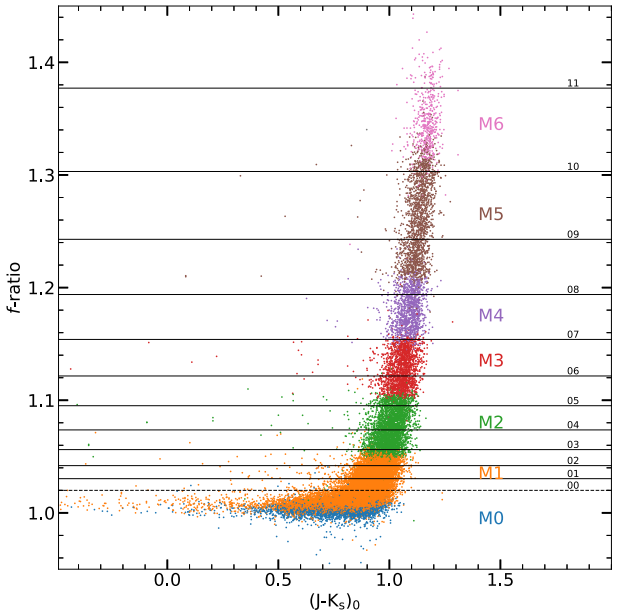

Figure 4. Relation between the reddening-corrected 2MASS $(J - K_s)_o$ colour index and the combined *f*-ratio from equation (2) for the 29 514 GALAH stars in our initial sample. The coloured bands mark the approximate location of the MKK spectral subtypes (M0III, M1III, ...). The finer, log-scale subdivision according to Table 4 is given by the horizontal lines and it is marked by the numbers to the right (00, 01, ...).

We initially selected to define a unique template for each of the 11 M0III↔M10III spectral subtypes of the original MKK classification scheme (Morgan, Keenan & Kellman 1943; Morgan & Keenan 1973), but quickly realized that at the high S/N and high resolution of GALAH spectra, any such subtype spans too wide a range in stellar properties for a single template to adequately represent them all. Similarly, equally spaced bins in *f*-ratio are not satisfactory, as they oversample at low *f* values. Therefore, we decided for a logarithmic progression, with Table 4 listing the 13 final bins, their interval in terms of *f*-ratio, and the number of true M giants contained in that bin. Their subdivision of the giant branch is shown in Fig. 4 (horizontal lines). The median of all the spectra in a given bin defines the template spectrum for that bin. Taking the median value eliminates any disturbance from cosmic ray hits or rare presence of emission components. In addition, the median computed over thousands of individual spectra has an extremely high S/N and it is completely insensitive to chemical peculiarities of individual stars.

The template is finally subtracted from continuum-normalized spectra of the true M giants within the given bin, and the residuals inspected for emission in Hα. In this first paper, we limit ourselves to consider only the M giants showing an Hα emission profile rising above a threshold of 0.5 on the subtracted spectrum. This returned a total of 223 stars.

4.5 Visual inspection

The spectra of these 223 stars were visually inspected for inconsistencies that could cause the Hα to appear in emission on the subtracted spectrum.

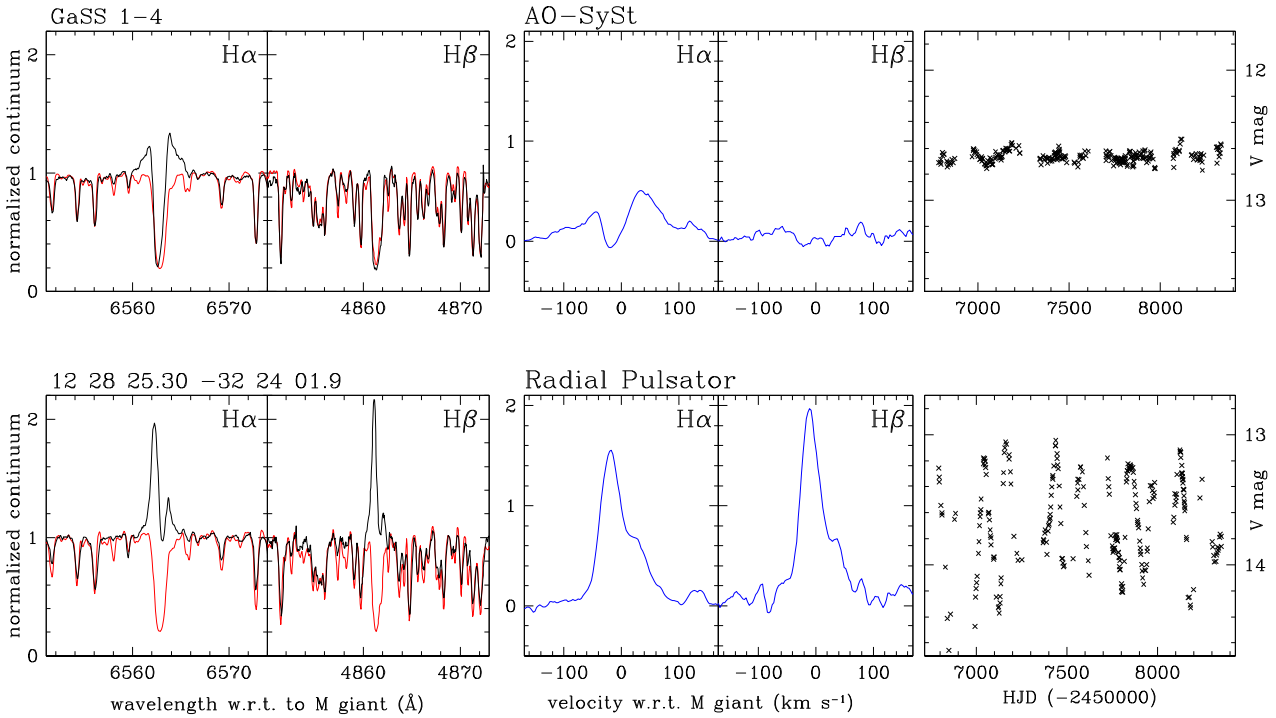

Figure 5. Left-hand panels: example Hα and Hβ profiles (in black) from RV-zeroed GALAH spectra of an SySt (top row) and of a radial pulsator (bottom row), compared with those of the template for the same *f*-ratio bin (in red, cf. Table 4). Centre panels: the result of subtracting the (red) template spectrum from the (black) object spectrum from the left-hand panels. Right-hand panel: the corresponding *V*-filter light curve from ASAS-SN sky patrol data.

Table 4. Intervals in combined *f*-ratio (equation 3) defining the template bins for the selected 15 824 M giants. $(J-K_s)_o$ is the median value within the bin for the reddening-corrected $(J-K_s)$ from 2MASS. The last column lists the number of stars in each bin. The template spectra for each bin are plotted in Fig. A1.

Bin	Left limit	Right limit	$(J-K_s)_o$	No. of stars
00	1.0200	1.0303	0.904	3419
01	1.0304	1.0419	0.935	2309
02	1.0420	1.0561	0.968	1732
03	1.0562	1.0736	0.994	1424
04	1.0737	1.0950	1.017	1282
05	1.0951	1.1214	1.043	1200
06	1.1215	1.1539	1.065	1048
07	1.1540	1.1938	1.088	919
08	1.1939	1.2428	1.110	917
09	1.2429	1.3030	1.141	849
10	1.3031	1.3770	1.166	638
11	1.3771	1.4679	1.182	77
12	1.4680	3.6559	1.139	10

Some spectra were found to suffer from a mismatch in radial velocity with the template. In these few cases, the radial velocity rv_guess from GALAH DR3, which is used to shift spectra in all four GALAH channels to rest frame, provides correct results for the blue, green, and infrared, but not for the red channel, resulting in an excess flux around Hα in the difference spectrum, which is obviously spurious.

Another more frequent cause for false positives was the presence of an emission component probably originating from the sky background that has not been fully cancelled out by the sky-subtraction procedure. This may happen e.g. when the target star is located in a region of the sky affected by diffuse background emission, like emission nebulae and H II regions. Such cases are easy to recognize because the Hα and Hβ emission lines are (a) typically quite sharp, single-component, and symmetric; (b) frequently accompanied by [N II] 6548, 6584 nebular emission lines (which do not form in the high-density environment of an accretion disc); and (c) usually displaced in velocity with respect to the M-giant spectrum by an amount larger than expected from orbital motion in a symbiotic binary. In multifibre spectroscopic surveys like GALAH, only a limited number of fibres are assigned to record the sky background. They are distributed over the field of view away from the position of known stars. This is perfectly fine for a great fraction of the sky away from the Galactic plane. There are however, here and there, regions of the sky affected by background emission due to diffuse nebulosity. The intensity of such emission may vary appreciably over limited angular distances, and the same may be the case for the internal nebular gas dynamics and therefore the resulting wavelength for Hα and Hβ emitted lines. Any sparse mapping realized by a limited number of sky fibres of such a complex 2D pattern can naturally result in non-null residuals of the sky-background subtraction, in addition to other caveats of sky subtraction as explained in Kos et al. (2017).

There was also a group of stars that presented an equal excess emission in Hα and Hβ on the subtracted spectrum, always with the same characteristic profile (steep red and blue ends, flat and rounded top), as if originating from a hydrogen deficiency compared with the template spectrum. These stars were also disregarded in the current selection process.

After a further few rejections for miscellaneous reasons, we were left with a final selection of 83 M giants showing genuine emission in Hα with an intensity in excess of 0.5 in the subtracted spectrum (the 83-sample hereafter). Stars with an emission in Hα weaker than 0.5, which are inherently more subtle to treat, will be investigated in a follow-up paper.

4.6 Filtering out the radial pulsators

Not all the objects in the 83-sample are necessarily valid candidate *acc*-SySt. The main false positives are expected to be the (large-amplitude) radial pulsators (e.g. Miras or SRa variables), which may give origin to emission lines (primarily hydrogen Balmer) deep in their atmosphere where shocks form.

It is of course not precluded that a Mira pairs with a compact companion to form an SySt. For example V407 Cyg, prior to its 2010 nova outburst, was primarily studied as a Mira suffering from possible dust-obscuration episodes (Munari, Margoni & Stagni 1990; Kolotilov et al. 1998) with little (or none) spectroscopic evidences for binarity (Hinkle et al. 2013). *Mira* itself (*o* Cet) is a well known *acc*-SySt: *Hubble* in the ultraviolet and *Chandra* at X-rays have spatially resolved its WD companion, the accretion disc, and the stream fuelling it (Karovska 2006). Such a plethora of multiwavelength information is however not available for a typical GALAH anonymous star, and to be on the safe side we decided – at the initial stage of our project represented by this paper – to filter out the radial pulsators. Such a pruning is based on converging photometric (light curve) and spectroscopic (Hβ/Hα emission ratio) criteria, described below.

We decided not to rely on existing compilations of known variables (as for example collected in the VSX[1] catalogue), because the adopted classification criteria (as well as amplitude and periods) are sometimes in disagreement among themselves and also in conflict with the naming conventions listed in the IAU General Catalog of Variable Stars.[2] We preferred instead to analyse in a homogeneous way their photometric behaviour ourselves. To this aim we downloaded the available photometry for the 83-sample from the ASAS-SN sky patrol survey (Shappee et al. 2014; Kochanek et al. 2017) and examine ourselves the resulting light curves, which are usually composed of hundreds of individual observations in either g or V bands distributed over a time interval of a few years, and therefore adequate to reveal the presence of long and stable periodicities related to radial pulsation. ASAS-SN sky patrol covers the whole accessible sky on both hemispheres every night, and the $12 < V_{JK} < 14$ mag range of our targets is ideally placed at the centre of ASAS-SN dynamic range, away from the bright saturation limit or the noisy detection threshold.

The light curve of a Mira shows regular, long period (from several months to longer than a year), and large amplitude (from a few to >10 mag) sinusoid-like variations (e.g. Hoffmeister et al. 1985; Sterken & Jaschek 2005). The large-scale radial pulsation is betrayed by the in-phase variation of the radial velocity of the absorption spectrum, with amplitudes of the order of ∼10–15 km s^{-1} (Joy 1926; Hoffmeister et al. 1985). Our pathfinder SU Lyn shows a significant variability (0.6 mag amplitude in V), but it lacks the larger amplitude and the regular beat of a Mira. As clearly illustrated by Fig. 2, the M giant in SU Lyn does not radially pulsate in any significant way (the absorption lines are stable in radial velocity to better than 2 km s^{-1}), and therefore no shocks form in the atmosphere which could lead to emission in the Balmer lines. Armed with these considerations, and to stay on the cautionary side, we selected to flag (in the 83-sample) all the stars showing ASAS-SN light curves with an amplitude in excess of 0.7 mag and a stable and clean sinusoid-like shape (cf. Fig. 5). Such a light curve could however arise also from orbital motion, for example from ellipsoidal distortion when the cool giant fills its Roche lobe and/or its side facing the companion is irradiated and heated up (e.g. as in the accreting-only and recurrent nova T CrB; Munari, Dallaporta & Cherini 2016). A spectroscopic confirmation of the radially pulsating nature is therefore required, and this needs to be accommodated within the single-epoch spectra (i.e. no revisit) of the GALAH survey.

In radially pulsating cool giants, outward moving material collides against the gas lifted during the previous cycle and now falling back inward. The resulting shock is hot enough to excite emission in the Balmer lines of hydrogen. Such shocks develop deep within the atmosphere, interior to the outer layers where absorption by TiO molecules occurs. The absorption by TiO begins around 4200 Å and, by superposition of successive bands (they all decline toward the red), their combined absorption grows rapidly stronger with wavelength (Fluks et al. 1994). As a consequence, emission in Hδ (4101 Å) and higher Balmer terms exits the atmosphere unscathed by TiO, and their flux declines with increasing upper n-quantum number in the usual way. What happens to the red of Hδ? Going from Hγ to Hβ and then Hα, we move into deeper and deeper overlapping absorption by TiO bands and the *observed* emission in the line becomes more and more absorbed. Saying it a different way (Joy 1926; Yamashita & Nariai 1977), in pulsating M giants the strongest line is Hδ and the intensity of successive Balmer emission lines declines either going to the blue or to the red (see exemplary spectrum for LQ Sgr presented by Bragaglia et al. 1995). In most astrophysical environments, the observed emission in Hα is invariably stronger than in Hβ, while in Miras the opposite is the case (Merrill 1940), because of the TiO absorption in the outer atmospheric layers. This offers a clear distinction between the emission originating from the accretion disc in an *acc*-SySt [in terms of equivalent widths: EW(Hα) > EW(Hβ)] from that expected to come from the internal shock regions of an M-type radial pulsator [EW(Hα) ≤ EW(Hβ)].

GALAH high-resolution spectra show a further distinction between the two types. In *acc*-SySt systems, a sharp absorption component appears superimposed to the broad Hα emission profile, generally *blueshifted* by about 5–25 km s^{-1} and half as wide as the photospheric Hα absorption line (FWHM ∼ 15–25 km s^{-1} as opposed to 45–50 km s^{-1}), which – by analogy with the prototype SU Lyn or other *acc*-SySt discussed by Jorissen et al. (2012) and Gorlova, Van Winckel & Jorissen (2012) – is believed to originate in the gentle wind blowing off the accretion disc or in the outflowing wind of the RG that engulfs the whole binary system. In the GALAH spectra of radially pulsating stars, the narrow absorption superimposed to the emission is instead generally *redshifted* as if coming from cooler material falling back toward the star after being lifted higher up during the previous pulsation cycle.

These photometric and spectroscopic criteria to separate candidate *acc*-SySt and radially pulsating objects in the 83-sample are illustrated in Fig. 5, which presents line profiles and light curves well typical of the rest of the sample: high amplitude and regular beating for the light curve of a pulsator, with strong Hβ and redshifted narrow absorption; lower amplitude and less regular light curve for the *acc*-SySt, an Hβ much weaker than Hα and blueshifted narrow absorption. By applying these criteria, 30 radial pulsators are pruned from the 83-sample, reducing the candidate *acc*-SySt to 53. Hereafter, we refer to them as the 53-sample.

4.7 Avoiding contamination by T Tau stars

T Tau pre-main sequence variables have been considered as possible contaminants in previous large-scale searches for new SySt, especially those based on IPHAS r, i, Hα photometric survey (Corradi

[1] http://vizier.u-strasbg.fr/viz-bin/VizieR-3?-source=B/vsx/
[2] http://www.sai.msu.su/gcvs/

et al. 2008, 2010, 2011; Rodríguez-Flores et al. 2014). T Tau stars are distributed over a wide range of spectral types, from mid-F down to the coolest M-types, may be heavily reddened, and present emission lines originating from the circumstellar disc, the spotted surface and the magnetic-confined accretion columns on the magnetic poles (Hartmann, Herczeg & Calvet 2016). T Tau stars can therefore mimic the red $r - i$ colour of SySt and similarly stand out in the $r -$ Hα photometric index. T Tau stars are less prone to be confused with SySt if spectra are available, especially if they cover a broad wavelength range (as those we have collected in Section 5.1 below for our program stars): the spectra of T Tau stars show the absorption features typical of a main-sequence star, not of a giant, and the emission lines are rather different both in assortment (Ca II H&K doublet usually quite strong in T Tau stars, while generally absent in SySt) and in their profile (in T Tau stars sporting narrow jet components superimposed on a broad pedestal coming from the rotating disc; Giannini et al. 2019). In addition, Li I 6707 Å is in strong absorption in most T Tau stars, whereas it is generally absent in SySt.

In the context of our search for new SySt, T Tau stars are however of no concern, because they cannot be confused with cool giants when the segregation is carried out on *Gaia* parallaxes, as we did. Of relevance to this paper are only T Tau stars with an M spectral type (M-TTau for short). The intrinsically brightest among M-TTau are those with the earliest M-types, M0V and M1V. The absolute magnitude of M0V and M1V stars are M(V) = 8.8 and 10.8, respectively, while that of M0III and M1III giants is M(V) = −0.5 (Drilling & Landolt 2000; Sowell et al. 2007). The inflated photospheric radius (not yet settled on the main sequence) and the contribution by the circumstellar disc may raise the intrinsic brightness of M-TTau above that of single and isolated dwarfs of the same spectral type, but they will never fill the huge ≥10 mag gap between main-sequence and giant stars of the M spectral type.

In confirmation of this, we have retrieved the *Gaia* EDR3 parallaxes for the brightest known M-TTau (selected from the compilation by Yang et al. 2012) and computed their M(V) magnitudes by adopting the photometric calibration of the *Gaia* Consortium (Evans et al. 2018). The absolute M(V) magnitudes of M-TTau turned out to be all fainter than +6.5, confirming that in no way an M-TTau may have slipped into our sample of M giants segregated on the base of *Gaia* parallaxes (see also Section 5.9 below). As a further check, we took the compilation of T Tau stars listed in SIMBAD and VSX, and checked if any matched the M-giants of the initial 15k-sample, and verified that none did.

4.8 Comparison with VV Cep binaries

There are binaries that host cool supergiants and massive hot companions, of which a comprehensive catalogue of 108 Galactic objects has been recently published by Pantaleoni González et al. (2020). The 23 entries from this catalogue with an M spectral type for the cool giant are summarized in Table A5, where we add distances, absolute magnitudes, and height above the galactic plane as derived from *Gaia* EDR3 parallaxes and the 2MASS JHK_s survey. Such objects are usually named VV Cep stars, from the best known member of the group, and while not related to SySt are sometimes discussed in parallel. We have not included δ Sge in Table A5 as it seems more related to other types of objects like TX CVn or 17 Lep than to VV Cep stars (Ginestet & Carquillat 2002; Pugh et al. 2015).

The VV Cep stars all have very massive components on very wide orbits. The orbital solution for VV Cep itself gives an orbital period of 20.3 yr, an orbital separation of 24.8 au, and individual masses of 18.2 and 18.6 $M_\odot$ for the M supergiant and the B-type companion, respectively (Bennett et al. 2004). Of interest to us is the fact that in VV Cep stars, the Balmer lines, and Hα in particular, may be seen in emission, with a line profile reminiscent of that seen in Be stars (in which the emission comes from an equatorial ring-like shell formed by material leaving the hot star that is rotating close to break-up velocity). While the hot component in VV Cep dominates the spectrum in the blue, that of the M supergiant takes over at red wavelength. With an Hα in emission superimposed, it could be questioned whether any of our candidate *acc*-SySt may indeed belong to VV Cep stars. This, however, can be safely excluded on two independent grounds.

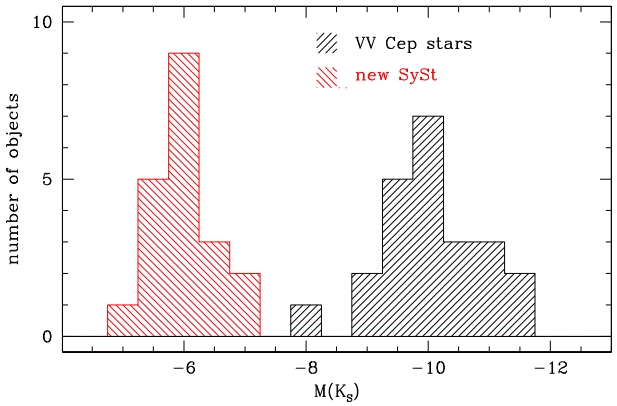

Figure 6. Distribution in $M(K_s)$ for the candidate *acc*-SySt compared to that of VV Cep stars.

First, M supergiants of VV Cep stars are intrinsically much brighter than the M giants characterizing our candidate *acc*-SySt. The two are compared in Fig. 6, with values taken from Table A2 for our program stars, and Table A5 for the VV Cep stars. The median absolute $M(K_s)$ magnitude for VV Cep stars is −10.0, that of the program stars only −5.9. Secondly, their distance over the Galactic plane is radically different. Being very massive and therefore very young, VV Cep are examples of extreme Population I (Pop I) stars, laying close to the Galactic plane, while our candidate *acc*-SySt belong to a much older population as discussed in Section 5.9 below. Their distributions in terms of height above the Galactic plane are compared in Fig. 7, with input data taken from Tables A2 and A5: the median value is just 50 pc for the VV Cep stars and a much larger 1.8 kpc for the new candidate *acc*-SySt.

5 THE FINALLY SELECTED 33 NEW CANDIDATE SYMBIOTIC STARS AND THEIR PROPERTIES

We have finally subjected the 53-sample to a series of follow-up observations from the ground and the space to pick-up the most promising objects. Based on the ensuing results, our final list of 33 proposed *acc*-SySt candidates is presented in Table 5 (where GaSS in their names stands for GALAH symbiotic star); they are divided in two groups, a primary and a supplementary sample. The division is based primarily on available follow-up observations (less for the supplementary sample) and amplitude of photometric variability (larger for the supplementary sample). A plot similar to Fig. 5, presenting the Hα, Hβ profiles and the light curve, is provided in Appendix A for all 33 objects (Figs A2–A8).

Gaia EDR3 lists parallaxes (π) for all the 33 program stars, and they are reported with their uncertainties ($\sigma(\pi)$) in Table A2. In

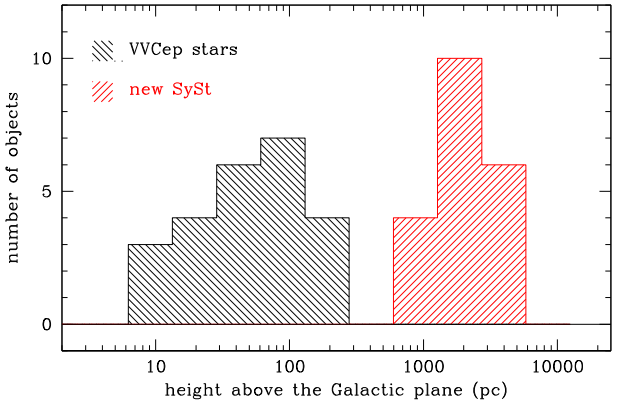

Figure 7. Distribution in height over the plane of the Galaxy for the candidate *acc*-SySt and for VV Cep stars.

Table 5, we provide distances, by direct inversion of parallax, for only 20 of them, namely those satisfying the condition $\sigma(\pi)/\pi < 0.2$. This is the limit recommended by the *Gaia* team (Bailer-Jones 2015; Luri et al. 2018). The parallaxes of the remaining program stars are too small in comparison to their formal uncertainties and even generally smaller than the *mean* 0.019 mas bias affecting *Gaia* EDR3 parallaxes as a whole (Lindegren et al. 2021). Such bias depends in a non-trivial way on (at least) the magnitude, colour, and ecliptic latitude of the sources, with no firm correcting recipe available yet. Improved parallaxes in future *Gaia* data releases will allow to derive valuable distances to (most of) the remaining program stars.

We now describe the follow-up observations that have led us to the compilation of Table 5. A complete description of such extensive follow-up observations is far beyond the scope and breadth of this paper. Full details, augmented by the results of further follow-up observations currently in progress, will be discussed elsewhere.

5.1 Near-UV upturn

The presence of a bright accretion disc is betrayed by an emission excess at wavelengths shorter than ∼4000 Å, as illustrated for SU Lyn in Fig. 1. With the long-slit B&C spectrograph attached to the Asiago 1.22-m telescope, highly efficient down to the atmospheric cut-off (∼3200 Å at the 1000 m above sea level location), we have observed most of the objects in the 53-sample located north of −29° in declination (Table A1 in Appendix A provides a logbook of these observations). At the Asiago +46° latitude, this corresponds to a

Table 5. The candidate accreting-only symbiotic stars (*acc*-SySt) discovered in this paper based on spectra from the GALAH survey. $E(B-V)$ is from Schlafly & Finkbeiner (2011). The spectral type is on the MKK scale and f is the template label bin^{-1} (see Table 4 and Fig. A1). V is from the APASS catalogue. ΔV is our estimate of the amplitude of variability on ASAS-SN sky patrol data (Section 4.6). 'P orb' lists possible orbital periods (for 2×P alternative see Section 5.7). 'dist' is the distance (in kpc) derived from *Gaia* EDR3 parallax for objects satisfying the conditions $\sigma(\pi)/\pi < 0.2$ (cf. Section 5). $RV_\odot$ is from GALAH DR3 (rv_guess). Objects marked 'var' in the 'Asiago RV' column show a variability in radial velocity (cf. Table 6 and Section 5.2). The column '*Swift*' marks with 'X' the objects counterpart to X-ray sources in the 2SXPS catalogue (Evans et al. 2020), and with 'UV' those found emitting in the ultraviolet UVM2 band in our *Swift* follow-up observations (cf. Table 8 and Section 5.5). U_{exc} lists the presence of emission excess at U-band wavelengths: 'pht' from photometric UBV observations (Massey 2002), 'spc' from our spectra (Section 5.1). An 'F' in the 'Flk' column marks the presence of flickering (Section 5.4). The final two columns provide the velocity (with respect to M giant) and the FWHM of the narrow absorption superimposed to the broader Hα emission (Section 4.6).

Name	RA (J2000)	Dec.	Galactic Long	Galactic Lat	$E(B-V)$ (mag)	Spectral type f		V (mag)	ΔV (mag)	P orb (d)	Dist (kpc)	$RV_\odot$ (km s^{-1})	Asiago RV	*Swift*	U_{exc}	Flk	Hα (wind) RV (km s^{-1})	Hα (wind) Width (km s^{-1})
Main sample																		
GaSS 1–1	04 52 35.65	−70 40 42.7	282.35	−35.19	0.23	M1	03	12.950	0.23			+264.28			pht	F	−21.9	19
GaSS 1–2	05 04 09.82	−70 12 17.6	281.44	−34.40	0.33	M2	04	12.725	0.43			+234.29			pht		−23.9	19
GaSS 1–3	06 22 21.17	−59 39 26.9	268.79	−26.77	0.04	M0	00	12.521	<0.05		8.2	+282.99		X			−2.1	24
GaSS 1–4	11 12 15.48	−32 07 19.3	279.61	26.22	0.10	M1	00	12.638	0.11	235	8.2	+141.44					−11.3	19
GaSS 1–5	11 22 10.22	−29 21 12.5	280.56	29.61	0.05	M2	02	13.469	0.33	311	10.1	+35.75					−7.4	21
GaSS 1–6	14 46 07.03	−37 53 38.7	326.64	19.64	0.06	M3	05	12.096	0.30	401	5.4	+33.35					−12.3	17
GaSS 1–7	14 57 25.03	−24 48 24.8	336.07	29.84	0.13	M1	02	13.497	0.35			−235.14			spc		−9.3	24
GaSS 1–8	15 23 54.79	−29 43 14.9	338.39	22.46	0.45	M1	00	13.637	0.16	224	7.4	−143.10					−17.1	24
GaSS 1–9	16 55 28.75	−03 09 45.0	15.77	23.92	0.27	M1	02	13.299	0.28			−131.58	var:		spc	F	−7.2	11
GaSS 1–10	17 07 24.58	−58 29 21.7	331.48	−10.65	0.15	M1	02	12.568	0.21			−100.12				F	−4.5	22
GaSS 1–11	17 50 33.15	−47 22 40.4	344.53	−10.21	0.14	M3	06	12.182	0.09	453	6.6	+58.19		UV		F	−22.0	27
GaSS 1–12	18 57 06.98	−22 16 56.1	13.46	−11.15	0.22	M4	07	11.761	0.85		4.6	+51.88	var	UV	spc:		−11.4	14
GaSS 1–13	19 27 26.71	−07 21 02.4	30.41	−11.33	0.32	M1	01	13.681	0.20	328		−373.27	var		spc	F	−13.5	19
GaSS 1–14	20 37 56.95	+00 27 53.7	46.25	−23.28	0.06	M2	05	13.019	0.52	381	8.6	−247.79	var:		spc:	F	−6.4	21
GaSS 1–15	21 10 01.51	+04 02 35.4	54.32	−28.20	0.08	M2	04	12.054	0.09	229	2.9	+49.94	var	X		F	−8.1	22
Supplementary sample																		
GaSS 1–16	05 31 40.32	−66 42 40.2	276.75	−32.60	0.10	M1	02	13.415	0.09			+302.18					−17.7	25
GaSS 1–17	07 06 36.52	−58 41 12.7	269.18	−21.04	0.09	M1	00	11.439	0.24		5.4	+119.77				F	−2.4	24
GaSS 1–18	12 08 19.12	−38 16 37.7	293.70	23.82	0.06	M1	02	13.068	0.33	338	8.7	+164.65					−16.9	26
GaSS 1–19	14 37 11.36	−78 36 33.9	308.20	−16.84	0.11	M1	01	13.422	0.15			+247.20					−7.1	26
GaSS 1–20	16 00 54.84	−16 28 32.5	355.07	26.66	0.25	M1	00	12.116	0.59			+44.76	var				−10.2	17
GaSS 1–21	16 12 42.83	−20 37 23.6	353.80	21.79	0.29	M4	06	13.757	0.70			−182.82			spc	F	−0.3	18
GaSS 1–22	16 14 17.67	−25 09 20.4	350.53	18.44	0.27	M1	00	11.907	0.32		5.8	−242.25					−8.2	31
GaSS 1–23	17 11 24.39	−12 14 19.9	9.87	15.73	0.44	M4	07	13.321	0.68		4.8	−167.23	var:		spc		−4.6	22
GaSS 1–24	17 17 44.36	−61 38 05.3	329.57	−13.48	0.09	M6	11	13.000	0.75			+171.01					2.5	19
GaSS 1–25	17 18 59.65	−17 47 37.5	6.13	11.14	0.23	M0	00	11.561	0.17		4.3	−81.87				F	−5.4	29
GaSS 1–26	18 07 34.98	−42 47 42.3	350.08	−10.60	0.10	M3	05	13.508	0.32			−1.74				F	−10.3	25
GaSS 1–27	18 32 00.28	−46 00 36.9	348.98	−16.00	0.06	M1	00	11.113	0.29	400	4.7	−42.51					−5.5	14
GaSS 1–28	19 01 02.81	−27 19 19.0	9.13	−14.03	0.20	M2	04	13.265	0.63	496	7.5	−106.75			spc		−4.8	21
GaSS 1–29	19 08 07.66	−47 44 06.7	349.44	−22.40	0.07	M2	04	14.585	0.33		7.0	+149.28					−4.3	23
GaSS 1–30	19 11 35.88	−35 10 50.8	2.41	−19.06	0.07	M0	00	11.120	0.21		5.6	−48.38					−6.1	20
GaSS 1–31	19 17 16.24	−22 02 53.2	15.65	−15.30	0.10	M1	02	11.505	0.54		4.3	+70.13	var				−2.6	14
GaSS 1–32	19 18 43.66	−29 15 29.8	8.82	−18.37	0.11	M1	01	11.444	0.21		5.3	−95.48					−10.1	23
GaSS 1–33	22 10 02.95	−06 18 07.2	53.99	−46.41	0.05	M1	02	15.434	0.41	682		−205.14			spc	F	−11.7	15

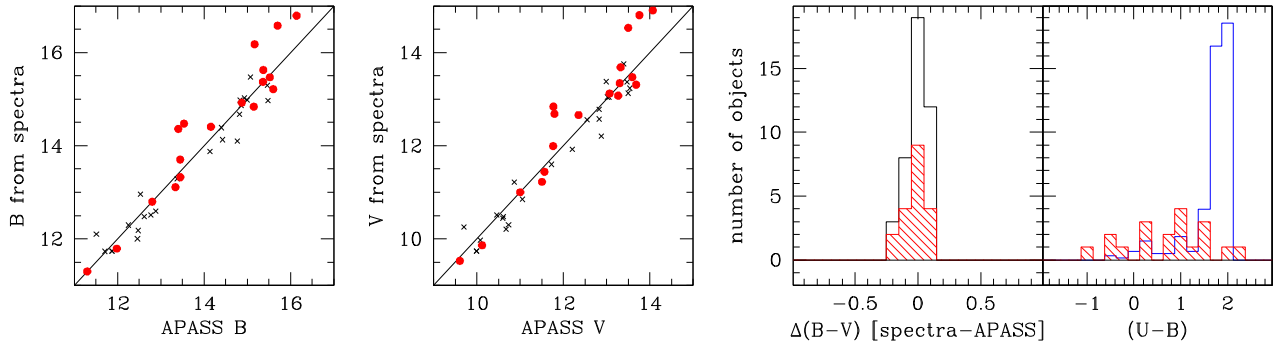

Figure 8. Left-hand panels: comparison between the average B and V magnitudes from APASS all-sky survey, and the corresponding values derived from Asiago 1.22-m flux-calibrated spectra for a subset of the 53-sample. The solid lines mark the 1:1 relation. Right-hand panels: histogram distribution of differences between Asiago and APASS derived $B - V$ colours, and distribution of $U - B$ colours derived from Asiago spectra. The line in blue shows the distribution of a hundred M giants from the solar neighbourhood as measured by Fluks et al. (1994). Red colour refers to SySt discovered in this paper, black to other GALAH M giants observed along with them (including also some radial pulsators).

horizon distance of 15°. The near-UV faintness of the program stars and the high atmospheric extinction at such large airmasses conspired to make such observations quite demanding to execute. A consistent number of spectrophotometric standards were observed in parallel each night at similarly large air-masses. Suitably high S/N at 3400–3600 Å was obtained for only a fraction of the attempted objects, and sometimes only after adding spectra collected at different revisits. The objects marked 'spc' in the U_{exc} column of Table 5 are those showing excess emission on spectra over the range $3400 \leq \lambda \leq 4000$ Å. There are clear hints for some of them that the amount of near-UV excess changes when spectra taken at different epochs are compared.

A quick summary of the photometric data extracted from spectra is presented in Fig. 8. The B and V data lie well on a 1:1 relation with APASS mean data, the scatter being at least in part related to the variability all objects display (as per column ΔV of Table 5). The difference in the $B - V$ colour (indicative of the accuracy of the *slope* of fluxed spectra) between APASS and spectra appears well distributed around 0.0 with a FWHM = 0.18 mag. The most interesting panel of Fig. 8 is the last one, showing the distribution of $U - B$ measured on spectra compared with the distribution of $U - B$ for a hundred M giants of the solar neighbourhood (suffering from negligible reddening) as measured by Fluks et al. (1994). It is clear how, on average, the $U - B$ colour of candidate *acc*-SySt is bluer that those of (supposedly) single, normal M giants, supporting the notion that for a sizeable fraction of them we have actually observed an excess in U as coming from the companion and the accretion disc. The candidate *acc*-SySt scoring an 'spc' in Table 5 are those with an $U - B$ bluer than +0.4 in Fig. 8, and 'spc:' for those between +0.4 and +0.8.

5.2 Radial velocity variability

Armed with evidence from Fig. 2 that the low amplitude, irregular variability affecting the M giant in SU Lyn does not reverberate into changes in radial velocity, we observed some of the 53-sample north of −25° in declination with the echelle spectrograph mounted on the Asiago 1.82-m telescope. The results are summarized in Table 6. As a check, some normal stars from the initial 15k-sample and a few radial pulsators from the 223-sample were also observed, with results presented in Table A3. In both tables, the quoted error for Asiago RVs is the *internal* error, i.e. that derived by comparing the RV obtained from different echelle orders by cross-correlation with spectra of IAU radial velocity standards of M spectral type. We selected to limit the measurement to 5 of the 32 orders covered by the Asiago echelle spectrograph, favouring those at redder wavelengths (where S/N is higher), and avoiding the orders with TiO band heads or telluric atmospheric absorptions that would affect the cross-correlation results. A comparison of Asiago RVs with the GALAH rv_guess and *Gaia* DR2 values in Table A3 for the GALAH M giants subsample returns a negligible offset and an rms ∼1.5 km s^{-1}. The latter could in part be accounted by variability of epoch radial velocities intrinsic to the sources.

From the data in Table 6, a clear RV variability has been observed for five objects, and borderline for an additional three. They are marked with 'var' in column 'Asiago RV' of Table 5. We favour an interpretation in terms of orbital motion for this RV variability.

5.3 Emission line variability

The candidate *acc*-SySt of this paper show a clear variability of the intensity and profile of Hα emission line on spectra collected with the Asiago 1.22-m and 1.82-m telescopes. An example is presented in Fig. 9. GaSS 1–31 showed a clear emission in Hα on the GALAH spectrum recorded on 2017 April 9, a weaker one on the Asiago spectrum for 2020 October 3, and no emission on 2020 July 5 (see also Section 5.5 below) and on 2020 October 17 (this last spectrum has been obtained at a lower resolving power – 12 000 because of 2 × 2 CCD binning – with an echelle spectrograph mounted on the Varese 84-cm telescope). The Hα of GaSS 1–12 has been always observed in emission on all three visits with the Asiago 1.82-m, with a varying degree of intensity and velocity of the emission relative to the M giant. Most interestingly, the last Asiago spectrum for 2020 October 3 shows the appearance of a second narrow absorption, blueshifted with respect to the primary one, an event reminiscent of what happened to SU Lyn in 2017 (cf. Fig. 2).

5.4 Optical flickering

The accretion in binaries is characterized by chaotic processes (e.g. density fluctuations in the accretion flow from the donor to the accreting star) that develop on time-scales (seconds, minutes, or a few hours) much shorter than those of other sources of variability (orbital motion, pulsation, rotation, outbursts, etc.). The possibility to detect flickering on optical photometric data depends primarily on its contrast with the steady sources in the system: the fainter the

Table 6. Heliocentric radial velocity of candidate GALAH SySt measured with the Asiago 1.82-m telescope+echelle spectrograph compared with the corresponding values of rv_guess listed in GALAH DR3. The mean radial velocity listed in *Gaia* DR2 is also given, with its formal error and the number of epoch transits over which it has been computed.

	Asiago 1.82-m echelle			GALAH DR3			*Gaia* DR2		
	UT middle	$RV_\odot$ (km s^{-1})	Err (km s^{-1})	UT middle	$RV_\odot$ (km s^{-1})	Err (km s^{-1})	$\langle RA_\odot \rangle$ (km s^{-1})	Err (km s^{-1})	N
GaSS 1–9	2020-07-04 22:30	− 130.06	0.51	2017-04-09 17:56	− 131.58	0.41	− 133.07	0.60	13
	2020-10-03 17:49	− 131.04	0.15						
GaSS 1–12	2019-09-11 19:13	61.11	0.48	2017-06-04 15:59	51.88				
	2020-07-05 23:15	56.22	0.21						
	2020-10-03 18:10	54.57	0.40						
GaSS 1–13	2020-07-04 22:54	− 362.31	1.23	2014-06-11 16:08	− 375.27	0.50	− 374.54	1.54	4
	2020-10-03 18:51	− 373.54	0.18						
	2020-10-29 17:13	− 375.50	0.26						
GaSS 1–14	2020-10-03 20:04	− 247.37	0.19	2016-08-13 12:56	− 247.79	0.40	− 250.47	0.61	10
	2020-10-29 17:55	− 248.79	0.12						
GaSS 1–15	2020-09-03 21:21	46.40	0.29	2017-09-06 12:14	49.94	0.29			
	2020-10-03 19:47	51.08	0.04						
	2020-10-29 18:15	51.34	0.10						
GaSS 1–20	2020-07-05 21:03	12.95	0.48	2017-06-03 13:27	44.76	0.43	9.36	0.82	10
GaSS 1–21	2020-07-05 20:42	− 182.39	1.70	2015-04-29 13:47	− 182.82	0.47	− 182.22	0.59	9
GaSS 1–23	2020-07-05 21:45	− 166.89	0.92	2016-08-16 09:36	− 167.23	0.45	− 169.53	1.01	10
GaSS 1–31	2020-07-05 23:36	69.59	0.15	2017-11-06 10:00	70.13	0.51	68.02	0.82	7
	2020-10-03 18:27	70.92	0.16						
	2020-10-17 18:20	68.72	0.72						
GaSS 1–33	2020-10-03 19:10	− 206.97	0.36	2014-07-08 17:31	− 205.14				
	2020-10-29 18:54	− 206.10	1.05						

two components of the binary, the easier for flickering to become observable (e.g. Hellier 2001). Therefore, if flickering is easy to observe in cataclysmic variable stars that radiate about 1 $L_\odot$ at optical wavelengths, it is an entirely different matter for symbiotic binaries in which the optical luminosity of the cool giant alone amounts to 10^2 $L_\odot$.

The regions in the disc responsible for flickering are hot (Warner 1995; Zamanov et al. 2020), and their emission is consequently rising toward the blue; that of the giant rises instead toward the red. Therefore, to reduce the background glare of the giant it is convenient to go as blue as possible (Skopal 2005). Detection of flickering at satellite ultraviolet wavelengths is straightforward as demonstrated by the *Swift* observations of SU Lyn by Mk16. On ground-based observations, the bluest photometric band is U (in its many variants: Landolt's U, u from Stromgren, or SLOAN u'). U band was relatively easy to observe in the old times of photoelectric photometers mounted on all-reflecting telescopes with bare aluminum surfaces, thanks to the high instrumental throughput (no coatings or refractive components) and the excellent sensitivity of photomultipliers like the standard RCA 31034A and Hamamatsu R934-02. Many searches for flickering in SySt were performed at that time (e.g. Slovak & Africano 1978; Mikolajewski et al. 1990; Tomov et al. 1996). The advent of CCDs, with their much lower sensitivity at U-band wavelengths, badly affected the study of flickering, with rarer attempts carried out (e.g. Dobrzycka, Kenyon & Milone 1996; Sokoloski, Bildsten & Ho 2001; Gromadzki et al. 2006; Zamanov et al. 2011). To further complicate the matter, the sensitivity of CCDs, which extends up and beyond 1 μm, allows signal to be recorded from the red-leak affecting most U filters, especially those of the modern multilayer dielectric type. Such a red-leak may be so severe in the case of cool giants that the fraction of recorded photons coming through the red-leak easily outnumbers those going through the proper transmission profile of the U band (Munari & Moretti 2012).

To search for flickering among our candidate *acc*-SySt we used a 50-cm telescope, with a 40-arcmin well-corrected field of view and quality photometric filters, operated robotically for ANS Collaboration in Chile at San Pedro de Atacama. For the above described limitations about U filters, we selected to search for flickering in B band, with interspersed observations in V band serving to construct the $B - V$ colour base for the transformation from the instantaneous local photometric system to the Landolt's standard one. Local photometric sequences were extracted from the APASS multi-epoch, all-sky $B\,V\,g\,r\,i$ photometric survey (Henden et al. 2016) in its DR8 version.

Given the much brighter emission of the M giant in B compared to U, the expected amplitude of observable flickering decreases to (at most) a few hundredths of a magnitude. To be detected, such a tiny amount of variation requires highly accurate observations and careful data reduction, under clear and stable skies as usually enjoyable in Atacama. We adopted integration times in B of 30 s for the brightest targets and 5 min for the faintest, with 60 s for the bulk of objects, thus ensuing that all objects have been observed at high S/N (>100 on each single point), while remaining short of the saturation thresholds and non-linear regime. Every 10 exposures in B, one was obtained in V to compute the coefficients of the transformation colour equations. The procedure was repeated identically for 70 min for each program star. The photometry was performed for most objects in aperture mode, their high galactic latitudes implying sparsely populated fields and therefore no need to revert to point spread function (PSF) fitting, which was instead necessary for three targets. On average, the 50 field stars closest on the image to the SySt, of a similar magnitude and well isolated from neighbouring stars were also measured on all recorded images in exactly the same way as the SySt. The photometry of these 50 field stars was then inspected looking for those with a $B - V$ colour as close as possible to the SySt in the centre. Typically five such stars were found, with a few cases scoring just two and others up to eight. These field stars with magnitude and

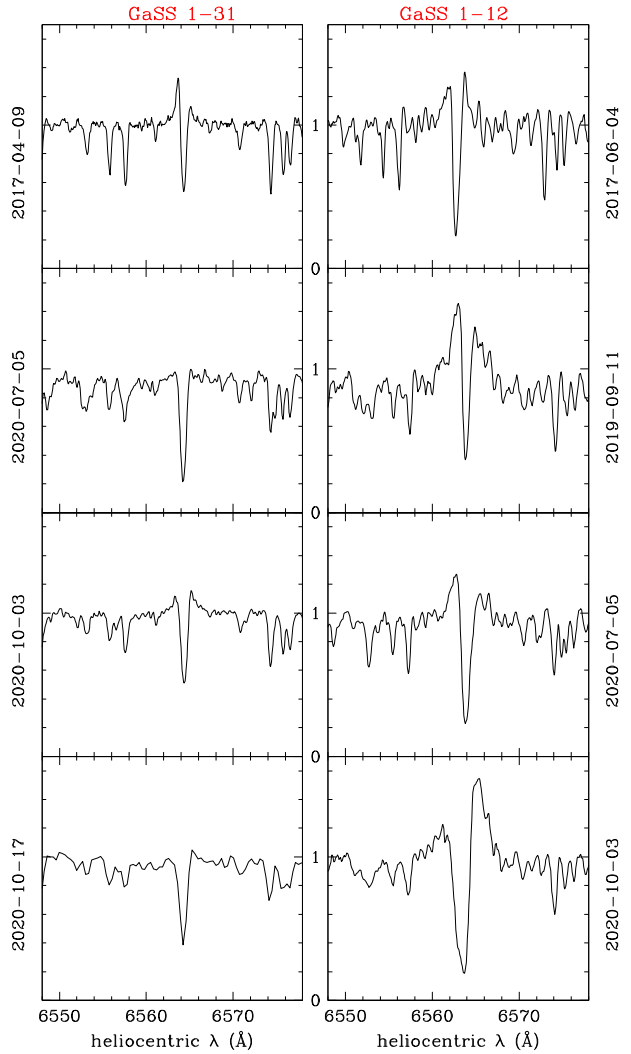

Figure 9. Example of variability observed on Hα comparing the original GALAH spectra (top row) with Asiago 1.82-m echelle spectra obtained at later epochs (the left-bottom spectrum is from Varese 84-cm telescope). Only GALAH spectra are corrected for telluric absorption lines.

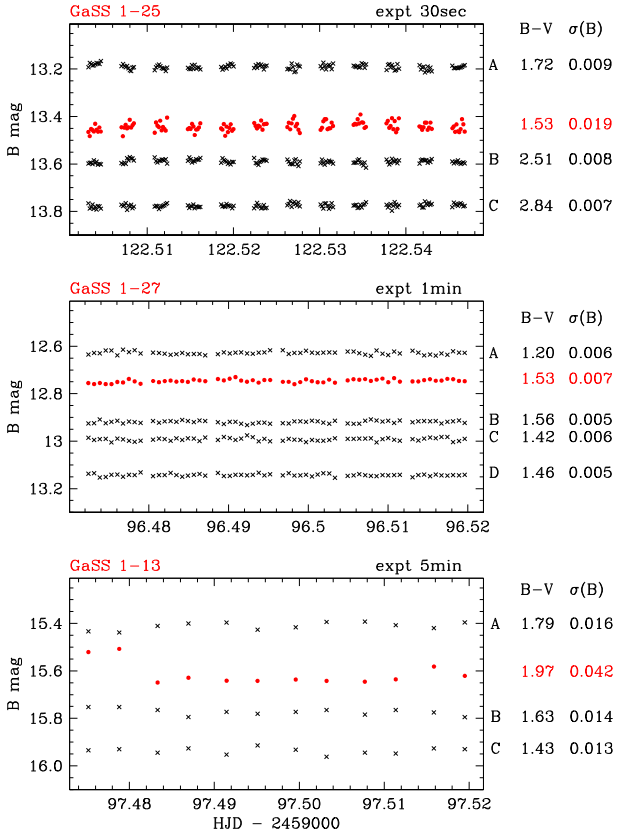

Figure 10. Examples of the *B*-band time series collected on the program stars, with 30 s, 1 min, and 5 min sampling time (from top to bottom), in search for flickering from the accretion disc. The regular gaps correspond to the acquisition of *V*-band frames for the calibration of colour equations to transform data to the standard Landolt system. The measured $B - V$ colour of the SySt (in red and filled circles) and of nearby field stars of similar brightness and colour (in black and crosses) is marked to the right, together with the dispersion around the median of the plotted *B*-band data. SySt on the top and bottom panels clearly show flickering well in excess of the noise affecting field stars, while that in the middle panel is constant at the same noise level of the field stars.

colour closely matching those of the SySt, serve as samplers of the observational noise above which the flickering has to be detected: the closely similar colour nulls the effects of differential atmospheric transmission, and the closely similar brightness nulls the non-linear effects in the differential statistical noise.

The candidate *acc*-SySt subjected to the search for flickering are listed in Table A4, together with the HJD of the central image for the 70 min time series, and the average of *B* and *V* measured magnitudes during such time series. The error of such *B* and *V* data is totally negligible in its Poissonian component, while the amount due to transformation from the local system to the APASS one (closely adherent to Landolt's) is systematic and constant for a given object and amounts on average to 0.008 mag (which obviously cancels out when comparing flickering data within a given time series).

An example of the collected data is presented in Fig. 10, with one object each for the 30 s, 1 min, and 5 min sample times. At the top and bottom panels we show objects with a clear detection of flickering well in excess of the noise affecting the field stars as usually quantified by their respective rms deviation from the mean (Dobrzycka et al. 1996), while in the centre we present a non-flickering symbiotic that remains stable at a few mmag level through the 70 min monitoring. GaSS 1–25 at the top of Fig. 10 exemplifies the frequent case of incessant flickering (e.g. RS Oph as observed by Dobrzycka et al. 1996), while the behaviour displayed by GaSS 1–13 at the bottom of Fig. 10, i.e. isolated flarings over an otherwise relative flat background, is a close match to that observed by Zamanov et al. (2017) in EF Aql.

The objects for which flickering was detected well above observational noise are marked with an 'F' in the 'Flk' column of Table 5. The detectability of flickering and its amplitude is usually dependent on the actual epoch of observation (Stoyanov et al. 2018). Orbital phases with the hotspot in plain view are favoured (WD at quadrature moving toward superior conjunction), while others can be detrimental, e.g. during eclipses or passage at apoastron in a highly eccentric orbit (with consequent reduction in mass transfer rate). Therefore, stars in Table 5 that failed to show flickering at the single epoch of our observation could do otherwise at a later revisit. This is also the case for SU Lyn. When it was observed in late 2015 by Mk16 its was in a high accretion state and it flickered wildly, while it was in a low accretion state and did not flicker when Dimitrov et al. (2018) performed their observations in 2018 January. Similarly, while large

Table 7. Results of the *Swift* X-Ray Telescope (XRT) and UltraViolet Optical Telescope (UVOT) observations of some of the candidate *acc*-SySt presented in this paper. The fluxes are in units of 10^{-13} erg cm^{-2} s^{-1}. The bottom three objects are radial pulsators observed for comparison. The data for 20 35 04.52–05 47 35.3 include also additional 485 s exposure obtained on 2019 September 8.

Name/RA, Dec.	Obs. date	Start time (UT)	XRT obs. duration (s)	0.3–10 keV count rate	0.3–10 keV flux	UVOT obs. duration (s)	UVM2 mag.
GaSS 1–11	13 June 2020	12:05	1885	<3.0e-3	<2.6e-13	1864	17.33 ± 0.06
GaSS 1–12	16 Sept 2019	00:02	1516	<3.2e-3	<2.8e-13	1701	16.21 ± 0.04
GaSS 1–31	14 June 2020	01:01	839	<3.7e-3	<3.3e-13	830	>19.92
05 11 30.88–61 29 03.6	10 June 2020	06:31	1973	<1.7e-3	<1.5e-13	1948	>20.65
20 06 56.32–28 35 32.3	11 Oct 2019	00:49	1536	<2.5e-3	<2.2e-13	1527	>20.71
20 35 04.52–05 47 35.3	04 Sept 2019	12:23	1504	<3.6e-3	<3.2e-13	1485	>20.82

amplitude flickering has always been the rule for MWC 560 (e.g. Lucy et al. 2020), it has disappeared altogether during the last couple of years (Zamanov et al. 2019).

We postpone a detailed analysis of the data collected during our search for flickering for the program stars to a follow-up paper. Derivation of temperature and radius of the region(s) responsible for the observed flickering (e.g. Zamanov et al. 2020) is straightforward but largely out of the goals of this paper. We similarly postpone the attempt of confirming a WD companion for our candidate *acc*-SySt by searching for possible quasi-periodicities or signatures of the WD rotation (e.g. Sokoloski & Bildsten 1999; Zhekov & Tomov 2019). Such analysis will strongly benefit from further observations we have planned for the SySt reported in this paper and are carrying out also for other SySt assigned to later papers in this series.

5.5 Satellite X-ray/UV observations

The presence and nature of the accreting source in *acc*-SySt systems, either a WD or a NS, is best defined by satellite observations performed in the UV and X-rays, where the peak of the emissivity for accretion-induced processes is located (e.g. Masetti et al. 2007a and references therein, and also Kuranov & Postnov 2015 for a recent review). The X-ray/UV properties of the *acc*-SySt prototype SU Lyn have been investigated by Mk16, Lopes de Oliveira et al. (2018), and Kumar et al. (2021) based on observations with *Swift*, *NuSTAR*, and *ASTROSAT* satellites. They found SU Lyn to show (i) a large (by a factor of a few hundred in flux) UV excess with respect to a 'normal' red giant; (ii) long-term (months to years) hard X–ray variations by an order of magnitude between low- and high-level states in the 15–35 keV hard X–ray emission; and (iii) fast UV variability during the high X-ray states (flickering). In the latter ones, the average X-ray flux was $\sim 10^{-11}$ erg cm^{-2} s^{-1} in the 0.3–50 keV band, with the spectrum modelled with a thermal plasma of temperature $kT \sim$ 20 keV, plus a fluorescent iron emission at 6.4 keV, absorbed by a hydrogen column density $N_{\rm H}$ as large as $\sim 3 \times 10^{22}$ erg cm^{-2}. This absorption has however little effect on the UV excess observed from this source. At a distance of 650 pc, this corresponds to unabsorbed X-ray luminosities of up to $\sim 10^{33}$ erg s^{-1} in the high state, and a factor of 10 larger in the UV. The passage from low- to high-level states in the UV and X-ray emission is attributed to large excursions in the transfer and accretion rates.

In anticipation of a devoted observing campaign, we have performed some quick exploratory observations of three of the candidate *acc*-SySt discovered in this paper with the *Swift* satellite (Gehrels et al. 2004), and for comparison of three of the identified radial pulsators considered as a control sample. The observations have been carried out in Target-of-Opportunity (ToO) mode. This type of observations is generally limited to roughly 2000 s per object, so this can be considered as a quick and rather shallow survey of our target sample. The pointings were performed in two time slots: the first one in 2019 September–October, and the second one in 2020 June. The results are summarized in Table 7.

Table 8. Unabsorbed accretion luminosity from the *Swift* data in Table 7 (see Section 5.6 for details).

Symbiotic star	$L_{\rm UV}$ (erg s^{-1})	$L_{\rm UV}$ ($L_\odot$)	$M_{\rm acc}$ ($M_\odot$ yr^{-1})
GaSS 1–11	1.43e34	3.7	1.7e-9
GaSS 1–12	3.30e34	8.5	4.0e-9
GaSS 1–31	<4.29e32	<0.11	<5.1e-11

Our *Swift* observations were acquired with the onboard instruments X-Ray Telescope (XRT; Burrows et al. 2005) and UltraViolet Optical Telescope (UVOT; Roming et al. 2005). The XRT allows covering the X-ray band between 0.3 and 10 keV band, whereas UVOT data were collected using the UV filter UVM2 (reference wavelength: 2246 Å; see Poole et al. 2008; Breeveld et al. 2011 for details). On-source pointings were simultaneously performed with the two instruments and lasted between ∼800 and ∼2000 s.

All observations were reduced within the FTOOLS environment (Blackburn 1995). The XRT data analysis was performed using the XRTDAS standard pipeline package (XRTPIPELINE v. 0.13.4) in order to produce screened event files. All X-ray data were acquired in photon counting (PC) mode (Hill et al. 2004) adopting the standard grade filtering (0–12 for PC) according to the XRT nomenclature. For each source, scientific data were extracted from the images using an extraction radius of 47 arcsec (20 pixels) centred at the optical coordinates of the source, while the corresponding background was evaluated in a source-free region of radius 94 arcsec (40 pixels) within the same XRT acquisition. In all cases, no emission above an S/N threshold S/N = 3 was detected. The XRT count rate upper limits in the 0.3–10 keV range were then measured within the XSPEC package.

X–ray flux limits were determined using the WEBPIMMS online tool[3] by assuming a spectral model similar to that of Mk16 for SU Lyn, i.e. a thermal plasma emission with temperature $kT = 17$ keV absorbed by a column density $N_{\rm H} = 2.9 \times 10^{22}$ cm^{-2}, which implies a count rate-to-flux conversion factor of $\sim 8.8 \times 10^{-11}$ erg cm^{-2} s^{-1} count^{-1}. We note that, with this model, the unabsorbed fluxes (in Table 8) in this same band are about 50 per cent larger than the absorbed ones.

[3] https://heasarc.gsfc.nasa.gov/cgi-bin/Tools/w3pimms/w3pimms.pl

Count rates on Level 2 (i.e. calibrated and containing astrometric information) UVOT images at the position of the objects of our sample were measured through aperture photometry using 5 arcsec apertures, whereas the corresponding background was evaluated for each image using a combination of several circular regions in source-free nearby areas. Magnitudes and upper limits were measured with the UVOTSOURCE task. The data were then calibrated using the UVOT photometric system described by Poole et al. (2008), and we included the recent (2020 November) fixings recommended by the UVOT team.

Of the three candidate *acc*-SySt observed with *Swift*, two were found to be strong UV emitters, confirming their symbiotic nature. The third, GaSS 1–31, was not detected. There may be a clear reason for that, though. The *Swift* pointing was carried out on 2020 June 14. Three weeks later, on 2020 July 5, we observed the same star with the Asiago 1.82-m and the echelle spectrograph. The Hα profile for that date is presented in Fig. 9, and does not show the faintest trace of an emission. In addition, the equivalent width of the Hα absorption is same as for field stars of the same spectral type (and greater than for the other dates in Fig. 9), indicating no partial filling from even very faint emission. In short, it looks like the emission from the accretion disc was 'switched-off' at the time of the *Swift* pointing, with consequent non-detection. An eclipse behind the M-giant seems improbable in view of the limited variability of the epoch GALAH and Asiago radial velocities listed in Table 6 (and their similarity with the average velocity provided by *Gaia* DR2), precluding a high orbital inclination for GaSS 1–31. It rather seems a drastic reduction in the mass accretion rate was taking place at the time of *Swift* observations. This could have been caused by a reduction in the wind blown-off by the M giant or passage at apoastron in a highly eccentric orbit. The spectrum taken a hundred days later (that for 2020 October 3 in Fig. 9) shows that accretion has weakly resumed, with both a reduction in the equivalent width of Hα absorption (partially filled-in) and emission wings extending above the local continuum.

None of the three radial pulsators we tried with *Swift* were detected, in spite of having been selected among those showing the strongest Hα and Hβ emission on GALAH spectra (far stronger than typically observed in *acc*-SySt). This supports the clear-cut role of satellite UV observations in segregating *acc*-SySt (Sahai et al. 2015), in particular from radial pulsators of similar spectral appearance on optical spectra.

A few final words are in order to explain the non-detection of GaSS 1–11 and GaSS 1–12 in X-rays in our shallow observations. The upper limit to their flux is about 0.01× the flux Mk16 recorded from SU Lyn during their *Swift* observations. Those observations of SU Lyn were obtained during an exceptionally bright state of the accretion disc (cf. Fig. 2 and the discussion at the end of Section 3), while the flux at other times (when the Hα shown by SU Lyn is much weaker and more similar in appearance to that revealed by GALAH spectra for our sample of 33 candidate *acc*-SySt) was just 1/10 of that (cf. Lopes de Oliveira et al. 2018). There are two other factors playing against GaSS 1–11 and GaSS 1–12. The most important is the distance. SU Lyn is just 0.65 kpc away, while GaSS 1–11 and GaSS 1–12 are, respectively, at 6.6 and 4.6 kpc distance according to *Gaia* EDR3 parallaxes, corresponding to dilution factors of 100 and 50. In addition, SU Lyn is seen face-on, while the unknown orbital inclination of GaSS 1–11 and GaSS 1–12 introduces a reduction in flux proportional to cos *i* and a further reduction for limb-darkening reasons. Considering all factors together, it is no wonder that GaSS 1–11 and GaSS 1–12 fell below the X-ray detection threshold of snapshot ToO with *Swift*.

Table 9. Flux recorded in Hα and corrected for reddening (F(Hα)), isotropic luminosity radiated in Hα at *Gaia* EDR3 parallax (L(Hα)), and accretion luminosity ($L_{\rm acc}$) derived as described in Section 5.6 for the program star with available Asiago spectra to flux calibrate GALAH spectra.

Symbiotic star	F(Hα) (erg cm^{-2} s^{-1})	L(Hα) (erg s^{-1})	$L_{\rm acc}$ (L$_\odot$)
GaSS 1–12	1.391E-13	3.52e+32	14
GaSS 1–14	3.307E-14	2.93e+32	12
GaSS 1–15	3.205E-14	3.23e+31	1
GaSS 1–23	7.257E-14	2.00e+32	8
GaSS 1–25	1.179E-13	2.61e+32	10
GaSS 1–28	2.785E-14	1.88e+32	7
GaSS 1–31	2.367E-13	5.24e+32	22

5.6 Accretion luminosities

We have previously stated that the aim of this paper is to search for new SySt accreting at low rates similar to SU Lyn. Mass accretion rate ($M_{\rm acc}$) and accretion luminosity ($L_{\rm acc}$) are related by the usual

$$L_{\rm acc} = G\frac{M_* M_{\rm acc}}{R_*}, \quad (4)$$

where M_* and R_* are the mass and radius of the accreting object, respectively. The accretion on a WD, as it is the case for SU Lyn, radiates most of its output in the UV and much less into X-rays, while the reverse applies to NSs and their much deeper potential well.

The UVM2 magnitudes of the candidate new SySt in Table 7 correspond to flux densities (in units of 10^{-15} erg cm^{-2} s^{-1} Å^{-1}) of 0.54, 1.52, and <0.05, for GaSS 1–11, GaSS 1–12, and GaSS 1–31, respectively (from the count rate-to-flux calibration given in Poole et al. 2008; Breeveld et al. 2011). Then, considering the distances and $E(B-V)$ colour excesses reported in Table 5, correcting for the Galactic reddening according to the prescription in section 3.2 of Kataoka et al. (2008) and the UV correction coefficients in their table 5, and assuming for the three objects a flat spectral distribution in the UV as Mk16 did for SU Lyn, we obtain the unabsorbed UV luminosities listed in Table 8. In the hypothesis of accretion on to a WD of mass 1 M$_\odot$, as Mk16 has inferred for SU Lyn, in Table 8 we report also the corresponding accretion rates.

For the other candidate new SySt that were not observed by *Swift*, an estimate of $L_{\rm acc}$ can be derived from the flux recorded in the Hα emission. If an emission line forms in an accretion disc, the flux radiated by the line and the flux emitted by the disc as a whole are related. The correlation can be tight, with temporal variations in $L_{\rm acc}$ that may be accurately tracked and replicated by L(Hα) (cf. Munari et al. 2019, their fig. 14).

GALAH spectra are unfortunately not flux calibrated. To circumvent the problem, we look for assistance from the fluxed Asiago spectra. After dereddening the Asiago spectra for the $E(B-V)$ values listed in Table 5, we used them to flux calibrate the GALAH spectra of the corresponding objects. Being primarily interested in deriving just an order-of-magnitude, and noting the candidate new SySt exhibit only a limited photometric variability (cf. Section 4.6 above), we ignore the fact that Asiago and GALAH spectra are not simultaneous. On the template-subtracted version of the flux-calibrated GALAH spectra, we measured the integrated flux of Hα emission line F(Hα) (therefore already corrected for reddening), and list it in Table 9, where we consider only the candidate new SySt with *Gaia* EDR3 distances in Table 5. If d is the distance, the luminosity L(Hα) radiated isotropically by the disc in Hα is obviously

$$L(\mathrm{H}\alpha) = 4\pi d^2 F(\mathrm{H}\alpha). \quad (5)$$

As customary practice, we may write a power-law proportionality between the luminosity radiated in the line and by the disc as a whole:

$$\log(L_{\rm acc}) = \alpha_{\rm H\alpha} + \beta_{\rm H\alpha}\ \log(L({\rm H}\alpha)), \quad (6)$$

where $\alpha_{\rm H\alpha}$ and $\beta_{\rm H\alpha}$ are coefficients specific to Hα. Adopting their value as calibrated by Mendigutía et al. (2011) on Herbig Ae/Be stars, we have derived the $L_{\rm acc}$ listed in the last column of Table 9. The accretion luminosities derived directly from *Swift* UV data or estimated from the flux radiated in Hα are similar, and confined to the 1–20 $L_{\odot}$ range, the same roughly spanned by SU Lyn while varying between high and low states. Interestingly, there is an estimate of $L_{\rm acc}$ for GaSS 1–12 both from the *Swift* UV observations and also from Hα emission line flux, and the two differ by less than a factor of 2. While this can be read as an indirect confirmation of the reliability of $L_{\rm acc}$ estimated from Hα, it also points to the constant variability of $L_{\rm acc}$ observed in *acc*-SySt. In fact, the F(Hα) of GaSS 1–12, measured on the fluxed version of the echelle spectra presented in Fig. 9, varies by more than the above 2× factor.

5.7 Orbital-like periodicities

The long-term light curves of SySt are usually reconstructed from multiband photometric campaigns (e.g. Skopal et al. 2007, 2012; Sekeráš et al. 2019), from investigating historical plate archives (e.g. Munari & Jurdana-Šepić 2002), or searching the public data bases of all-sky patrol surveys (e.g. Gromadzki et al. 2009; Gromadzki, Mikołajewska & Soszyński 2013; Munari et al. 2021). Aside from the obvious effect of eclipses for systems seen at high inclination, the orbital motion may also affect the light curve of SySt seen at intermediate inclinations.

The basic type of orbital-induced modulation of the light curve of non-eclipsing SySt is shown in Fig. 11 (top panel adapted from Munari 2019, bottom panel from Munari et al. 2016), aiming to highlight the interplay between the irradiation effect and the ellipsoidal distortion. The figure compares the light curve of an *acc*-SySt (T CrB) and of a *burn*-SySt (LT Del), both seen at a sufficiently high orbital inclination to clearly show orbital modulation even if not high enough to present eclipses. In both systems the RG fills its Roche lobe, and the consequent ellipsoidal distortion imparts a characteristic double-maxima/double-minima shape to the orbitally modulated light curve at the reddest wavelengths. The hotter companion irradiates the facing side of the RG, thus heating its photosphere and partially ionizing the atmosphere above it, with the consequence to make the system brighter when the irradiated side of the RG is in full view (Kenyon 1986). The effect is larger going to bluer wavelengths. Obviously, the brighter and hotter the companion, the stronger the irradiation, and the wider the resulting modulation of the light curve. In a *burn*-SySt like LT Del the irradiation is so strong that it dominates over the ellipsoidal distortion in the *B*-band light curve of Fig. 11. On the contrary, in *acc*-SySt like T CrB the companion is much fainter and cooler compared to *burn*-SySt, and the amount of irradiation on the RG is amply reduced, with the net result that the *B*-band light curve may, or may not, show secondary minima shallower than primary ones.

A search for periodicity on the light curve of a SySt with an ellipsoidally distorted RG tends to return *half* the value of the true period: for T CrB in Fig. 11 it would be 114 d instead of 228 d. It is the spectroscopic orbit that would solve the P versus 2×P uncertainty in favour of 228 d. Such an uncertainty usually plagues analysis of data gathered from all-sky patrol surveys that scan the heaven in white light or through just one photometric filter. The P versus 2×P

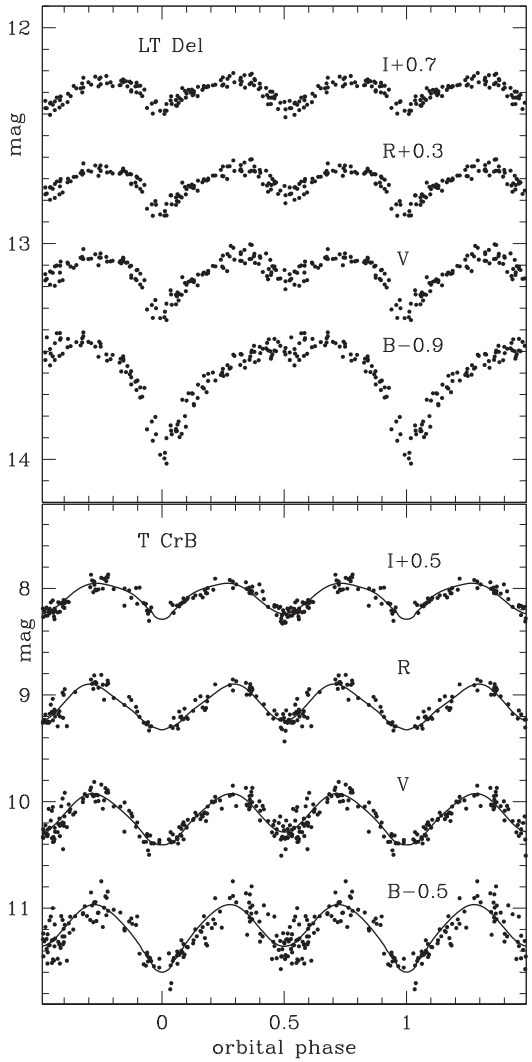

Figure 11. Examples of the modulation of the *B V R I* light curves induced by orbital motion in non-eclipsing SySt (see Section 5.7). Note the increasing impact of flickering going toward the bluer bands for the accreting-only T CrB, and its absence for the burning-type LT Del.

ambiguity can be resolved without the need of supporting radial velocities if the light curves of SySt cover both the bluest and the reddest photometric bands, provided that the irradiation of the RG by the companion is large enough to induce a measurable difference in the depth of primary and secondary minima at the bluest wavelengths.

We have searched the ASAS-SN photometric data for the 33 candidate *acc*-SySt looking for a type of light-curve modulation that could be orbitally induced along the lines of the description above. We found a suitable shape for 12 of them, and they are presented in Fig. 12, with the corresponding periods listed in Table 5. Their length is rather typical for SySt, the majority of known cases going from 7 months to 2.5 yr (Mikołajewska 2003). ASAS-SN collects data in just one photometric band, so not much can be said to resolve the ambiguity between P and 2×P. However, for GaSS 1–27 and GaSS 1–28, a slight difference in the depth of minima seems present, enough to lift the ambiguity. Given the limited time span of ASAS-SN coverage, such a difference could also result from other causes for photometric variability, and needs confirmation over more orbital cycles. Even more so for a possible third case for unequal minima, that of GaSS 1–33, and its sparsely covered light curve (cf. Fig. 12).

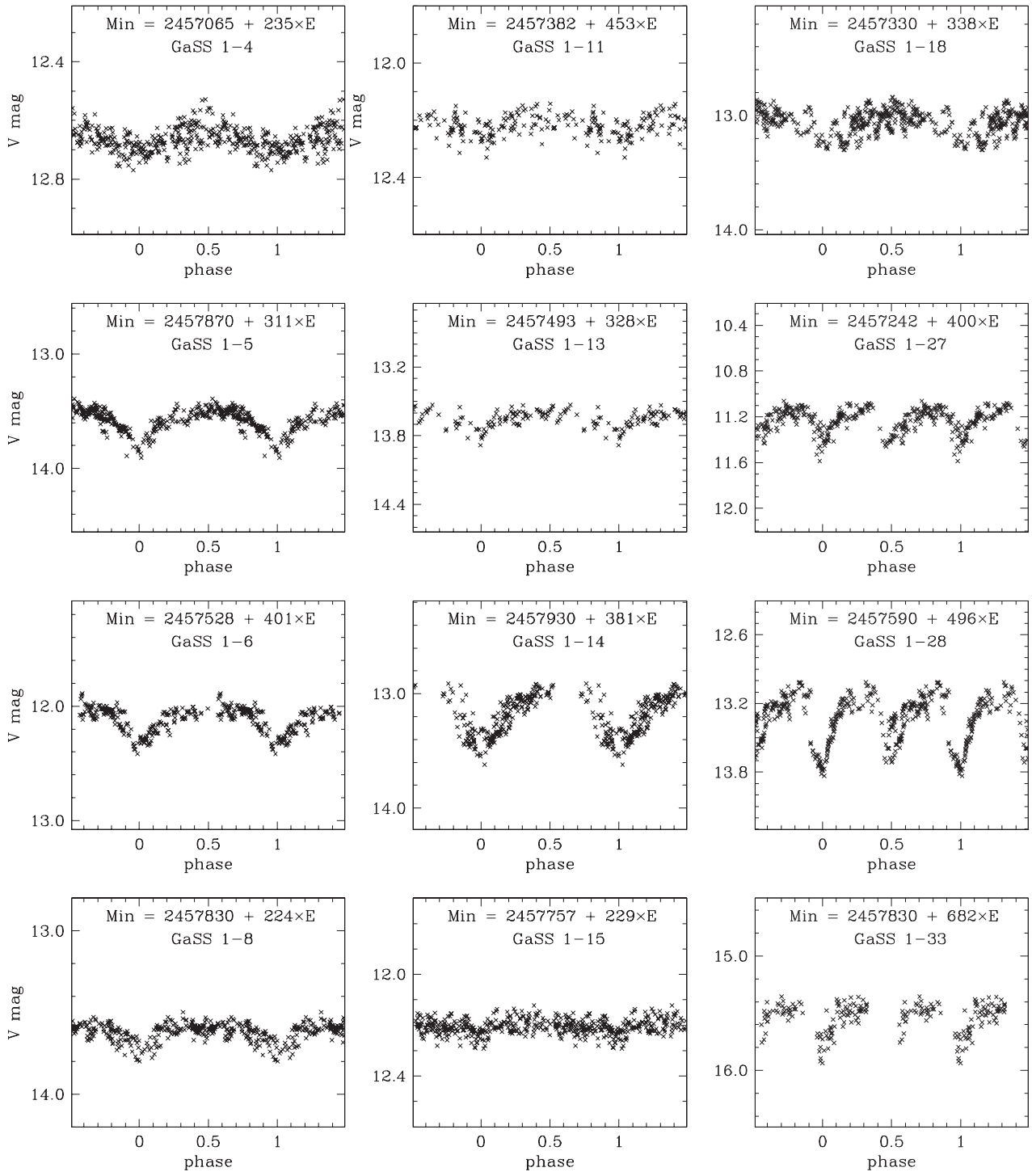

Figure 12. Phased light curves (see ephemeris at the top of each panel) for the 12 candidate *acc*-SySt marked in Table 5 as showing a modulation reminiscent of orbital motion.

A borderline case is that of GaSS 1–8, with just a hint of a secondary minimum around phase 0.5, which could be spurious.

The remaining objects in Fig. 12 show equal-depth minima, so the actual orbital period could be twice the value listed in Table 5 and on the ephemerides in their respective panels of Fig. 12. To help resolve the controversy, we have started a *B V R I* monitoring of all 12 objects, but the fruits of this effort will be collected only in a few years' time, when at least a few orbital cycles will be covered.

Overall, the light curves presented in Fig. 12 suggest that the irradiation of the RG by the companion is in general rather low for the new candidate SySt discovered in this paper, which agrees with the low accretion levels estimated in Section 5.6 above.

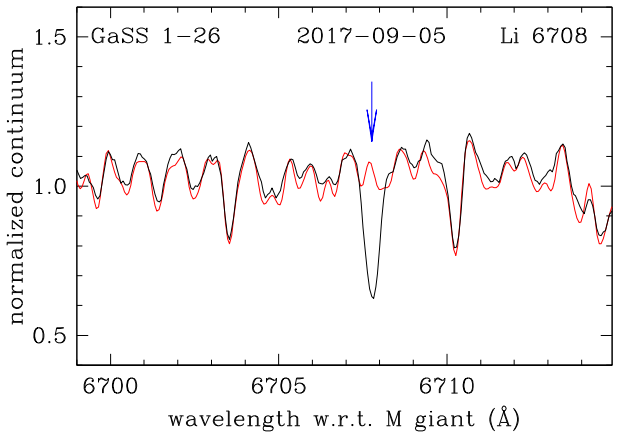

Figure 13. The GALAH spectrum of GaSS 1–26 (black) around the position of Li I 6707.8 Å compared with that (red) of the template for the same *f*-ratio bin. The overabundance of Li I is quite obvious.

5.8 Lithium

Wallerstein et al. (2008), in their chemical analysis of high-resolution spectra of M giants in SySt, found that the recurrent novae and accreting-only systems T CrB and RS Oph show an overabundance of ^{7}Li in their spectra. None of the other SySt in their large sample showed ^{7}Li enhancement and none was known to have undergone nova outbursts similar to T CrB and RS Oph. The overabundance of ^{7}Li in T CrB has been recently revised upward to $A(\mathrm{Li}) = 2.4 \pm 0.1$ by Woodward et al. (2020). The apparent link between ^{7}Li and nova outbursts has been further reinforced when the SySt V407 Cyg erupted in 2010. ^{7}Li overabundance was discovered earlier in V407 Cyg by Tatarnikova et al. (2003) at a time when the object was simply known as a Mira variable with a possible companion, and therefore attributed to indigenous production via the Cameron & Fowler (1971) mechanism activated in the Mira variable. We know now that also V407 Cyg undergoes nova outbursts, and this sheds an alternative explanation for its ^{7}Li overabundance.

The production of ^{7}Li during nova eruptions has been predicted theoretically (e.g. José & Hernanz 1998; Rukeya et al. 2017; Starrfield et al. 2020) and confirmed observationally (e.g. Izzo et al. 2015; Tajitsu et al. 2015; Molaro et al. 2016). Up to $\sim 1 \times 10^{-5}$ of the whole mass of the ejecta can be in the form of ^{7}Li, actually ^{7}Be that will decay into ^{7}Li. The large amounts produced during outbursts (especially those occurring on white dwarfs of the carbon–oxygen type), suggests that novae could be the main producer of ^{7}Li in the Milky Way (Molaro et al. 2020).

It is tempting to attribute the overabundance of ^{7}Li observed in T CrB, RS Oph, and V407 Cyg to pollution of the cool giant by the ejecta of the nova outbursts experienced by the WD companion. Their eruptions occur at a high frequency (eight have been observed in historic times for RS Oph) such that they could replenish the surface of the cool giant with ^{7}Li faster than convection can dilute ^{7}Li into the interior of the star. Alternatively, ^{7}Li could instead come from the interior of the cool giant, and conditions leading to an efficient transport of ^{7}Li to the surface could also lead more probably to nova outbursts as a consequence of a higher mass-loss rate and/or an enrichment in CNO nuclei.

In analogy with T CrB, RS Oph, and V407 Cyg, we have searched for ^{7}Li overabundance in our 33 candidate new SySt by comparing with the template spectrum for their *f*-ratio, and found a clear case of enhancement in GaSS 1–26, as shown in Fig. 13. The object is completely anonymous (no matching entry in SIMBAD, VSX, and similar catalogues) and its optical variability is inconspicuous (cf. Fig. A7 in Appendix A).

We have subjected GaSS 1–26 to a search for flickering and got a robust detection (cf. Table 5), which supports its binary nature and the presence of an accreting companion in the form of a WD.

Armed with that, we turned to the Harvard plate stack in search for an unnoticed nova outburst in the distant past. DASCH project provides access to calibrated scans of the huge collection of sky patrol photographic plates obtained over a century with Harvard astrographs located in both hemispheres (Grindlay et al. 2009). The area of the sky where GaSS 1–26 is located has not yet been included in the available DASCH data releases (1–6). We have been however granted access to the data for the area of sky around GaSS 1–26 prior to their publication in DASCH DR7, currently planned for 2021 July. This led to some initial excitement when two plates for 1908 June 6 and 1916 September 17 were logged as reporting GaSS 1–26 much brighter than at other epochs and at a blue magnitude compatible with a nova outburst. This pair of observations belongs to a time interval with very few Harvard plates covering the GaSS 1–26 position and being deep enough to have recorded it in quiescence (we measured it at $B = 15.4$ during our search for flickering, cf. Table A4, thus quite faint for the photographic means of the time). To assess if any nova outburst had really affected GaSS 1–26 in 1908 and/or 1916, we asked for and were provided with a scan of both plates (Edward Los, private communication). Inspection of these scans reveals the presence of artefacts at the astrometric position for GaSS 1–26, in the form of ink from a pen marking for the 1908 plate and a scratch on the emulsion for the 1916 one. Therefore, no nova outburst affected GaSS 1–26 in either 1908 or 1916. Even if the search on Harvard plates for unnoticed past nova outbursts has not been fruitful, it should be extended to other photographic plate archives, although not many cover the Southern hemisphere at faint magnitudes and over protracted periods of times, and even less have preserved the plates in good conditions and provide access to them in person or via digitized scans.

In favour of a possible pollution scenario for the ^{7}Li in GaSS 1–26 is the fact that indigenous ^{7}Li production via the Cameron & Fowler (1971) mechanism is expected to occur during hot-bottom burning (HBB) conditions, when the outer part of the burning H-shell is included in the envelope convection. A key aspect of HBB is the existence of a lower mass limit for it to occur, which depends on metallicity (Herwig 2005). The minimum initial mass for HBB is $M_{\mathrm{ini}} \geq 5\ \mathrm{M}_\odot$ at solar metallicity (Forestini & Charbonnel 1997), which can decrease down to 3 $\mathrm{M}_\odot$ for very metal-poor stars (Siess, Livio & Lattanzio 2002). The latter is obviously not the case given the otherwise normal spectrum displayed by GaSS 1–26. The faintness and negligible reddening place GaSS 1–26 at a great distance from us; its *Gaia* EDR3 parallax is affected by a large error, but it seems safe to argue that a lower limit to the distance is 10 kpc. At a galactic latitude $-10\overset{\circ}{.}6$, it means a height over the galactic plane of $z \geq 1.9$ kpc. It would be rather atypical to find a young and massive $M_{\mathrm{ini}} \geq 5\ \mathrm{M}_\odot$ star at such a large height above the Galactic plane.

5.9 Evolutionary status

The nature of the candidate new SySt will be investigated in detail elsewhere, including their chemical partition and Galactic orbits. However, some preliminary comments seem in order here.

To assess the evolutionary status of the candidate *acc*-SySt, we have taken their $J\ H\ K_{\mathrm{S}}$ near-IR photometry from 2MASS survey (Cutri et al. 2003) and after correcting for reddening and distance

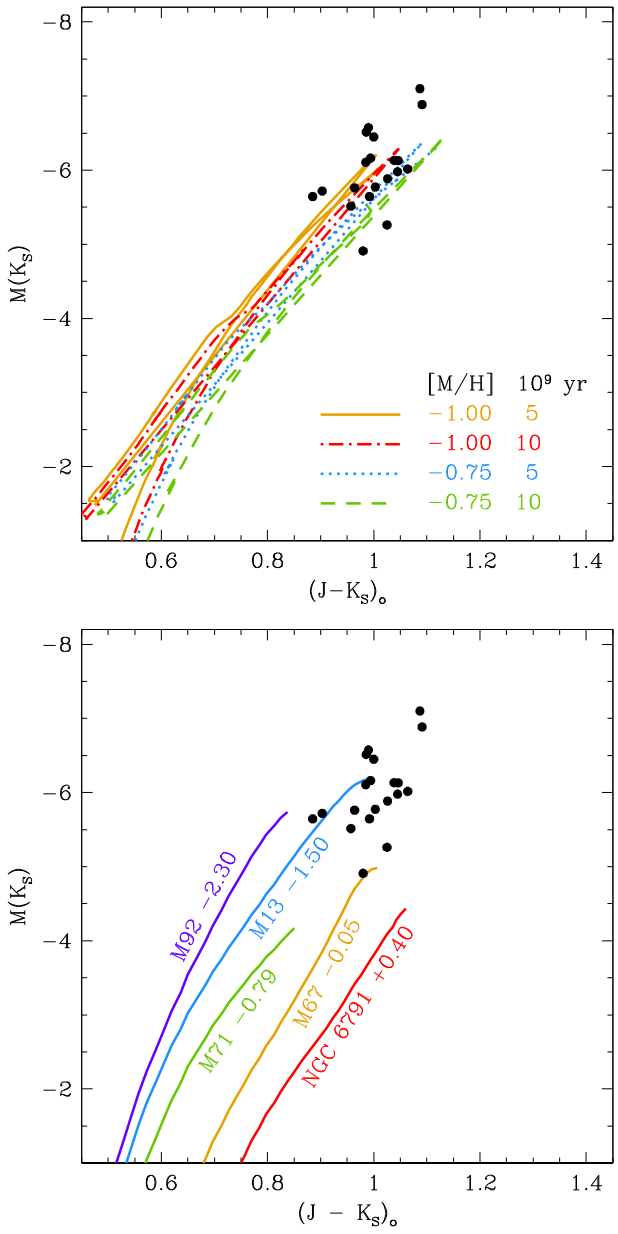

Figure 14. Location of the candidate *acc*-SySt on the near-IR isochrone plane, compared with Padova PARSEC isochrones (top) and observed ones (bottom) for clusters spanning a range in metallicity (see Section 5.9 for details).

given in Table 5, we have plotted their positions on the absolute $M(K_s)$/dereddened $(J-K_s)_o$ plane in Fig. 14.

On the top panel of Fig. 14, the comparison is carried out against the Padova PARSEC isochrones (Bressan et al. 2012; Marigo et al. 2017; Pastorelli et al. 2020). It provides evidence that the candidate *acc*-SySt are all located close to the tip of the giant branch, and that they are relatively old and metal-poor objects. This conforms with their significant height z above the Galactic plane as given in Table A2. For that age and metallicity, their mass estimated from the isochrones ranges from 1.03 to 1.22 $M_\odot$. Similar conclusions are drawn by comparison with the observed isochrones compiled by Karaali, Bilir & Gökçe (2013) for a sample of clusters spanning a large range of observed metallicities, as illustrated in the bottom panel of Fig. 14.

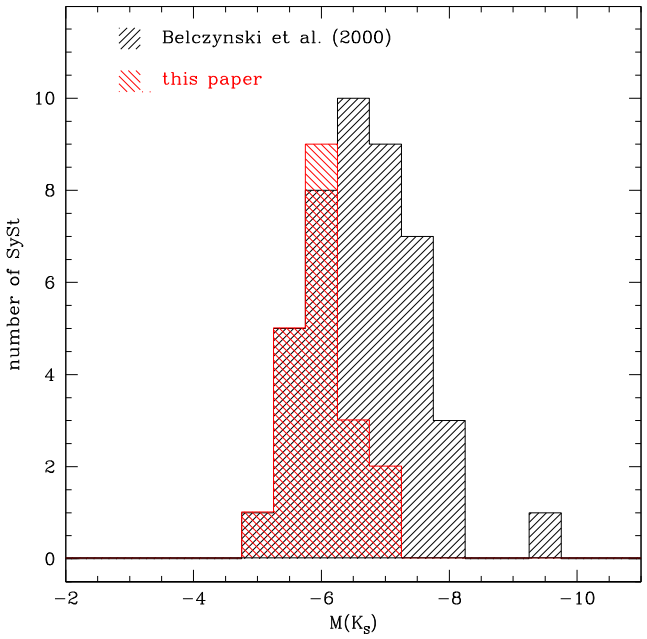

Figure 15. Distribution in absolute 2MASS K_s magnitude of Belczyński et al. (2000) SySt with an M spectral type, and those from this paper. Only objects with a *Gaia* EDR3 parallax satisfying the accuracy condition $\sigma(\pi)/\pi$ <0.2 are plotted.

How do the red giants of the candidate new SySt compare to well-established SySt? This is addressed in Fig. 15, where their distributions in $M(K_s)$ are compared. For the well-established SySt we adopted the catalogue by Belczyński et al. (2000), and retained only the 44 objects with a giant of M spectral type and with a *Gaia* EDR3 parallax accurate enough to satisfy the inversion condition $\sigma(\pi)/\pi$ <0.2. To compute their $M(K_s)$ we adopted for them the interstellar extinction estimated from the Schlegel–Finkbeiner–Davis (SFD) reddening maps (Schlegel, Finkbeiner & Davis 1998).

The distribution in Fig. 15 of the new and the well-established SySt is the same. The fact that GALAH is a magnitude-limited survey ($12 < V_{JK} < 14$) means that intrinsically brighter objects need to be at larger distances to fall between the limits in magnitude. The lack of GALAH candidate *acc*-SySt at the brighter $M(K_s)$ values in Fig. 15 simply reflects the fact that current *Gaia* EDR3 parallaxes are not accurate enough to satisfy the condition $\sigma(\pi)/\pi$ <0.2 for the most distant, and therefore intrinsically brightest objects. It may be guessed that future *Gaia* data releases will push forward the horizon of parallax accuracy and allow to include the remaining candidate *acc*-SySt and let them populate the histogram of Fig. 15.

6 CONCLUSIONS AND FUTURE PROSPECTS

We present the discovery and characterization of 33 bona fide candidates of the accreting-only type of SySt. So far, this class of binary systems has evaded a thorough scientific scrutiny, otherwise received by its counterpart, the nuclear-burning class of SySt. Both describe the same underlying configuration, a binary system composed of a red giant and a (degenerate) companion, however, they are distinguished by the physical processes under way inside the system and the consequent observational implications, favouring the study of *burn*-SySt. Because *acc*-SySt are believed to be much more abundant in the Galaxy than *burn*-SySt, while the ratio of known (investigated) objects is just the reverse, it is important to

uncover this hidden population of interacting binary stars in order to assess the viability of SySt as progenitors of Type Ia supernovae, their impact on the pollution of the interstellar medium (ISM), and to better understand the cycle of exchange between the accreting-only and the nuclear-burning phases.

To this end, we have investigated a large sample of 600 255 stars from the GALAH spectroscopic all-sky survey, which, given its unbiased observational strategy, promises to enable the envisaged statistical analysis, while supported by a suite of follow-up observations, provides a rich source of information on individual SySt. The first 33 candidates presented in this paper were selected using relatively conservative criteria: parallax and colour cut, strength of molecular (TiO) absorption bands, prominence of Hα emission line, and rejection based on the presence of various observational and reduction artefacts. Furthermore, the photometric light curves were checked to filter out radial pulsators, and great care was taken to reinforce our diagnostics for the symbiotic nature of program stars, building on the knowledge provided by the prototype *acc*-SySt SU Lyn and by conducting follow-up ground- and space-based observations examining the near-UV excess, RV and emission line variability, optical flickering, and X-ray/UV luminosities.

One of the 33 objects, Gass 1–26, shows a clear enhancement in ^{7}Li, which makes it an excellent candidate for follow-up observations aiming to illuminate the possible connection between pollution by novae outbursts and the galactic lithium abundance. Future studies will extend the analysis presented in this work in diverse directions, including:

(i) weaker emission features in spectra will be considered, as we currently only accept Hα profiles which, after subtraction of the template spectrum, reach higher than 0.5 above the adjacent continuum;

(ii) other spectral diagnostic features will be established to identify *acc*-SySt despite a possible absence of emission lines, for example a peculiar chemical signature in the spectrum of a giant star that was polluted by eruptions from the compact companion and thus by nuclearly processed material;

(iii) earlier spectral types of the primary stars will be investigated, also to account for the more metal-poor systems that do not achieve the same large radius and low surface temperatures as M giants;

(iv) automatic and manual inspection of legacy observations is being carried out, such as digging through diverse photometric archives and historical plates stacks in order to find e.g. past active phases or nova outbursts;

(v) existing and future high-energy instruments/surveys (e.g. *Swift*, *eROSITA*) can be exploited for follow-up observations or cross-matching of catalogued detections;

(vi) combining the chemical abundances and galactic orbits with the aid of the next *Gaia* releases will provide the means to confirm/reject the belief of SySt being an old population, primarily belonging to the bulge, thick disc, and halo. This view is built from the infrared characteristics of their cool giants, but it is heavily biased by how (and where in the Galaxy) the classical SySt were discovered by objective prism surveys of half a century ago. Determining the parent stellar population of SySt has a profound implication considering that Type Ia are the only type of supernovae known to erupt in elliptical galaxies, whose stellar populations resemble the bulge of our Galaxy.

The proposed future work will greatly expand the number of characterized *acc*-SySt and thus provide the community with large enough samples for a statistical study of the population of SySt as a whole, including ascertain the actual nature of the accreting objects and the relative statistics among the possible alternatives. In the meantime, we encourage the readers to further investigate the 33 candidates presented here and help confirm their symbiotic nature with further follow-up observations.

ACKNOWLEDGEMENTS

This research has made use of the ASI Science Data Center Multimission Archive; it also used the NASA Astrophysics Data System Abstract Service, which is operated by the Jet Propulsion Laboratory, California Institute of Technology, under contract with the National Aeronautics and Space Administration. This research has also made extensive use of the SIMBAD and VIZIER data bases operated at CDS, Strasbourg, France. We thank Dr Jamie Kennea and the *Swift* team for the quick approval and the rapid acquisition of the observations we requested. We thank R. Jurdana for the initial contact, and J. Grindlay and E. Los for grating access to DASCH data and scans prior to publication. NM acknowledges financial support through ASI–INAF agreement 2017-14-H.0, and UM through MAINSTREAM – PRIN INAF 2017 'The origin of lithium: a key element in astronomy' (PI: Paolo Molaro). We would also like to thank S. Dallaporta, G. Cherini, and F. Castellani (ANS Collaboration) for contributing to the photometric observations of SU Lyn. This work was supported by the Swedish strategic research programme eSSENCE. GT was supported by the project grant 'The New Milky Way' from the Knut and Alice Wallenberg Foundation and by the grant 2016-03412 from the Swedish Research Council. GT acknowledges financial support of the Slovenian Research Agency (research core funding no. P1-0188 and project N1-0040). This research made use of ASTROPY (http://www.astropy.org) a community-developed core PYTHON package for Astronomy (Astropy Collaboration et al. 2013, 2018).

DATA AVAILABILITY

The data underlying this paper will be shared on reasonable request to the corresponding author.

REFERENCES

Akras S., Guzman-Ramirez L., Leal-Ferreira M. L., Ramos-Larios G., 2019, ApJS, 240, 21
Allen D. A., 1982, in Friedjung M., Viotti R., eds, Astrophysics and Space Science Library Vol. 95, IAU Colloq. 70, The Nature of Symbiotic Stars. Reidel, Dordrecht, p. 27
Allen D. A., 1984, Proc. Astron. Soc. Aust., 5, 369
Angeloni R. et al., 2014, MNRAS, 438, 35
Angeloni R. et al., 2019, AJ, 157, 156
Astropy Collaboration et al., 2013, A&A, 558, A33
Astropy Collaboration et al., 2018, AJ, 156, 123
Bailer-Jones C. A. L., 2015, PASP, 127, 994
Barden S. C. et al., 2010, in McLean I. S., Ramsay S. K., Takami H., eds, Proc. SPIE Vol. 7735, Ground-Based and Airborne Instrumentation for Astronomy III. SPIE, Bellingham, p. 773509
Belczyński K., Mikołajewska J., Munari U., Ivison R. J., Friedjung M., 2000, A&AS, 146, 407
Bennett P. D., Brown A., Fawcett S. M., Yang S., Bauer W. H., 2004, in Hilditch R. W., Hensberge H., Pavlovski K., eds, ASP Conf. Ser. Vol. 318, Spectroscopically and Spatially Resolving the Components of the Close Binary Stars. Astron. Soc. Pac., San Francisco, p. 222
Blackburn J. K., 1995, in Shaw R. A., Payne H. E., Hayes J. J. E., eds, ASP Conf. Ser. Vol. 77, Astronomical Data Analysis Software and Systems IV. Astron. Soc. Pac., San Francisco, p. 367
Bozzo E. et al., 2018, A&A, 613, A22
Bragaglia A., Duerbeck H. W., Munari U., Zwitter T., 1995, A&A, 297, 759

Breeveld A. A., Landsman W., Holland S. T., Roming P., Kuin N. P. M., Page M. J., 2011, in McEnery J. E., Racusin J. L., Gehrels N., eds, AIP Conf. Proc. Vol. 1358, Gamma Ray Bursts 2010. Am. Inst. Phys., New York, p. 373
Bressan A., Marigo P., Girardi L., Salasnich B., Dal Cero C., Rubele S., Nanni A., 2012, MNRAS, 427, 127
Buder S. et al., 2021, MNRAS, in press (arXiv:2011.02505)
Burrows D. N. et al., 2005, Space Sci. Rev., 120, 165
Cameron A. G. W., Fowler W. A., 1971, ApJ, 164, 111
Chen P. S., Liu J. Y., Shan H. G., 2019, Ap&SS, 364, 132
Cheung C. C., Donato D., Wallace E., Corbet R., Dubus G., Sokolovsky K., Takahashi H., 2010, Astron. Telegram, 2487, 1
Corradi R. L. M. et al., 2008, A&A, 480, 409
Corradi R. L. M. et al., 2010, A&A, 509, A41
Corradi R. L. M., Sabin L., Munari U., Cetrulo G., Englaro A., Angeloni R., Greimel R., Mampaso A., 2011, A&A, 529, A56
Cutri R. M. et al., 2003, VizieR Online Data Catalog: II/246
de Laverny P., Recio-Blanco A., Worley C. C., Plez B., 2012, A&A, 544, A1261
De Silva G. M. et al., 2015, MNRAS, 449, 2604
Dimitrov V. V. et al., 2018, preprint (arXiv:1811.03317)
Dobrzycka D., Kenyon S. J., Milone A. A. E., 1996, AJ, 111, 414
Drew J. E. et al., 2005, MNRAS, 362, 753
Drilling J. S., Landolt A. U., 2000, in Cox A. N., ed., Allen's Astrophysical Quantities, 4th edn. Springer-Verlag, New York, p. 381
Drozd K., Mikołajewska J., Darnley M., Iłkiewicz K., Caldwell N., Shara M., 2019, in Griffin R. E., ed., Proc. IAU Symp. Vol. 339, Southern Horizons in Time-Domain Astronomy. Cambridge Univ. Press, Cambridge, p. 291
Evans D. W. et al., 2018, A&A, 616, A4
Evans P. A. et al., 2020, ApJS, 247, 54
Fluks M. A., Plez B., The P. S., de Winter D., Westerlund B. E., Steenman H. C., 1994, A&AS, 105, 311
Forestini M., Charbonnel C., 1997, A&AS, 123, 241
Freeman K., Bland-Hawthorn J., 2002, ARA&A, 40, 4871
Fujimoto M. Y., 1982, ApJ, 257, 767
Gaia Collaboration, 2020, VizieR On-line Data Catalog: I/350
Gaia Collaboration et al., 2018, A&A, 616, A11
Gehrels N. et al., 2004, ApJ, 611, 1005
Giannini T. et al., 2019, A&A, 631, A44
Ginestet N., Carquillat J. M., 2002, ApJS, 143, 513
Giroletti M. et al., 2020, A&A, 638, A130
Gonçalves D. R., Magrini L., Munari U., Corradi R. L. M., Costa R. D. D., 2008, MNRAS, 391, L84
Gonçalves D. R., Magrini L., Martins L. P., Teodorescu A. M., Quireza C., 2012, MNRAS, 419, 854
Gonçalves D. R., Magrini L., de la Rosa I. G., Akras S., 2015, MNRAS, 447, 993
Gorlova N., Van Winckel H., Jorissen A., 2012, Balt. Astron., 21, 165
Grindlay J., Tang S., Simcoe R., Laycock S., Los E., Mink D., Doane A., Champine G., 2009, in Osborn W., Robbins L., eds, ASP Conf. Ser. Vol. 410, Preserving Astronomy's Photographic Legacy: Current State and the Future of North American Astronomical Plates. Astron. Soc. Pac., San Francisco, p. 101
Gromadzki M., Mikolajewski M., Tomov T., Bellas-Velidis I., Dapergolas A., Galan C., 2006, Acta Astron., 56, 97
Gromadzki M., Mikołajewska J., Whitelock P., Marang F., 2009, Acta Astron., 59, 169
Gromadzki M., Mikołajewska J., Soszyński I., 2013, Acta Astron., 63, 405
Hartmann L., Herczeg G., Calvet N., 2016, ARA&A, 54, 135
Hellier C., 2001, Cataclysmic Variable Stars - How and Why they Vary. Springer-Verlag, London
Henden A. A., Templeton M., Terrell D., Smith T. C., Levine S., Welch D., 2016, VizieR On-line Data Catalog: II/336
Henize K. G., 1976, ApJS, 30, 491
Herwig F., 2005, ARA&A, 43, 435
Hill J. E. et al., 2004, in Flanagan K. A., Siegmund O. H. W., eds, Proc. SPIE Vol. 5165, X-Ray and Gamma-Ray Instrumentation for Astronomy XIII. SPIE, Bellingham, p. 217
Hinkle K. H., Fekel F. C., Joyce R. R., Wood P., 2013, ApJ, 770, 28
Hoffmeister C., Richter G., Wenzel W., 1985, Variable Stars. Springer-Verlag, Berlin
Howell S. B. et al., 2014, PASP, 126, 3981
Izzo L. et al., 2015, ApJ, 808, L14
Jorissen A., 2003, in Corradi R. L. M., Mikolajewska R., Mahoney T. J., eds, ASP Conf. Ser. Vol. 303, Symbiotic Stars Probing Stellar Evolution. Astron. Soc. Pac., San Francisco, p. 25
Jorissen A., Van Eck S., Dermine T., Van Winckel H., Gorlova N., 2012, Balt. Astron., 21, 39
José J., Hernanz M., 1998, ApJ, 494, 680
Joy A. H., 1926, ApJ, 63, 281
Karaali S., Bilir S., Gökçe E. Y., 2013, Publ. Astron. Soc. Aust., 30, e011
Karovska M., 2006, in Wilson A., ed., Proceedings of the X-ray Universe 2005 (ESA SP-604). ESA, Noordwijk, p. 183
Kataoka J. et al., 2008, ApJ, 672, 787
Kenyon S. J., 1986, The Symbiotic Stars. Cambridge Univ. Press, Cambridge
Kenyon S. J., Fernandez-Castro T., 1987, AJ, 93, 938
Kenyon S. J., Webbink R. F., 1984, ApJ, 279, 252
Kenyon S. J., Livio M., Mikolajewska J., Tout C. A., 1993, ApJ, 407, L81
Kippenhahn R., 1955, Astron. Nachr., 282, 73
Kniazev A. Y. et al., 2009, MNRAS, 395, 1121
Kochanek C. S. et al., 2017, PASP, 129, 104502
Kolotilov E. A., Munari U., Popova A. A., Tatarnikov A. M., Shenavrin V. I., Yudin B. F., 1998, Astron. Lett., 24, 451
Koornneef J., 2009, A&A, 500, 247 (special issue 500/01: reprint of 1983, A&A, 128, 84)
Kos J. et al., 2017, MNRAS, 464, 12591
Kumar V., Srivastava M. K., Banerjee D. P. K., Joshi V., 2021, MNRAS, 500, L12
Kuranov A. G., Postnov K. A., 2015, Astron. Lett., 41, 114
Landolt A. U., 1992, AJ, 104, 340
Lee T. A., 1970, ApJ, 162, 217
Lindegren L. et al., 2021, A&A, 649, A4
Lopes de Oliveira R., Sokoloski J. L., Luna G. J. M., Mukai K., Nelson T., 2018, ApJ, 864, 46
Lü G., Yungelson L., Han Z., 2006, MNRAS, 372, 1389
Lü G.-L., Zhu C.-H., Postnov K. A., Yungelson L. R., Kuranov A. G., Wang N., 2012, MNRAS, 424, 2265
Lucy A. B. et al., 2020, MNRAS, 492, 3107
Luna G. J. M., Sokoloski J. L., Mukai K., Nelson T., 2013, A&A, 559, A6
Luri X. et al., 2018, A&A, 616, A9
Lutovinov A., Suleimanov V., Manuel Luna G. J., Sazonov S., de Martino D., Ducci L., Doroshenko V., Falanga M., 2020, New Astron. Rev., 91, 101547
Marigo P. et al., 2017, ApJ, 835, 77
Martell S. L. et al., 2017, MNRAS, 465, 32031
Masetti N., Orlandini M., Palazzi E., Amati L., Frontera F., 2006, A&A, 453, 295
Masetti N., Rigon E., Maiorano E., Cusumano G., Palazzi E., Orlandini M., Amati L., Frontera F., 2007a, A&A, 464, 277
Masetti N. et al., 2007b, A&A, 470, 331
Masetti N., Munari U., Henden A. A., Page K. L., Osborne J. P., Starrfield S., 2011, A&A, 534, A89
Massey P., 2002, ApJS, 141, 81
Mendigutía I., Calvet N., Montesinos B., Mora A., Muzerolle J., Eiroa C., Oudmaijer R. D., Merín B., 2011, A&A, 535, A99
Merc J., Gális R., Wolf M., 2019a, Astron. Nachr., 340, 598
Merc J., Gális R., Wolf M., 2019b, Res. Notes Am. Astron. Soc., 3, 28
Merloni A. et al., 2012, preprint (arXiv:1209.3114)
Merrill P. W., 1940, The Spectra of Long-Period Variable Stars. Univ. Chicago Press, Chicago, IL
Merrill P. W., Burwell C. G., 1950, ApJ, 112, 72
Mikołajewska J., 2003, in Corradi R. L. M., Mikolajewska R., Mahoney T. J., eds, ASP Conf. Ser. Vol. 303, Symbiotic Stars Probing Stellar Evolution. Astron. Soc. Pac., San Francisco, p. 9
Mikołajewska J., Caldwell N., Shara M. M., 2014, MNRAS, 444, 586

Mikołajewska J., Shara M. M., Caldwell N., Iłkiewicz K., Zurek D., 2017, MNRAS, 465, 1699
Mikolajewski M., Mikolajewska J., Tomov T., Kulesza B., Szczerba R., Wikierski B., 1990, Acta Astron., 40, 129
Miszalski B., Mikołajewska J., 2014, MNRAS, 440, 1410
Miszalski B., Mikołajewska J., Udalski A., 2013, MNRAS, 432, 3186
Mohamed S., Podsiadlowski P., 2012, Balt. Astron., 21, 88
Molaro P., Izzo L., Mason E., Bonifacio P., Della Valle M., 2016, MNRAS, 463, L117
Molaro P., Izzo L., Bonifacio P., Hernanz M., Selvelli P., della Valle M., 2020, MNRAS, 492, 4975
Morgan D. H., 1992, MNRAS, 258, 639
Morgan W. W., Keenan P. C., 1973, ARA&A, 11, 29
Morgan W. W., Keenan P. C., Kellman E., 1943, An Atlas of Stellar Spectra, with an Outline of Spectral Classification. Univ. Chicago Press, Chicago, IL
Mukai K. et al., 2016, MNRAS, 461, L1 (Mk16)
Munari U., 2019, in Beccari G., Boffin H. M. J., eds, The Impact of Binary Stars on Stellar Evolution. Cambridge Univ. Press, Cambridge, p. 77
Munari U., Jurdana-Šepić R., 2002, A&A, 386, 237
Munari U., Moretti S., 2012, Balt. Astron., 21, 22
Munari U., Renzini A., 1992, ApJ, 397, L87
Munari U., Margoni R., Stagni R., 1990, MNRAS, 242, 653
Munari U., Dallaporta S., Cherini G., 2016, New Astron., 47, 7
Munari U. et al., 2019, MNRAS, 488, 5536
Munari U., Valisa P., Vagnozzi A., Dallaporta S., Hambsch F. J., Frigo A., 2021, Contr. Astron. Obser. Skalnate Pleso, 51, 103
Nuñez N. E., Nelson T., Mukai K., Sokoloski J. L., Luna G. J. M., 2016, ApJ, 824, 23
O'Brien T. J. et al., 2006, Nature, 442, 279
Pantaleoni González M., Maíz Apellániz J., Barbá R. H., Negueruela I., 2020, Res. Notes Am. Astron. Soc., 4, 12
Pastorelli G. et al., 2020, MNRAS, 498, 3283
Pearse R. W. B., Gaydon A. G., 1976, The Identification of Molecular Spectra, 4th edn. Chapman and Hall, London
Poole T. S. et al., 2008, MNRAS, 383, 627
Pugh T., Gray D. F., Griffin R. F., 2015, MNRAS, 454, 2344
Ricker G. R. et al., 2015, J. Astron. Telesc. Instrum. Syst., 1, 014003
Rodríguez-Flores E. R., Corradi R. L. M., Mampaso A., García-Alvarez D., Munari U., Greimel R., Rubio-Díez M. M., Santander-García M., 2014, A&A, 567, A49
Roming P. W. A. et al., 2005, Space Sci. Rev., 120, 95
Roth M. M. et al., 2018, A&A, 618, A3
Rukeya R., Lü G., Wang Z., Zhu C., 2017, PASP, 129, 074201
Sabbadin F., Falomo R., Ortolani S., 1987, A&AS, 67, 541
Sahai R., Sanz-Forcada J., Sánchez Contreras C., Stute M., 2015, ApJ, 810, 77
Sanduleak N., Stephenson C. B., 1973, ApJ, 185, 899
Schlafly E. F., Finkbeiner D. P., 2011, ApJ, 737, 103
Schlegel D. J., Finkbeiner D. P., Davis M., 1998, ApJ, 500, 525
Sekeráš M. et al., 2019, Contr. Astron. Obser. Skalnate Pleso, 49, 19
Shappee B. J. et al., 2014, ApJ, 788, 48
Sharma S. et al., 2018, MNRAS, 473, 20041
Sheinis A. et al., 2015, J. Astron. Telesc. Instrum. Syst., 1, 0350021
Siess L., Livio M., Lattanzio J., 2002, ApJ, 570, 329
Skopal A., 2005, A&A, 440, 995
Skopal A., Cariková Z., 2015, A&A, 573, A8
Skopal A., Vittone A. A., Errico L., Otsuka M., Tamura S., Wolf M., Elkin V. G., 2006, A&A, 453, 279
Skopal A., Vaňko M., Pribulla T., Chochol D., Semkov E., Wolf M., Jones A., 2007, Astron. Nachr., 328, 909
Skopal A., Shugarov S., Vaňko M., Dubovský P., Peneva S. P., Semkov E., Wolf M., 2012, Astron. Nachr., 333, 242
Skrutskie M. F. et al., 2006, AJ, 131, 11631
Slovak M. H., Africano J., 1978, MNRAS, 185, 591
Sokoloski J. L., Bildsten L., 1999, ApJ, 517, 919
Sokoloski J. L., Bildsten L., Ho W. C. G., 2001, MNRAS, 326, 553
Sokoloski J. L. et al., 2006, ApJ, 636, 1002
Sokoloski J. L., Lawrence S., Crotts A. P. S., Mukai K., 2017, preprint (arXiv:1702.05898)
Sowell J. R., Trippe M., Caballero-Nieves S. M., Houk N., 2007, AJ, 134, 1089
Starrfield S., Iliadis C., Hix W. R., 2008, in Bode M. F., Evans A., eds, Cambridge Astrophys. Ser. 43, Classical Novae, 2nd edn. Cambridge Univ. Press, Cambridge, p. 77
Starrfield S., Bose M., Iliadis C., Hix W. R., Woodward C. E., Wagner R. M., 2020, ApJ, 895, 70
Sterken C., Jaschek C., 2005, Light Curves of Variable Stars. Cambridge Univ. Press, Cambridge
Stoyanov K. A. et al., 2018, Bulgarian Astron. J., 28, 42
Tajitsu A., Sadakane K., Naito H., Arai A., Aoki W., 2015, Nature, 518, 381
Tatarnikova A. A., Marrese P. M., Munari U., Tomov T., Whitelock P. A., Yudin B. F., 2003, MNRAS, 344, 1233
Tomov T. et al., 1996, A&AS, 116, 1
Turnshek D. E., Turnshek D. A., Craine E. R., Boeshaar P. C., 1985, An Atlas of Digital Spectra of Cool Stars. Western Research Company, Tucson
Walker A. R., 1983, MNRAS, 203, 25
Wallerstein G., Harrison T., Munari U., Vanture A., 2008, PASP, 120, 492
Warner B., 1995, Cambridge Astrophys. Ser. 28, Cataclysmic Variable Stars. Cambridge Univ. Press, Cambridge
Wittenmyer R. A. et al., 2018, AJ, 155, 841
Woodward C. E., Pavlenko Y. V., Evans A., Wagner R. M., Ilyin I., Strassmeier K. G., Starrfield S., Munari U., 2020, AJ, 159, 231
Yamashita Y., Nariai K., 1977, An Atlas of Representative Stellar Spectra. Univ. Tokyo Press, Tokyo
Yang H. et al., 2012, ApJ, 744, 121
Yungelson L., Livio M., Tutukov A., Kenyon S. J., 1995, ApJ, 447, 656
Yungelson L. R., Kuranov A. G., Postnov K. A., 2019, MNRAS, 485, 851
Zamanov R., Boeva S., Latev G., Stoyanov K., Bode M. F., Antov A., Bachev R., 2011, Inf. Bull. Var. Stars, 5995, 1
Zamanov R. K. et al., 2017, Astron. Nachr., 338, 680
Zamanov R., Stoyanov K., Nikolov G., Kurtenkov A., Boeva S., Latev G., Tomov T., 2019, Astron. Telegram, 13236
Zamanov R. K., Boeva S., Stoyanov K. A., Latev G., Spassov B., Kurtenkov A., Nikolov G., 2020, Astron. Nachr., 341, 430
Zhekov S. A., Tomov T. V., 2019, MNRAS, 489, 2930
Zhu C., Lü G., Wang Z., Zhang J., 2010, New Astron., 15, 144

APPENDIX A: ADDITIONAL TABLES AND FIGURES

In this section, we present ancillary information that might be useful to the interested reader. First, we provide some details that concern follow-up observations of 33 candidate *acc*-SySt when searching for signs of the near-UV upturn (Table A1) and flickering (Table A4). Furthermore, we compute values for the position and luminosity for the 33 systems based on information given by the cross-match with external catalogues in Table A2. The radial velocity information measured or collected for some of the candidate *acc*-SySt in Table 6 is expanded for comparison reasons to include some GALAH radially pulsating and field M giants in Table A3. The list of VV Cep stars discussed in Section 4.8 is provided in Table A5. Finally, Fig. A1 displays the region of high S/N normalized template spectra around Hα and Hβ lines. These templates were used for subtraction from candidate *acc*-SySt spectra in order to detect prominent Hα emission features, with details of the subtraction results complemented by the ASAS-SN *V*-filter light curves plotted in Figs A2–A8.

Table A1. Log of low-resolution spectroscopic observations obtained with the Asiago 1.22-m+B&C+300 ln mm^{-1} (3300–8000 Å, 2.31 Å pixel^{-1}) in search for the near-UV upturn. The exposure time is in seconds.

SySt	UT middle		Expt
GaSS 1–7	2020-06-18	20:40	120
GaSS 1–7	2020-06-27	20:32	960
GaSS 1–9	2019-08-09	19:59	480
GaSS 1–9	2019-08-16	19:43	480
GaSS 1–9	2019-09-01	19:48	1200
GaSS 1–9	2020-06-27	22:31	960
GaSS 1–9	2020-08-25	19:18	480
GaSS 1–12	2019-08-16	20:27	720
GaSS 1–12	2019-08-19	20:54	960
GaSS 1–12	2019-09-01	19:27	1200
GaSS 1–12	2020-08-25	20:11	480
GaSS 1–13	2020-08-25	21:37	480
GaSS 1–13	2020-10-13	18:05	1800
GaSS 1–14	2019-08-30	18:59	480
GaSS 1–14	2019-09-01	20:18	960
GaSS 1–14	2019-12-06	17:24	1200
GaSS 1–15	2020-09-02	21:58	960
GaSS 1–15	2020-10-13	19:49	1800
GaSS 1–21	2020-06-19	21:24	720
GaSS 1–21	2020-06-27	21:54	1200
GaSS 1–23	2019-08-16	19:57	1200
GaSS 1–23	2019-08-19	19:41	960
GaSS 1–23	2019-09-01	19:58	1200
GaSS 1–23	2020-08-25	19:37	480
GaSS 1–25	2020-08-25	19:27	480
GaSS 1–28	2019-09-03	19:44	1200
GaSS 1–31	2020-08-25	20:20	480
GaSS 1–31	2020-10-13	17:30	1800
GaSS 1–33	2020-08-27	22:18	1440
GaSS 1–33	2020-10-13	20:28	3600

Table A2. *Gaia* EDR3 parallax and its uncertainty for the candidate *acc*-SySt, distance and height above the Galactic plane for stars with $\sigma(\pi)/\pi$ <0.2, and corresponding absolute V and K_s magnitudes from APASS and 2MASS values.

	EDR3		d	z	$M(V)$	$M(K_s)$
	π	err(π)	(kpc)	(kpc)	(mag)	(mag)
GaSS 1–1	0.0149	0.0125				
GaSS 1–2	0.0249	0.0114				
GaSS 1–3	0.1216	0.0100	8.2	3.7	−2.2	−5.8
GaSS 1–4	0.1226	0.0169	8.2	3.6	−2.2	−6.1
GaSS 1–5	0.0988	0.0157	10.1	5.0	−1.7	−5.5
GaSS 1–6	0.1843	0.0218	5.4	1.8	−1.7	−5.9
GaSS 1–7	0.0476	0.0216				
GaSS 1–8	0.1358	0.0153	7.4	2.8	−2.1	−5.6
GaSS 1–9	0.0974	0.0311				
GaSS 1–10	0.0715	0.0159				
GaSS 1–11	0.1523	0.0263	6.6	1.2	−2.3	−6.9
GaSS 1–12	0.2183	0.0321	4.6	0.9	−1.9	−7.1
GaSS 1–13	0.0423	0.0223				
GaSS 1–14	0.1163	0.0170	8.6	3.4	−1.8	−6.0
GaSS 1–15	0.3503	0.0257	2.9	1.4	−0.5	−4.5
GaSS 1–16	0.0219	0.0137				
GaSS 1–17	0.1861	0.0111	5.4	1.9	−2.5	−6.2
GaSS 1–18	0.1154	0.0157	8.7	3.5	−1.8	−5.6
GaSS 1–19	0.0589	0.0125				
GaSS 1–20	0.1327	0.0343				
GaSS 1–21	0.0391	0.0247				
GaSS 1–22	0.1711	0.0218	5.8	1.8	−2.7	−6.6
GaSS 1–23	0.2094	0.0245	4.8	1.3	−1.5	−6.0
GaSS 1–24	0.0902	0.0233				
GaSS 1–25	0.2306	0.0183	4.3	0.8	−2.3	−6.1
GaSS 1–26	0.0633	0.0171				
GaSS 1–27	0.2143	0.0177	4.7	1.3	−2.3	−5.7
GaSS 1–28	0.1326	0.0187	7.5	1.8	−1.4	−5.8
GaSS 1–29	0.1422	0.0157	7.0	2.7	+0.1	−5.3
GaSS 1–30	0.1799	0.0194	5.6	1.8	−2.7	−6.5
GaSS 1–31	0.2344	0.0170	4.3	1.1	−2.3	−6.1
GaSS 1–32	0.1877	0.0228	5.3	1.7	−2.5	−6.4
GaSS 1–33	0.0665	0.0327				

Table A3. Heliocentric radial velocity of some GALAH radially pulsating and field M giants observed along with the candidate SySt of Table 6. The values measured with the Asiago 1.82-m telescope+echelle spectrograph are compared with the corresponding values of rv_guess listed in GALAH DR3. The mean radial velocity listed in *Gaia* DR2 is also given, with its formal uncertainty and the number of epoch transits over which it has been computed.

RA	Dec.	Asiago 1.82-m echelle			GALAH DR3			*Gaia* DR2		
		UT middle	$RV_\odot$ (km s^{-1})	Err (km s^{-1})	UT middle	$RV_\odot$ (km s^{-1})	Err (km s^{-1})	$\langle RV_\odot \rangle$ (km s^{-1})	Err (km s^{-1})	N
					Radial pulsators					
19 17 30.06	− 18 47 02.1	2020-10-30 17:16	− 28.14	0.51	2017-05-07 18:28	− 34.63	0.03	− 32.82	2.87	2
20 35 04.52	− 05 47 35.3	2020-10-29 17:32	− 120.82	1.13	2014-07-09 15:39	− 121.61	0.21			
23 31 17.83	− 00 30 39.4	2019-12-09 18:30	− 34.67	0.49	2017-07-24 17:27	− 37.11	0.37	− 35.81	0.93	6
		2020-01-15 17:06	− 36.17	0.33						
		2020-10-29 19:59	− 39.47	0.31						
					Other GALAH M giants					
03 40 25.30	14 30 00.6	2020-01-13 20:42	11.46	0.21	2016-01-10 10:47	9.94	0.48	9.45	0.70	6
05 21 50.50	01 51 26.8	2019-12-07 01:50	− 16.54	0.29	2015-08-30	− 14.65		− 16.44	1.84	6
		2020-01-13 20:56	− 17.47	0.10	2015-12-27 13:09	− 12.42	0.31			
06 19 12.30	− 17 35 20.8	2020-01-13 22:17	121.14	0.43	2017-01-06 13:35	120.96	0.40	121.47	0.80	7
10 00 41.60	− 21 35 54.7	2020-04-10 20:13	188.45	0.58	2016-04-24 09:55	189.81	0.61	191.32	1.02	6
10 32 55.50	12 51 30.4	2020-04-10 20:34	132.32	0.12	2017-02-05 15:42	131.48	0.39	135.27	1.79	3
10 51 30.19	00 43 59.5	2020-04-10 21:04	165.91	0.36	2017-01-27 14:10	163.82	0.33	163.32	0.82	2
12 08 10.13	− 09 07 52.8	2020-04-10 21:50	45.34	0.22	2016-04-03 12:48	47.24	0.33	45.68	0.43	20
12 16 50.58	− 06 31 19.3	2020-04-10 22:04	83.14	0.19	2017-01-31 15:22	81.32	0.63	83.23	0.32	28
17 19 00.39	− 17 45 42.9	2020-07-05 21:21	− 23.56	0.91	2017-05-09 15:29	− 23.62	0.61			
19 59 58.75	08 04 07.3	2020-10-29 16:57	− 57.45	0.05	2016-10-08 09:34	− 57.27	0.02	− 57.85	0.15	3
20 00 03.82	07 22 39.7	2020-10-31 16:52	3.28	0.02	2016-10-08 09:34	2.65	0.15	2.14	0.14	14
20 05 15.00	08 54 02.5	2020-10-31 16:59	− 0.49	0.05	2016-05-31 19:34	− 0.07	0.24	− 1.14	0.42	6
22 04 33.89	− 08 14 49.9	2020-10-29 20:43	20.63	0.18	2014-07-11 17:59	19.40	0.01			
22 34 17.16	− 05 04 57.7	2020-10-29 20:55	− 20.77	0.52	2015-11-11 10:06	− 19.89	0.09			

Table A4. The B and V columns report the photometry of the candidate *acc*-SySt as measured during the search for flickering. The given HJD is the middle UT of the 70 min duration of the time series photometry. For the candidate SySt listed in Table 5 as showing flickering, the next three columns list, respectively, the $\sigma(B)$ of the B-band time series for the SySt, and the extremes of the distribution in $\sigma(B)$ of the field stars (of similar colour and magnitude as the investigated SySt, see Section 5.4 and Fig. 10) that were used to evaluate the flickering status of the candidate *acc*-SySt.

	HJD (–245 9000)	B (mag)	V (mag)	σ_B(SySt) (mag)	$\sigma_B(1)$ (mag)	$\sigma_B(2)$ (mag)
GaSS 1–1	117.834	14.248	13.078	0.015	0.008	0.010
GaSS 1–2	117.878	14.374	12.899			
GaSS 1–3	102.882	14.067	12.497			
GaSS 1–9	94.496	15.429	13.321	0.029	0.014	0.016
GaSS 1–10	118.497	14.659	13.032	0.034	0.017	0.018
GaSS 1–11	95.543	13.825	12.083	0.015	0.009	0.010
GaSS 1–12	96.546	13.874	12.122			
GaSS 1–13	97.497	15.605	13.641	0.041	0.014	0.016
GaSS 1–14	129.530	14.792	12.976	0.019	0.006	0.008
GaSS 1–15	97.549	13.838	12.092	0.020	0.010	0.011
GaSS 1–16	124.865	15.125	13.385			
GaSS 1–17	120.852	13.137	11.419	0.012	0.006	0.007
GaSS 1–21	130.986	15.921	14.010	0.054	0.027	0.029
GaSS 1–23	94.546	15.419	13.301			
GaSS 1–25	122.525	13.441	11.541	0.019	0.007	0.009
GaSS 1–26	146.505	15.427	13.723	0.042	0.018	0.022
GaSS 1–27	96.496	12.746	11.213			
GaSS 1–28	128.526	15.415	13.566			
GaSS 1–30	124.526	12.964	11.213			
GaSS 1–31	125.504	13.007	11.193			
GaSS 1–32	126.502	13.336	11.473			
GaSS 1–33	130.531	17.076	15.403	0.048	0.022	0.028

Table A5. The VV Cep stars selected from the catalogue of Pantaleoni González et al. (2020). The distance, height over the galactic plane and absolute infrared magnitude $M(K_s)$ are computed from *Gaia* EDR3 and 2MASS values.

Name	RA	Dec.	Dist (kpc)	z (pc)	K_s (mag)	$M(K_s)$ (mag)	Spectrum	
V641 Cas	00 09 26.3	+63 57 14	2.9	75	1.7	− 10.8	M3	Iab
KN Cas	00 09 36.4	+62 40 04	4.6	15	4.3	− 9.3	M1	Iab
V554 Cas	01 10 20.1	+62 30 40	2.6	−13	2.7	− 9.8	M2	I
AZ Cas	01 42 16.5	+61 25 16	3.3	−49	4.1	− 8.9	M0	Ib
XX Per	02 03 09.4	+55 13 57	2.5	−274	2.0	− 10.1	M4	Ib
HDE 237006	02 49 08.8	+58 00 48	2.5	−59	3.1	− 9.2	M1	Ib
WY Gem	06 11 56.2	+23 12 25	1.9	76	1.9	− 9.7	M2	Iab
V926 Mon	07 02 06.7	−03 45 17	1.1	12	2.0	− 8.2	M2	Ib
KQ Pup	07 33 48.0	−14 31 26	0.7	33	0.1	− 9.3	M2	Iab
V624 Pup	08 00 41.4	−32 50 25	5.0	−125	4.2	− 9.5	M2	Iab
WY Vel	09 21 59.1	−52 33 52	1.9	−61	0.4	− 11.3	M3	Ib:
HDE 300933	10 38 03.0	−56 49 02	3.1	79	1.8	− 10.8	M2	Iab/Ib
V730 Car	10 44 57.3	−59 56 06	2.4	−36	2.5	− 9.6	M1	Iab
HD 101007	11 36 56.9	−61 10 58	2.1	15	2.0	− 9.8	M3	Ib
V772 Cen	11 41 49.4	−63 24 52	2.3	−65	2.1	− 9.9	M2	Ib
CD-61.3575	12 44 16.1	−61 56 21	2.2	35	1.6	− 10.3	M2	Ia
CD-58.6089	15 34 41.4	−58 42 40	4.1	−163	3.4	− 9.8	M2	Ib
α Sco	16 29 24.5	−26 25 55	0.2	46	− 4.1	− 10.3	M0.5	Iab
FR Sct	18 23 22.8	−12 40 52	2.4	14	2.1	− 10.4	M2.5	Iab
V381 Cep	21 19 15.7	+58 37 25	1.8	201	0.8	− 10.8	M1	Ib
VV Cep	21 56 39.1	+63 37 32	1.0	123	− 0.0	− 10.2	M2	Ia–Iab
HDE 235749	22 11 35.7	+55 16 04	4.0	−55	3.3	− 9.9	M2	Ib
U Lac	22 47 43.4	+55 09 30	4.2	−263	1.9	− 11.4	M4	Iab

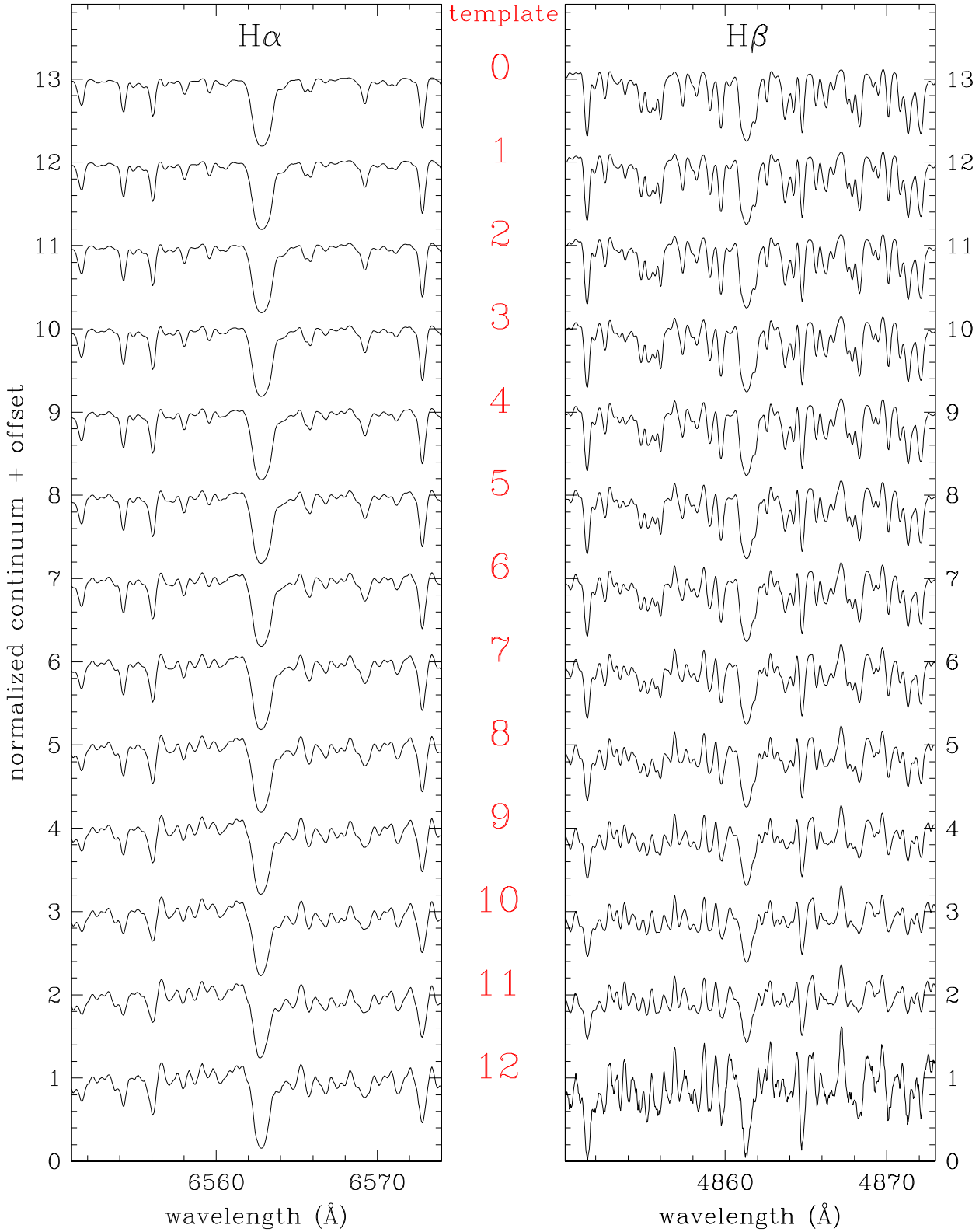

Figure A1. Sequence of templates as listed in Table 4. The template label/bin is indicated in red, and the template spectra are ordered from earlier to later M-type going from top to bottom. The bottommost spectrum is of relatively lower S/N due to the small number of spectra that were used in constructing this template (see Table 4).

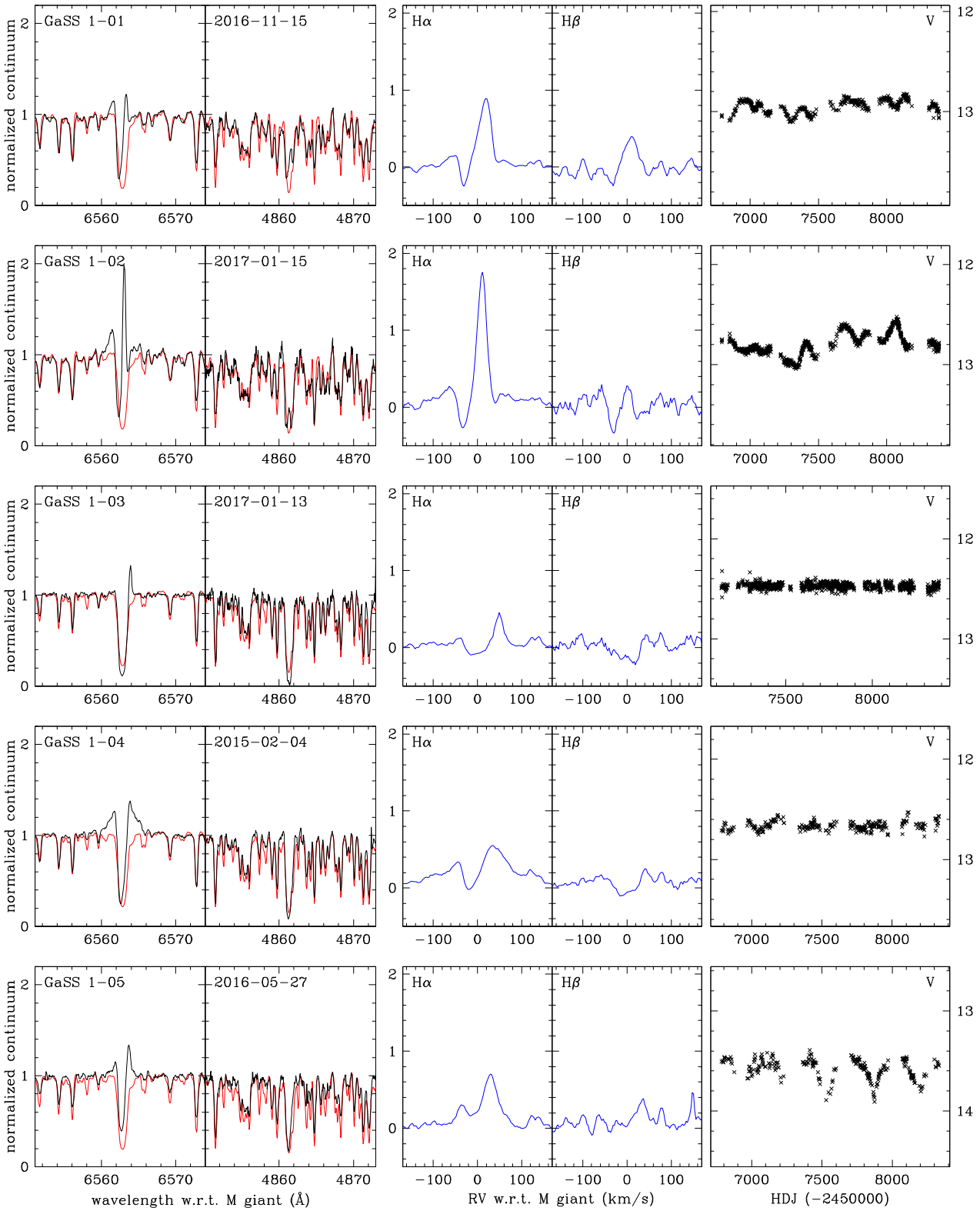

Figure A2. Left-hand panels: Hα and Hβ profiles (in black) compared to respective templates (in red) for program stars GaSS 1–1 to GaSS 1–5. Centre panels: the result of subtracting the template from the object spectrum. Right-hand panel: *V*-filter light curve from ASAS-SN sky patrol data.

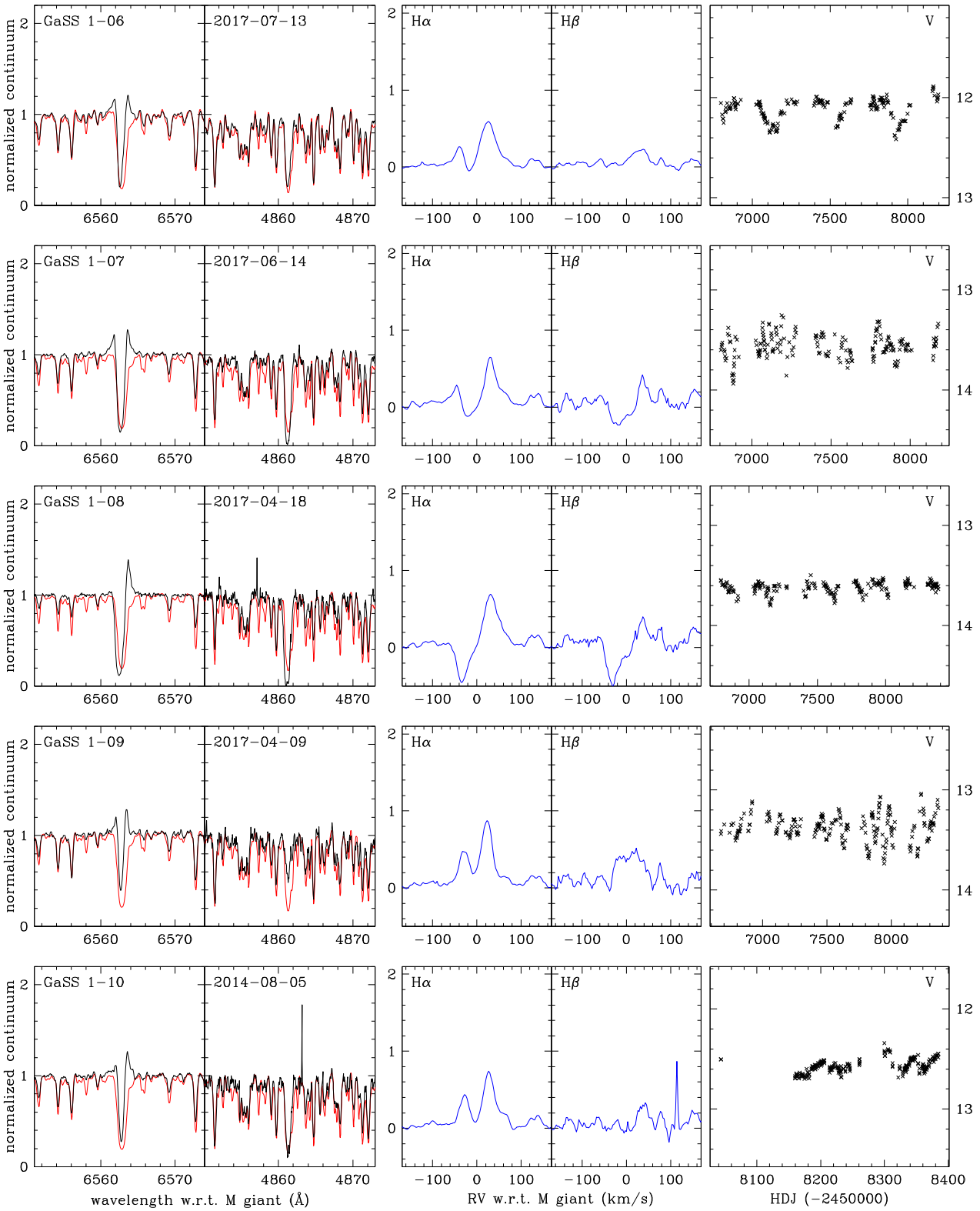

Figure A3. Similar to Fig. A2 but for program stars GaSS 1–6 to GaSS 1–10.

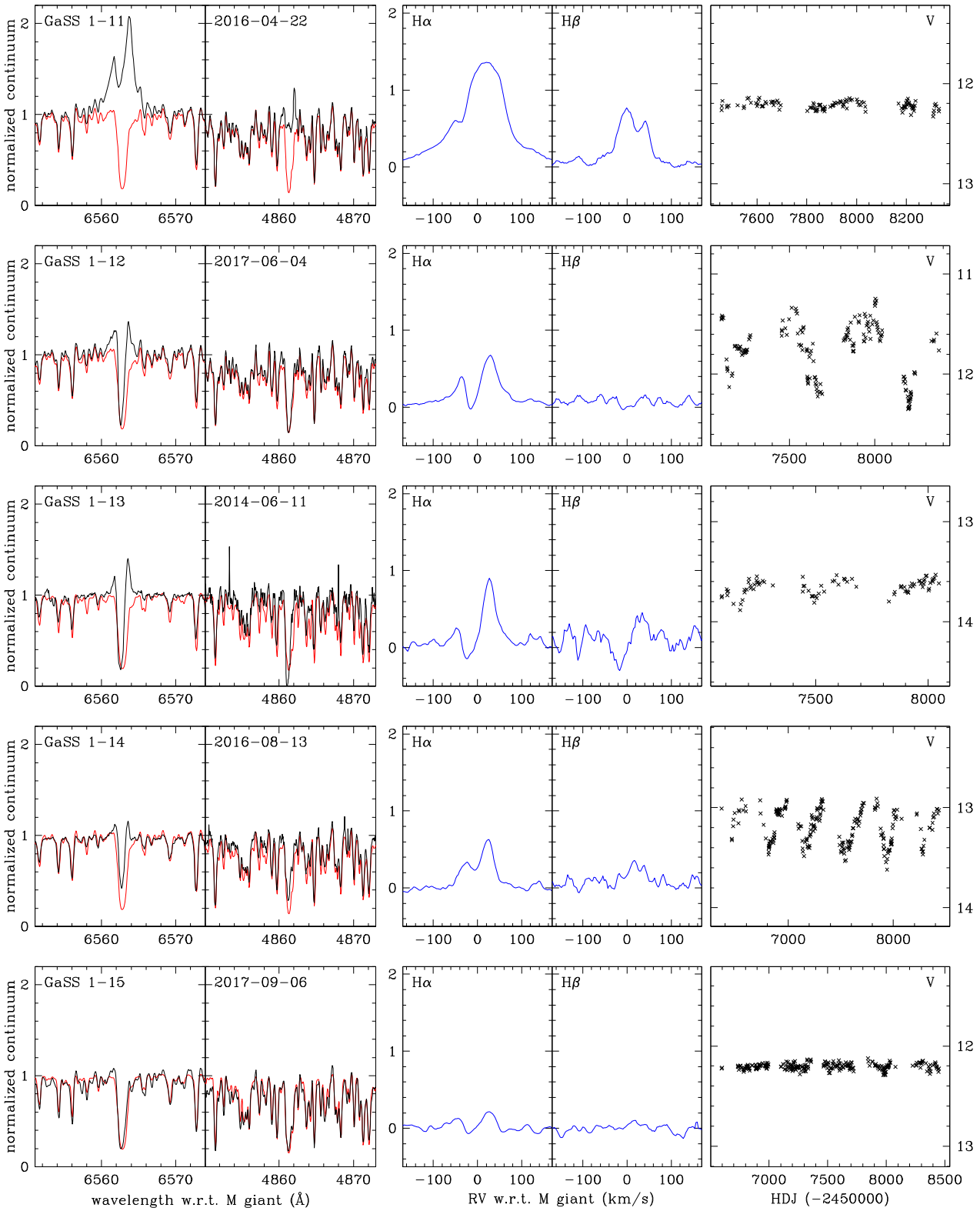

Figure A4. Similar to Fig. A2 but for program stars GaSS 1–11 to GaSS 1–16.

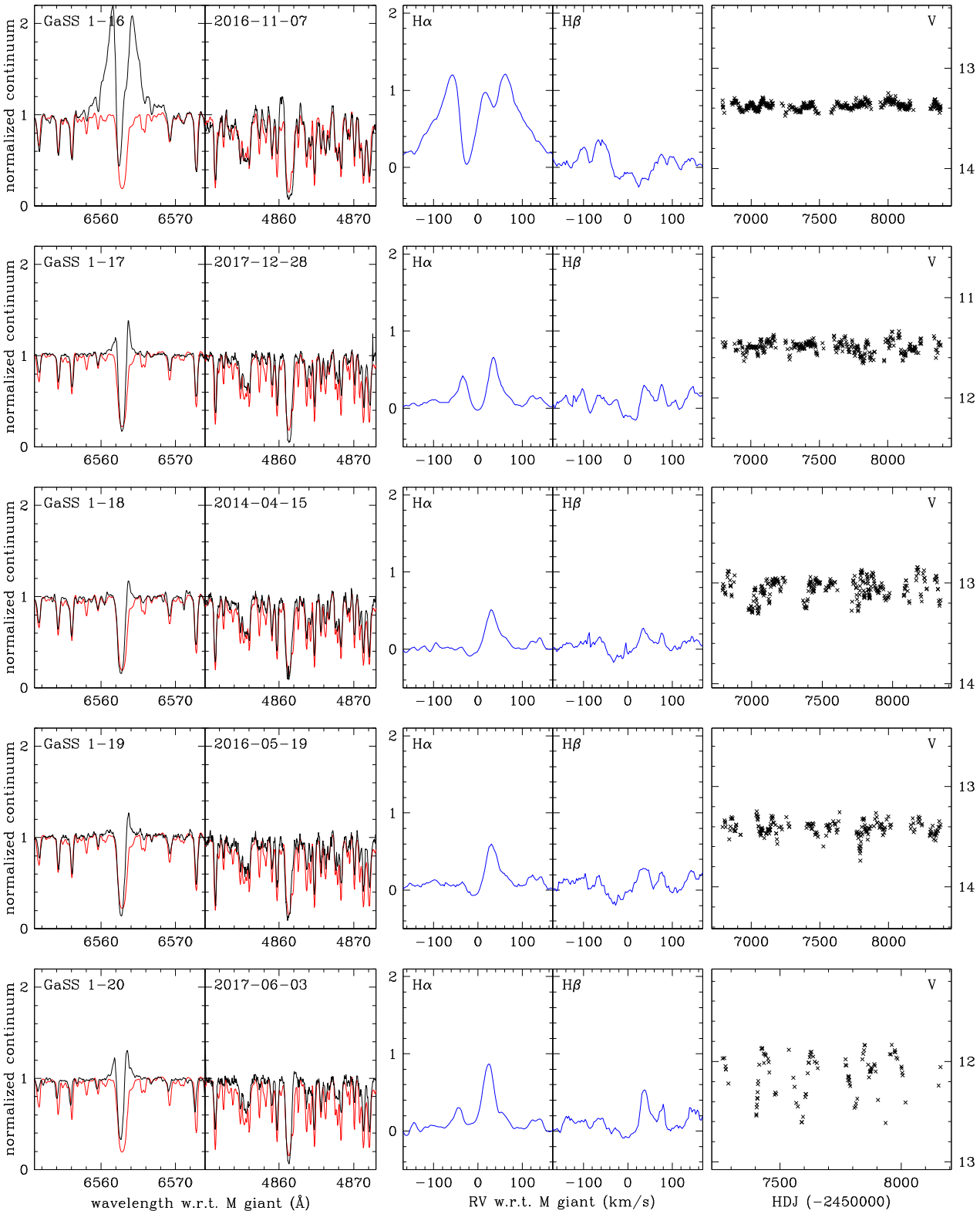

Figure A5. Similar to Fig. A2 but for program stars GaSS 1–16 to GaSS 1–20.

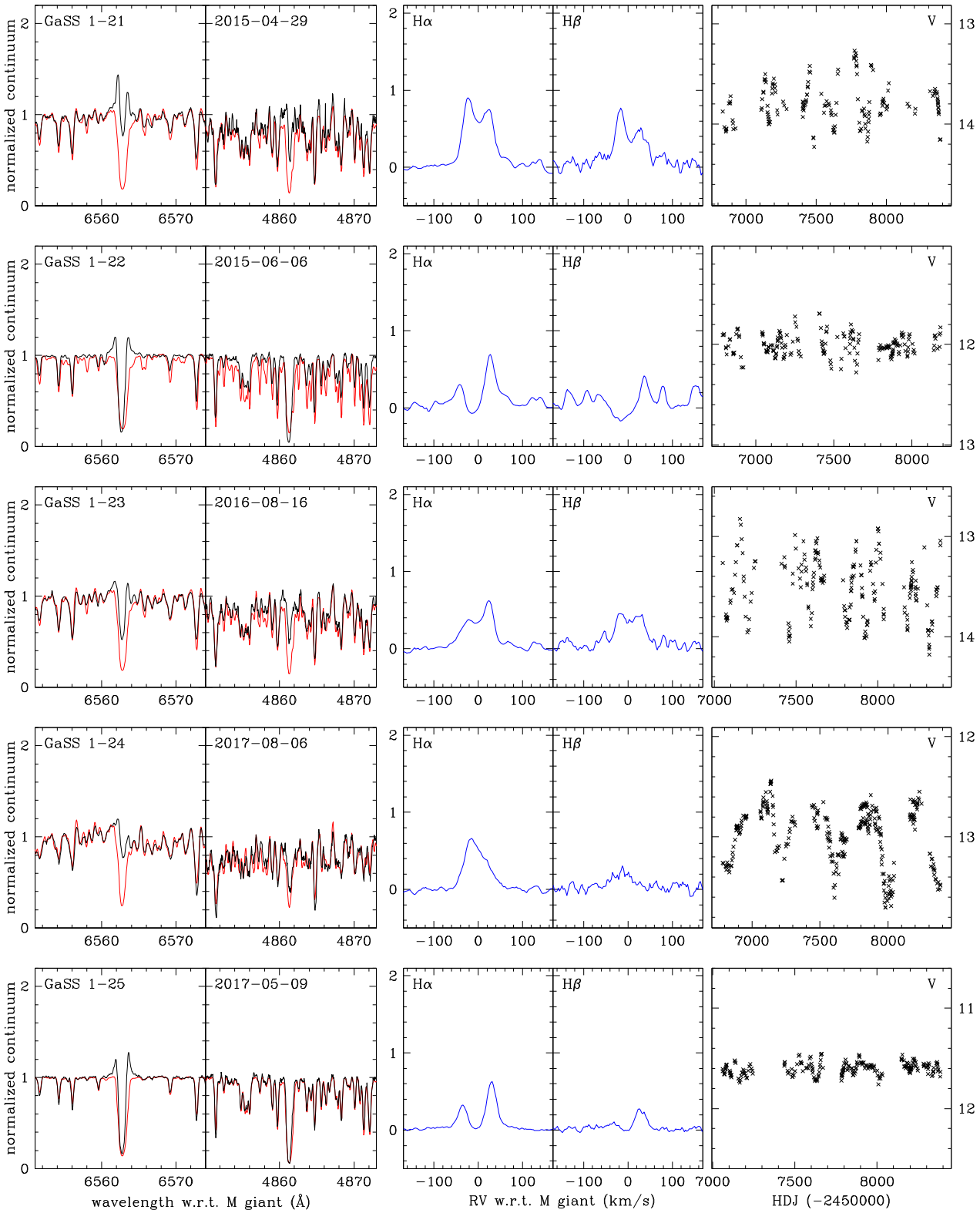

Figure A6. Similar to Fig. A2 but for program stars GaSS 1–21 to GaSS 1–25.

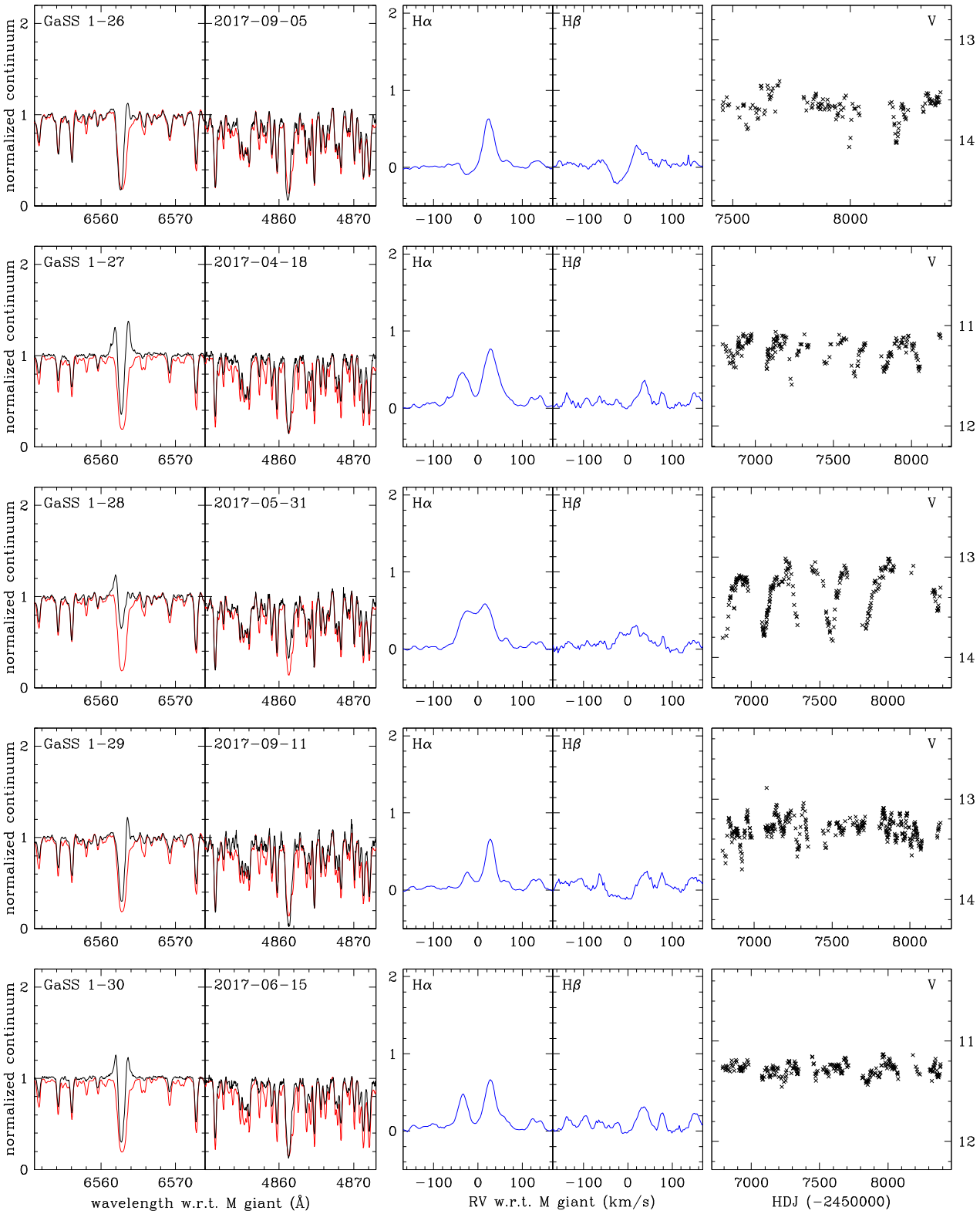

Figure A7. Similar to Fig. A2 but for program stars GaSS 1–26 to GaSS 1–30.

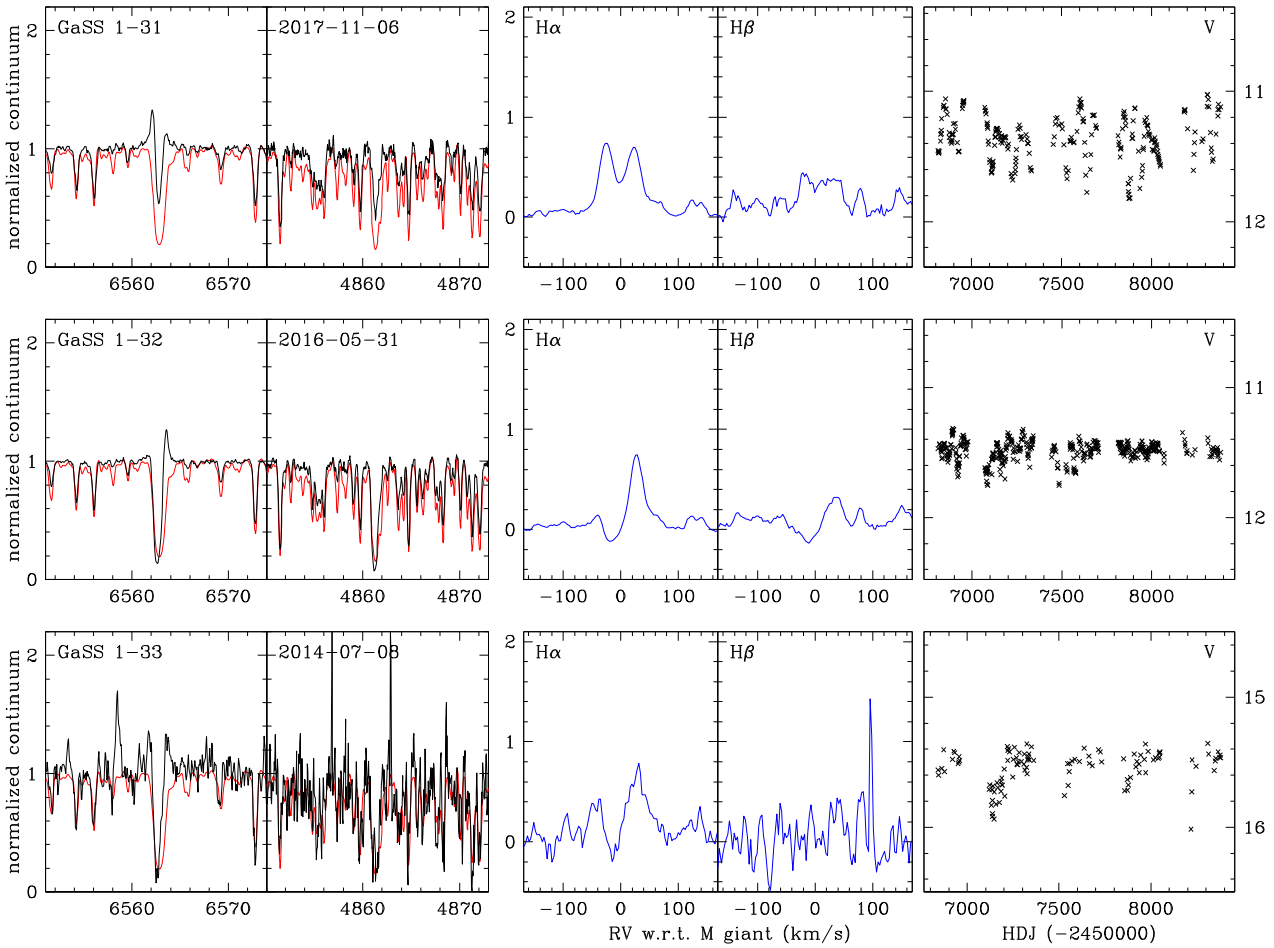

Figure A8. Similar to Fig. A2 but for program stars GaSS 1–31 to GaSS 1–33.

This paper has been typeset from a TEX/LATEX file prepared by the author.

List of astronomical key words (Updated on 2020 January)

This list is common to *Monthly Notices of the Royal Astronomical Society, Astronomy and Astrophysics*, and *The Astrophysical Journal*. In order to ease the search, the key words are subdivided into broad categories. No more than *six* subcategories altogether should be listed for a paper.

The subcategories in boldface containing the word 'individual' are intended for use with specific astronomical objects; these should never be used alone, but always in combination with the most common names for the astronomical objects in question. Note that each object counts as one subcategory within the allowed limit of six.

The parts of the key words in italics are for reference only and should be omitted when the keywords are entered on the manuscript.

General
editorials, notices
errata, addenda
extraterrestrial intelligence
history and philosophy of astronomy
miscellaneous
obituaries, biographies
publications, bibliography
sociology of astronomy
standards

Physical data and processes
acceleration of particles
accretion, accretion discs
asteroseismology
astrobiology
astrochemistry
astroparticle physics
atomic data
atomic processes
black hole physics
chaos
conduction
convection
dense matter
diffusion
dynamo
elementary particles
equation of state
gravitation
gravitational lensing: micro
gravitational lensing: strong
gravitational lensing: weak
gravitational waves
hydrodynamics
instabilities
line: formation
line: identification
line: profiles
magnetic fields
magnetic reconnection
(magnetohydrodynamics) MHD
masers
molecular data
molecular processes
neutrinos
nuclear reactions, nucleosynthesis, abundances
opacity
plasmas
polarization
radiation: dynamics
radiation mechanisms:general
radiation mechanisms: non-thermal
radiation mechanisms: thermal
radiative transfer
relativistic processes
scattering
shock waves
solid state: refractory
solid state: volatile
turbulence
waves

Astronomical instrumentation, methods and techniques
atmospheric effects
balloons
instrumentation: adaptive optics
instrumentation: detectors
instrumentation: high angular resolution
instrumentation: interferometers
instrumentation: miscellaneous
instrumentation: photometers
instrumentation: polarimeters
instrumentation: spectrographs
light pollution
methods: analytical
methods: data analysis
methods: laboratory: atomic
methods: laboratory: molecular
methods: laboratory: solid state
methods: miscellaneous
methods: numerical
methods: observational
methods: statistical
site testing
space vehicles
space vehicles: instruments
techniques: high angular resolution
techniques: image processing
techniques: imaging spectroscopy
techniques: interferometric
techniques: miscellaneous
techniques: photometric
techniques: polarimetric
techniques: radar astronomy
techniques: radial velocities
techniques: spectroscopic
telescopes

Astronomical data bases
astronomical data bases: miscellaneous
atlases
catalogues
surveys
virtual observatory tools

Software
software: data analysis
software: development
software: documentation
software: public release
software: simulations

Astrometry and celestial mechanics
astrometry
celestial mechanics
eclipses
ephemerides
occultations
parallaxes
proper motions
reference systems
time

The Sun
Sun: abundances
Sun: activity
Sun: atmosphere
Sun: chromosphere
Sun: corona
Sun: coronal mass ejections (CMEs)
Sun: evolution
Sun: faculae, plages
Sun: filaments, prominences
Sun: flares
Sun: fundamental parameters
Sun: general
Sun: granulation
Sun: helioseismology
Sun: heliosphere
Sun: infrared
Sun: interior
Sun: magnetic fields
Sun: oscillations
Sun: particle emission
Sun: photosphere
Sun: radio radiation
Sun: rotation
(Sun:) solar–terrestrial relations
(Sun:) solar wind
(Sun:) sunspots
Sun: transition region
Sun: UV radiation
Sun: X-rays, gamma-rays

Planetary systems
comets: general

comets: individual: . . .
Earth
interplanetary medium
Kuiper belt: general

Kuiper belt objects: individual: . . .
meteorites, meteors, meteoroids
minor planets, asteroids: general
minor planets, asteroids: individual: . . .
Moon
Oort Cloud
planets and satellites: atmospheres
planets and satellites: aurorae
planets and satellites: composition
planets and satellites: detection
planets and satellites: dynamical evolution and stability
planets and satellites: formation
planets and satellites: fundamental parameters
planets and satellites: gaseous planets
planets and satellites: general

planets and satellites: individual: . . .
planets and satellites: interiors
planets and satellites: magnetic fields
planets and satellites: oceans
planets and satellites: physical evolution
planets and satellites: rings
planets and satellites: surfaces
planets and satellites: tectonics
planets and satellites: terrestrial planets
planet–disc interactions
planet–star interactions
protoplanetary discs
zodiacal dust

Stars
stars: abundances
stars: activity
stars: AGB and post-AGB
stars: atmospheres
(stars:) binaries *(including multiple)*: close
(stars:) binaries: eclipsing
(stars:) binaries: general
(stars:) binaries: spectroscopic
(stars:) binaries: symbiotic
(stars:) binaries: visual
stars: black holes
(stars:) blue stragglers
(stars:) brown dwarfs
stars: carbon
stars: chemically peculiar
stars: chromospheres
(stars:) circumstellar matter
stars: coronae
stars: distances
stars: dwarf novae
stars: early-type
stars: emission-line, Be
stars: evolution
stars: flare
stars: formation
stars: fundamental parameters
(stars:) gamma-ray burst: general
(stars:) **gamma-ray burst: individual: . . .**
stars: general
(stars:) Hertzsprung–Russell and colour–magnitude diagrams
stars: horizontal branch
stars: imaging
stars: individual: . . .
stars: interiors

stars: jets
stars: kinematics and dynamics
stars: late-type
stars: low-mass
stars: luminosity function, mass function
stars: magnetars
stars: magnetic field
stars: massive
stars: mass-loss
stars: neutron
(stars:) novae, cataclysmic variables
stars: oscillations *(including pulsations)*
stars: peculiar *(except chemically peculiar)*
(stars:) planetary systems
stars: Population II
stars: Population III
stars: pre-main-sequence
stars: protostars
(stars:) pulsars: general
(stars:) **pulsars: individual: . . .**
stars: rotation
stars: solar-type
(stars:) starspots
stars: statistics
(stars:) subdwarfs
(stars:) supergiants
(stars:) supernovae: general
(stars:) **supernovae: individual: . . .**
stars: variables: Cepheids
stars: variables: Scuti
stars: variables: general
stars: variables: RR Lyrae
stars: variables: S Doradus
stars: variables: T Tauri, Herbig Ae/Be
(stars:) white dwarfs
stars: winds, outflows
stars: Wolf–Rayet

Interstellar medium (ISM), nebulae
ISM: abundances
ISM: atoms
ISM: bubbles
ISM: clouds
(ISM:) cosmic rays
(ISM:) dust, extinction
ISM: evolution
ISM: general
(ISM:) HII regions
(ISM:) Herbig–Haro objects

ISM: individual objects: . . .
(except planetary nebulae)
ISM: jets and outflows
ISM: kinematics and dynamics
ISM: lines and bands
ISM: magnetic fields
ISM: molecules
(ISM:) photodissociation region (PDR)
(ISM:) planetary nebulae: general
(ISM:) **planetary nebulae: individual: . . .**
ISM: structure
ISM: supernova remnants

The Galaxy
Galaxy: abundances
Galaxy: bulge
Galaxy: centre
Galaxy: disc
Galaxy: evolution
Galaxy: formation
Galaxy: fundamental parameters
Galaxy: general
(Galaxy:) globular clusters: general
(Galaxy:) **globular clusters: individual: . . .**
Galaxy: halo
Galaxy: kinematics and dynamics
(Galaxy:) local interstellar matter
Galaxy: nucleus
(Galaxy:) open clusters and associations: general
(Galaxy:) **open clusters and associations: individual: . . .**
(Galaxy:) solar neighbourhood
Galaxy: stellar content
Galaxy: structure

Galaxies
galaxies: abundances
galaxies: active
galaxies: bar
(galaxies:) BL Lacertae objects: general
(galaxies:) **BL Lacertae objects: individual: . . .**
galaxies: bulges
galaxies: clusters: general

galaxies: clusters: individual: . . .
galaxies: clusters: intracluster medium
galaxies: disc
galaxies: distances and redshifts
galaxies: dwarf
galaxies: elliptical and lenticular, cD
galaxies: evolution
galaxies: formation
galaxies: fundamental parameters
galaxies: general
galaxies: groups: general

galaxies: groups: individual: . . .
galaxies: haloes
galaxies: high-redshift

galaxies: individual: . . .
galaxies: interactions
(galaxies:) intergalactic medium
galaxies: irregular
galaxies: ISM
galaxies: jets
galaxies: kinematics and dynamics
(galaxies:) Local Group
galaxies: luminosity function, mass function
(galaxies:) Magellanic Clouds
galaxies: magnetic fields
galaxies: nuclei
galaxies: peculiar
galaxies: photometry
(galaxies:) quasars: absorption lines
(galaxies:) quasars: emission lines
(galaxies:) quasars: general

(galaxies:) **quasars: individual: . . .**
(galaxies:) quasars: supermassive black holes
galaxies: Seyfert
galaxies: spiral
galaxies: starburst
galaxies: star clusters: general

galaxies: star clusters: individual: . . .
galaxies: star formation
galaxies: statistics
galaxies: stellar content
galaxies: structure

Cosmology
(cosmology:) cosmic background radiation
(cosmology:) cosmological parameters
(cosmology:) dark ages, reionization, first stars
(cosmology:) dark energy
(cosmology:) dark matter
(cosmology:) diffuse radiation
(cosmology:) distance scale
(cosmology:) early Universe
(cosmology:) inflation
(cosmology:) large-scale structure of Universe
cosmology: miscellaneous
cosmology: observations
(cosmology:) primordial nucleosynthesis
cosmology: theory

Resolved and unresolved sources as a function of wavelength
gamma-rays: diffuse background
gamma-rays: galaxies
gamma-rays: galaxies: clusters
gamma-rays: general
gamma-rays: ISM
gamma-rays: stars
infrared: diffuse background
infrared: galaxies
infrared: general
infrared: ISM
infrared: planetary systems
infrared: stars
radio continuum: galaxies
radio continuum: general
radio continuum: ISM
radio continuum: planetary systems
radio continuum: stars
radio continuum: transients
radio lines: galaxies
radio lines: general
radio lines: ISM
radio lines: planetary systems
radio lines: stars
submillimetre: diffuse background
submillimetre: galaxies
submillimetre: general
submillimetre: ISM
submillimetre: planetary systems
submillimetre: stars
ultraviolet: galaxies
ultraviolet: general
ultraviolet: ISM
ultraviolet: planetary systems
ultraviolet: stars
X-rays: binaries
X-rays: bursts
X-rays: diffuse background
X-rays: galaxies
X-rays: galaxies: clusters
X-rays: general
X-rays: individual: . . .
X-rays: ISM
X-rays: stars

Transients
(transients:) black hole mergers
(transients:) black hole - neutron star mergers
(transients:) fast radio bursts
(transients:) gamma-ray bursts
(transients:) neutron star mergers
transients: novae
transients: supernovae
transients: tidal disruption events